



1N-05  
381 821

P. 136

# TECHNICAL NOTE

D-248

LONGITUDINAL AERODYNAMIC CHARACTERISTICS OF  
A FOUR-PROPELLER DEFLECTED SLIPSTREAM VTOL MODEL  
INCLUDING THE EFFECTS OF GROUND PROXIMITY

By Richard E. Kuhn and Kalman J. Grunwald

Langley Research Center  
Langley Field, Va.

NATIONAL AERONAUTICS AND SPACE ADMINISTRATION

WASHINGTON

November 1960

NATIONAL AERONAUTICS AND SPACE ADMINISTRATION

TECHNICAL NOTE D-248

LONGITUDINAL AERODYNAMIC CHARACTERISTICS OF  
A FOUR-PROPELLER DEFLECTED SLIPSTREAM VTOL MODEL  
INCLUDING THE EFFECTS OF GROUND PROXIMITY

By Richard E. Kuhn and Kalman J. Grunwald

SUMMARY

Results are presented of a wind-tunnel investigation of the longitudinal stability, control, and performance characteristics of a model of a four-propeller deflected-slipstream VTOL airplane in the transition speed range. These results indicate that steady level-flight transition and descending flight-path angles up to  $7^\circ$  or  $8^\circ$  out of the region of ground effect can be accomplished without wing stall being encountered. In general, the pitching moments out of ground proximity can be adequately trimmed by programming the stabilizer incidence to increase with increasing flap deflection, except for a relatively large diving moment in the hovering condition. The deflection of the slipstream onto the horizontal tail in proximity of the ground substantially increases the diving moment in hovering, unless the tail is set at a large nosedown incidence.

INTRODUCTION

A wind-tunnel investigation has been made of a 1/5-scale model of a current deflected-slipstream VTOL (vertical take-off and landing) airplane to determine the performance and the stability and control characteristics in hovering and in transition to forward flight. The investigation in the transition speed range was made in the 17-foot test section of the Langley 300-MPH 7- by 10-foot tunnel and the hovering investigation was made in a large room.

The investigation covered the complete range of flap deflections and power conditions through the transition speed range from hovering to forward (flaps retracted) flight. The present paper presents the results of the investigation of the longitudinal stability, control, and performance characteristics, including tests in the ground-effect region. An analysis of some of the significant longitudinal stability, control, and performance characteristics is included.

## SYMBOLS

The force and moment coefficients presented are based on the dynamic pressure in the slipstream. This system is used because, when a wing is located in a propeller slipstream, large forces and moments can be produced even though the free-stream velocity decreases to zero and in this condition coefficients based on the free-stream dynamic pressure approach infinity and therefore become meaningless. The coefficients based on the slipstream dynamic pressure are indicated in the present paper by the use of the subscript *s*. The relations between the thrust and dynamic pressure in the slipstream have been derived in reference 1. The more familiar coefficient forms based on the free-stream dynamic pressure can be found

by dividing by  $(1 - C_{T,s})$ ; that is  $C_L = \frac{C_{L,s}}{1 - C_{T,s}}$ . The positive sense of

forces, moments, and angles is indicated in figure 1. The pitching moments are presented with reference to the center of gravity located at the projection of the wing 40-percent-chord point on the thrust line as shown in figure 2.

<i>b</i>	wing span, 6.55 ft
<i>c</i>	wing chord, 1.166 ft
<i>c<sub>a</sub></i>	aileron chord, 0.466 ft
<i>c<sub>R</sub></i>	rear flap chord, 0.466 ft
<i>c<sub>S</sub></i>	sliding flap chord, 0.565 ft
<i>c<sub>t</sub></i>	horizontal-tail chord, 0.666 ft
<i>C<sub>h,a</sub></i>	aileron hinge-moment coefficient, $\frac{\text{Aileron hinge moment}}{q_s S_a c_a}$
<i>C<sub>h,R</sub></i>	rear-flap hinge-moment coefficient, $\frac{\text{Rear-flap hinge moment}}{q_s S_R c_R}$
<i>C<sub>h,S</sub></i>	sliding-flap hinge-moment coefficient, $\frac{\text{Sliding-flap hinge moment}}{q_s S_S c_S}$
<i>C<sub>L</sub></i>	lift coefficient based on free stream, $\frac{L}{\frac{\rho}{2} V^2 S}$

$C_{L,s}$	lift coefficient based on slipstream, $\frac{L}{q_s S}$
$C_{m,s}$	model pitching-moment coefficient, $\frac{M_Y}{q_s S c}$
$\Delta C_{m,s}$	increment of pitching-moment coefficient due to tail fan
$C_{m,t}$	horizontal-tail pitching-moment coefficient, $\frac{M_t}{q_s S_t c_t}$
$C_{N,t}$	horizontal-tail normal-force coefficient, $\frac{\text{Tail normal force}}{q_s S_t}$
$C_{T,s}$	thrust coefficient, $\frac{T}{q_s N \frac{\pi}{4} D^2}$
$C_{X,s}$	longitudinal-force coefficient, $\frac{F_X}{q_s S}$
D	propeller diameter, 1.55 ft
F	resultant force, lb
$F_X$	longitudinal force, lb
h	height of landing-gear wheels above ground, ft
$i_t$	horizontal-tail incidence, deg
$i_n$	incidence of thrust axis relative to fuselage reference line, deg
L	lift, lb
$M_Y$	pitching moment, ft-lb
$M_t$	horizontal-tail pitching moment, ft-lb
n	propeller rotational speed, rpm
N	number of propellers

$q_s$	dynamic pressure in slipstream, $\frac{\rho V^2}{2} + \frac{T}{N \frac{\pi}{4} D^2}$ , lb/sq ft
$S$	wing area, 7.65 sq ft
$S_a$	aileron area per semispan, 0.692 sq ft
$S_R$	inboard-rear-flap area per semispan, 0.724 sq ft
$S_S$	sliding flap area per semispan, 1.72 sq ft
$S_t$	horizontal-tail area, 2.47 sq ft
$T$	total thrust, lb
$T_t$	tail-fan thrust, lb
$V$	free-stream velocity, ft/sec
$V_k$	free-stream velocity, knots
$\alpha$	angle of attack, deg
$\beta_{0.75}$	propeller blade angle, measured at 75 percent radius, deg
$\delta_{tab}$	tab deflection, deg
$\delta_{f,S}$	sliding-flap deflection, deg
$\delta_{f,R}$	rear-flap deflection, deg
$\epsilon$	downwash angle, deg
$\rho$	mass density of air, slugs/cu ft
$\theta$	slipstream turning angle (static tests), $\arctan \frac{L}{F_X}$ , deg
$\gamma$	flight-path angle, deg
Subscripts:	
$O$	power-off-flaps retracted condition

s based on slipstream value  
 S sliding flap  
 R rear flap

### MODEL

L  
 7  
 3  
 5  
 A drawing of the model with pertinent dimensions is presented as figure 2, and photographs of the model mounted for testing are presented as figure 3. The wing employed an NACA 4415 airfoil section (fig. 4) and was set at  $5^\circ$  noseup incidence to the fuselage reference line, which was usually parallel to the propeller thrust axis. The flap system consisted of a 50-percent-chord sliding flap and a 30-percent-chord slotted flap as shown in figure 4. The radius of the sliding flap was 20 percent of the wing chord, and the ordinates of the slotted flap are shown on figure 4. The combinations of flap deflections used in the investigation and the convention adopted to designate the flap deflections as used on the figures and throughout the text are as follows:

Sliding-flap deflection, $\delta_{f,S}$ , deg	Rear-flap deflection, $\delta_{f,R}$ , deg	Designation: $\delta_{f,S}/\delta_{f,R}$
0	0	0/0
10	8.2	10/8.2
20	15	20/15
30	20.7	30/20.7
40	24	40/24
50	25	50/25
<sup>a</sup> 60	<sup>a</sup> 26	60/26

<sup>a</sup>Used in static tests only.

In addition, the rear or slotted flap was constructed in two pieces so that the outboard element could be deflected as an aileron. A few tests were made with the inboard element deflected  $40^\circ$  and with the sliding flap and aileron retracted, in order to obtain some data on a conventional partial-span flap configuration. Sketches of a full-span slat and full-span flap extension used in only a few tests are shown in figure 4.

The model was equipped with a large vertical tail to which the horizontal tail was attached in a high position (figs. 1 and 2). A small adjustable trailing-edge tab was provided on the horizontal tail.

For a few tests, the model was fitted with a pneumatically driven tail fan (figs. 1 and 2) in order to investigate the effect of the influence of the slipstream from the tail fan on the model characteristics.

The model construction consisted of a steel frame to carry the loads and a wooden covering to give the desired contours. The three-bladed propellers were made of aluminum alloy and were driven by variable-frequency electric motors. The speed of each propeller was determined by observing a stroboscopic-type indicator to which was fed the output frequency of small alternators connected to each of the motor shafts. The outboard propellers rotated against the tip vortex and for most of the tests the inboard propellers rotated in the opposite direction. For a few tests the direction of rotation of the inboard propellers was reversed so that they rotated in the same direction as their adjacent outboard propellers. For the basic configuration the thrust axis was oriented  $5^\circ$  below the wing-chord plane. Alternate nacelle mounting blocks were used in a few tests to mount the propellers with their thrust axes parallel to the wing chord plane. The thrust line passed through the moment reference point for both conditions.

The lift, longitudinal force, and pitching moment were measured with an internally mounted strain-gage balance. In addition the hinge moments of the aileron, the sliding flap, and the inboard part of the rear flap were measured by strain-gage beams. The moment reference points for these hinge moments are shown in figure 4. The horizontal-tail normal force and pitching moment (about the tail quarter-chord point) were also measured by strain-gage beams.

The flap settings were fixed by interchangeable blocks and the stabilizer was set at fixed positions by inserting dowels in appropriate predrilled setting holes.

The landing gear was built with round rods rather than with the streamline tubing used on the airplane and was installed for all but a few tests as indicated on the data figures.

#### TESTS AND CORRECTIONS

The investigation was made in the 17-foot test section of the Langley 300-MPH 7- by 10-foot tunnel, which is described in the appendix to reference 2. In order to minimize the time required for the tests, the operating conditions were chosen so that only two propeller blade angles were required. A blade angle of  $5^\circ$  was used for tests at thrust coefficients of 0.60 or more and a blade angle of  $13^\circ$  was used for the lower thrust coefficients and for the propeller-windmilling tests. A propeller rotational-speed of 6,000 rpm was used with the  $5^\circ$  blade angle

and of 4,000 with the 13° blade angle. The thrust of the four propellers was determined at each tunnel speed used by taking the difference between the longitudinal force measured with the propellers operating and with the propellers off at zero angle of attack with the flaps retracted.

The slipstream dynamic pressure varied from about 3.8 to 5.0 pounds per square foot. A free-stream dynamic pressure of 5.0 pounds per square foot was used for the propeller-off and propeller-windmilling tests. The Reynolds number of the flow in the slipstream based on the wing chord of 1.166 feet varied from  $0.42 \times 10^6$  to  $0.49 \times 10^6$ .

The test procedure consisted in setting the propeller rotational speed with the model at zero angle of attack and then increasing the tunnel speed until zero longitudinal force was reached. This tunnel speed, which then corresponded to the condition for steady level flight at zero angle of attack, was held constant as the data were taken through the angle-of-attack range. Usually, subsequent tests were also made at tunnel dynamic pressures above and below the tunnel speed for steady level flight at zero angle of attack in order to provide data for the conditions of acceleration and deceleration.

Corrections to the free-stream velocity for blockage and slipstream contraction were estimated and were considered negligible. The jet-boundary corrections applied to the angle of attack and longitudinal force were estimated for a square test section by a method similar to that of reference 3. Inasmuch as these corrections depend on the circulation about the wing, it was necessary to subtract the direct thrust contribution to lift before applying them. The following relations were used:

$$\alpha = \alpha_{\text{measured}} + 0.239C_{L,1}$$

$$C_{X,s} = C_{X,s,\text{measured}} - 0.0042(C_{L,1})^2(1 - C_{T,s})$$

where  $C_{L,1}$  is the increment of lift coefficient that is approximately proportional to circulation and is obtained by subtracting the direct thrust contribution as follows:

$$C_{L,1} = \frac{C_{L,s} - C_{T,s} \frac{4 \frac{\pi}{4} D^2}{S} \frac{F}{T} \sin(\theta + \alpha)}{1 - C_{T,s}}$$

L  
7  
3  
5

where  $\theta$  and  $F/T$  are the turning angle and thrust-recovery factor, respectively, determined from static tests.

### PRESENTATION OF RESULTS

The figures in which results of the investigation are presented are listed, for convenience, in the following table:

	Figures
Complete model data:	
Static data . . . . .	5 to 8
Effect of flap deflection and thrust coefficient:	
Horizontal tail off . . . . .	9 to 13
Horizontal tail on . . . . .	14 to 19
Effect of ground proximity . . . . .	20 to 23
Effect of horizontal-tail incidence . . . . .	24 to 28
Effect of thrust-line incidence and direction of inboard propeller rotation . . . . .	29 to 31
Effect of tail fan . . . . .	32 to 34
Effect of tab deflection . . . . .	35
Effect of leading-edge slat and chord extension . . . . .	36 to 38
Effect of inboard flap . . . . .	39 to 40
Effect of landing gear . . . . .	41
Flap and aileron hinge moments:	
Static data . . . . .	7
Effect of flap deflection . . . . .	9 to 13
Effect of thrust-line incidence and direction of propeller rotation . . . . .	29 to 31
Horizontal-tail normal force:	
Static data . . . . .	6
Effect of thrust coefficient and flap deflection . . . . .	14 to 17, 19
Effect of horizontal-tail incidence . . . . .	24 to 27
Effect of tail fan . . . . .	32 to 34
Effect of tab deflection . . . . .	35
Horizontal-tail pitching moments:	
Effect of thrust coefficients, flaps retracted . . . . .	14
Effect of horizontal-tail incidence . . . . .	24
Effect of tail fan . . . . .	32
Effect of tab deflection . . . . .	35

	Figures
Analysis:	
Steady-level-flight transition:	
Performance out of ground proximity . . . . .	42 to 45
Effect of ground proximity . . . . .	46
Trim and control:	
Out of ground proximity . . . . .	47 to 49
Effect of ground proximity . . . . .	50
Stability . . . . .	51
Climb and descent characteristics:	
Effect of flap deflection . . . . .	52
Effect of horizontal-tail incidence . . . . .	53
Effect of ground proximity . . . . .	54
Effect of slat . . . . .	55

The basic data obtained from the investigation are presented in figures 5 to 41. Complete analysis of all the data obtained has not been attempted; however, a few of the more significant results are analyzed on the basis of the performance and the stability and control characteristics that can be predicted from the tunnel data. These results are presented in figures 42 to 55. A gross weight of 3,600 pounds was assumed for the purpose of this analysis.

## DISCUSSION

### Hovering Characteristics

The basic hovering characteristics are presented in figures 5 to 8. With a flap-deflection combination  $\delta_{f,S}/\delta_{f,R}$  of 50/25, a turning angle  $\theta$  of approximately  $67^\circ$  and a thrust-recovery factor  $F/T$  of approximately 0.8 was obtained. Thus, for a gross weight of 3,600 pounds, a thrust of about 4,500 pounds and a noseup attitude of approximately  $23^\circ$  (as expected) would be required to hover out of ground effect. It is emphasized that these results apply only to the configuration having a ratio of propeller diameter to wing chord of the model as tested. If the propeller diameter were increased, the turning angle would be expected to decrease in approximately inverse proportion to the increase in propeller diameter (fig. 2 of ref. 4).

In proximity of the ground, the turning angle decreased slightly and the thrust recovery factor increased slightly as compared with values obtained out of ground effect. The most important effect of ground proximity was to increase the nosedown pitching moment. This increase was found to be due to the deflection of the slipstream from the ground onto the horizontal tail. The high noseup attitude (about  $26^\circ$ ) required

for hovering within ground proximity brings the tail very near the ground even with the high-tail configuration employed. Thus, a tail incidence of  $-26^\circ$  is required merely to place the horizontal tail parallel with the ground, and the data of figure 6 indicate that an additional increment of about  $11^\circ$  (or a total incidence of  $-37^\circ$ ) is required to provide pitching moments equal to those obtained out of ground proximity.

### Steady-Level-Flight Transition

The effect of thrust coefficient on the basic aerodynamic characteristics with various flap deflections is shown in figures 9 to 13 for the tail-off condition and in figures 14 to 19 for the tail-on condition. From polars of the lift against longitudinal force (part (a) of figures 9 to 19), it can be seen that in general wing stall is not encountered in the steady level-flight condition ( $C_{X,s} = 0$ ) but is delayed somewhat until the configuration is in the descent or deceleration condition ( $C_{X,s, \text{negative}}$ ). The one exception to this result is that obtained with the flaps retracted, where the stall occurs in the climb or acceleration condition; however, this stall occurs at high thrust coefficients and at angles of attack above  $25^\circ$  and is not believed likely to be encountered in practice.

The data of figures 9 to 19 have been used to estimate the attitude and thrust required for steady-level-flight transition as shown in figure 42. As discussed previously, a thrust of 4,500 pounds and a noseup attitude of  $23^\circ$  is required for hovering with  $\delta_{f,S}/\delta_{f,R} = 50/25$ . Thrust decreases rapidly with forward speed and is fairly independent of flap deflection within the ranges investigated.

The angle of attack, power required, and the flap deflections used in the analysis of the steady level-flight transition are shown in figure 43. The transition starts, of course, with hovering at a  $23^\circ$  attitude with flap deflections  $\delta_{f,S}/\delta_{f,R}$  of 50/25. The angle of attack is decreased, and zero angle of attack is reached at about 15 knots, after which flap deflection is progressively decreased, while angle of attack is held at  $0^\circ$ . Also shown in figure 43 are the angle of attack and power required as calculated from power-off data for the flaps retracted (from fig. 9) and for inboard flaps deflected  $40^\circ$  (from fig. 39). The power required was calculated from the data of reference 5 with propeller rotational speed assumed constant at 2,000 rpm.

It should be noted that, although the thrust required at about 40 knots decreased to a minimum of about 20 percent of that required for hovering (fig. 42), the power required decreased to only 50 percent of hovering power. This unexpected result is attributed to the extremely

low blade angles required for the low thrusts with the wide propeller blades (activity factor of 165 per blade) used with the model, as is shown in figure 44, where the blade angle  $\beta_{0.75}$  and the horsepower required for level flight is plotted as a function of airspeed. The effect of decreasing the activity factor is also shown in figure 44. Of course, with narrower blades, higher efficiencies are available at these intermediate speeds because blade angles are slightly higher.

L  
7  
3  
5

The low blade angles required may become a problem in the event of propeller malfunction or power failure. If the propellers were arranged to go to their low pitch stops under these conditions, very high drag would be encountered if failure should occur in the cruise condition, or large rolling moments would result if an outboard propeller failed at or near hovering. A possible means of avoiding such low blade angles and thus minimizing these problems would be to vary the propeller rotational speeds as a means of achieving power and thrust control during transition and to hold the blade angle fixed. This method is illustrated in figure 45 for the propeller blades with an activity factor of 165. A somewhat smaller variation in propeller rotational speed would be expected with narrower blades. This system may, however, impose problems of too slow response in change in propeller rotational speed, to a pilot command for thrust change, which would have to be evaluated before a constant-blade-angle system could be considered.

The effect of ground proximity  $h/D$  on the attitude and power required in transition is shown in figure 46. The presence of the ground causes the power required to remain almost as high as the hovering power up to speeds of about 20 knots. This power requirement is necessary because of flow separation from the flaps. Similar results have been observed with another deflected-slipstream configuration (ref. 2) and suggest that transition should not be attempted very near the ground.

#### Trim and Control

The untrimmed pitching moments for the airplane in steady-level-flight transition are shown in figure 47 for tail-off condition and for the condition with the horizontal tail on and at zero incidence. A nosedown moment of about 2,400 foot-pounds exists in hovering for the configuration as tested. This moment would require a down load from the tail fan of about 120 pounds for trim out of ground proximity. The effects of this loss in lift on the power required in hovering were not considered in computing the thrust and power required of figures 42 to 45.

The diving moment in hovering could be reduced by either lowering the thrust axis or moving the center of gravity of the airplane rearward

or by a combination of these two. Of course, moving the center of gravity rearward would reduce the longitudinal stability. There is ample stability in the flap-retracted condition (fig. 24) and some reduction could probably be tolerated for this condition, but in the intermediate range of flap settings the airplane already exhibits attitude instability with the present center-of-gravity location.

As the airplane departs from hovering and gains forward speed, the pitching moment changes to a noseup moment (fig. 47). The large nose-up moments experienced with the horizontal tail at zero incidence are due to the large downwash angles. The downwash angles at the horizontal tail have been estimated from the horizontal-tail normal-force data of figures 24 to 27 (part (c)) and are shown in figure 48. The downwash angle was estimated from

$$\epsilon = \alpha + i_t - \frac{C_{N,t}}{(C_{N\alpha})_t}$$

where the variation of horizontal-tail normal-force coefficient with respect to angle of attack  $(C_{N\alpha})_t$  was estimated from the power-off

data of figure 24(c). The downwash at the tail is shown to increase with increasing flap deflection, and the variation of downwash angle with angle of attack, in general, increases with increasing thrust coefficient. Thus, power is destabilizing. At flap deflections  $\delta_{f,S}/\delta_{f,R}$  above 30/20.7 (power on), the normal force at the horizontal tail was so small that reliable data could not be obtained.

The method of computing the downwash at the horizontal tail from the foregoing equation assumes that the dynamic pressure at the horizontal tail is equal to the free-stream dynamic pressure. The tail-effectiveness data of figure 49 indicate that this assumption is fairly accurate. In figure 49 the power-on horizontal-tail effectiveness

$\frac{\partial M_Y}{\partial i_t}$  for several flap deflections is compared with the effectiveness

computed from the power-off, flaps-retracted data obtained by assuming free-stream dynamic pressure at the tail throughout the transition speed range. Apparently, the horizontal tail is located high enough on this configuration so that essentially free-stream dynamic pressure exists at the horizontal tail throughout the transition out of the ground-effect region.

Some difficulty was experienced with the strain-gage instrumentation used in obtaining the tail normal-force data. Comparison of the measured data with that calculated from the model lift and pitching-moment data indicates that the angles of attack for zero normal force (zero tail contribution) are approximately correct but that at other angles of attack the tail normal-force coefficients are too large. The general trends of the data and the downwash estimated from them are believed correct, however.

In figure 49 are also plotted the downwash and stabilizer incidence required for trim through the steady-level-flight transition. Because of the high downwash angles and the noseup pitching moments (tail-off data of fig. 47) that must be trimmed by the horizontal tail, relatively high noseup tail incidences are required for trim. Below about 25 knots the dynamic pressure at the horizontal tail is so low that the tail becomes ineffective as a trimming device, and tail settings above  $20^\circ$  to  $25^\circ$  are probably not needed.

The effect of ground proximity on the pitching moments is shown in figure 50. Very close to the ground ( $h/D = 0.33$ ) the deflection of the slipstream onto the horizontal tail, as discussed previously, causes a large additional diving moment which persists up to a speed of 20 to 25 knots. Also, as discussed previously, this diving moment could be reduced considerably by using a nosedown horizontal-tail incidence of about  $-35^\circ$ . Note, however, that at speeds of about 25 knots and above, large noseup stabilizer settings are required for trim out of the region of ground effect. Thus, the horizontal tail will have to move through about a  $60^\circ$  angle range if trim is to be maintained in passing from the region of ground effect to the region out of ground effect.

Other possible means of reducing this diving moment would be by lowering the thrust axis, moving the center of gravity rearward, providing ample tail-fan thrust for both trim and control, or a combination of these methods. In addition, increasing  $\delta_{f,S}/\delta_{f,R}$  above 50/25 should provide some relief in that, with a larger turning angle resulting, the tail would not be so close to the ground and thus would partially be out of the redirected slipstreams. This would require increased power in hovering to overcome the larger turning losses involved, however.

### Stability

The attitude stability  $\frac{\partial M_Y}{\partial \alpha}$  and speed stability parameters  $\frac{\partial M_Y}{\partial v_k}$  through the transition speed range were estimated from the data in figures 14 to 19 and are presented in figure 51. The attitude stability was computed directly from the measured slopes of the pitching-moment

coefficient with respect to angle of attack from  $\frac{\partial M_Y}{\partial \alpha} = \frac{\partial C_{m,s}}{\partial \alpha} q_s S c$ .

The attitude-stability parameter  $\frac{\partial M_Y}{\partial \alpha}$  that would be obtained if the

power-off flaps-retracted level of stability  $\left(\frac{\partial C_{m,s}}{\partial \alpha}\right)_0$  were maintained

throughout the speed range is also presented for comparison. It can be

seen that below a speed of about 35 knots the configuration exhibits attitude instability. Experience with other deflected-slipstream configurations (refs. 6 and 7) has shown that some attitude instability is to be expected and is due partly to the downward shift of the center-of-propeller thrust with increasing angle of attack as discussed in reference 1 and partly to the increased variation of downwash with angle of attack as shown in figure 48.

The speed-stability parameter  $\frac{\partial M_y}{\partial V_k}$  was estimated from the variation of  $C_{M,s}$  with thrust coefficient at a constant angle of attack (figs. 14 to 19, parts (b)). Both the propeller blade angle and rotational speed were also assumed constant. It was necessary, first of all, to determine the variation of thrust with airspeed from the propeller data of reference 5. This calculation was made by using the equilibrium speed and thrust conditions of figures 42 and 43 as basic conditions. From these data the variation of thrust coefficient and slipstream dynamic pressure with velocity was readily calculated and from these, the variation of pitching moment with velocity was calculated.

As would be expected from previous experience (refs. 6 and 7) with deflected slipstream configurations, the model exhibits positive speed stability in hovering flight and throughout the speed range.

It should also be observed that these results apply in the unstalled regime of flight. Examination of the data of figures 14 to 19 indicates that, in general, beyond the stall the configuration would exhibit more attitude stability but also would exhibit speed instability. The full significance of data such as that presented in figure 51 cannot be assessed without a complete dynamic analysis in which at least three degrees of freedom are considered.

#### Climbing and Descending Flight

The effects of angle of climb and descent on the performance and trim parameters are presented in figures 52 to 55. In general, these data might also be used to gain some insight into the effects of accelerating or decelerating flight. Climb corresponds to accelerating flight and descent corresponds to decelerating flight. A descent angle of  $10^\circ$  ( $\gamma = -10^\circ$ ) would correspond to a deceleration of  $0.17g$ . Although the specific values of power, velocity, and moment would not apply exactly, the variations would be in the same direction, thus a decrease in pitching moment with increase in climb angle would also indicate a decrease in moment with acceleration.

The wing stall shows up on the curves (figs. 52 through 55) as a break in the smooth variation of the parameters with flight-path angle. In general, out of the region of ground effect, the stall occurs at a flight-path angle of about  $-7^\circ$  or  $-8^\circ$  or more (deceleration of 0.12g). The data also indicate in general that very little additional power is required to fly above the stall; however, relatively large increases in angle of attack are involved. There is no way of determining from the data obtained whether the configuration would be controllable above the stall, but general experience would indicate that not only would more adequate power be needed to fly in this regime, but also very powerful roll and yaw controls would have to be provided.

### Effect of Thrust-Line Incidence and Direction of Inboard Propeller Rotation

The wing was set at a noseup incidence of  $5^\circ$  with respect to the propeller thrust line. In order to determine the effect that incidence might have on the stall characteristics, the model could also be fitted with alternate nacelle mounting blocks that placed the thrust line parallel to the wing chord plane. A few tests were made with this wing setting with  $\delta_{f,S}/\delta_{f,R} = 30/20.7$ . The results shown in figures 29 to 31 indicate only a very slight delay in the stall with the thrust line parallel to the wing chord plane ( $i_n = 0$ ).

The direction of propeller rotation used in most tests, shown in figure 2, resulted in a tendency for the slipstream from both propellers on each side to increase the angle of attack over that part of the wing between the nacelles. It was thought that this increase in local angle of attack might contribute to the stall, and a few tests were made to determine the effects of reversing the direction of rotation of the inboard propellers and thus of decreasing the local angle of attack. These results are also shown in figures 29 to 31 and show very small effects.

### Effect of Tail Fan

The variation of the pressure required to drive the tail-fan motor and of the increment in pitching-moment coefficient due to the tail fan (based on the propeller slipstream dynamic pressure of 5.0 lb/sq ft) with tail-fan rotational speed under static conditions is shown in figure 8. The moment coefficient of 0.06 at the maximum for rotational speed investigated would correspond to a downward tail-fan thrust of about 80 pounds on the airplane.

The results at forward speed (figs. 32 to 34) indicate that the tail fan provides an increment of pitching moment but does not change the basic stability of the configuration. Also the tail normal-force and pitching-moment data indicate that the slipstream from the tail fan alters the flow field in the region of the horizontal tail but produces only an incremental change in the normal force and moment which does not change with angle of attack.

#### Effect of Slat

As pointed out previously, wing stall occurs at moderate angles of descent in the intermediate range of transition speeds. Previous experience (ref. 8) indicated that the stall could be delayed to much steeper descent conditions with deflected-slipstream configurations by adding a leading-edge slat. Another means whereby it was thought that similar results might be obtained was by increasing the flap chord to increase the wing area. The results of tests of such devices are presented in figures 36 to 38 and in figure 55. Increasing the flap chord is shown in figure 37 to be much less effective than adding the slat. The slat extended the unstalled region of flight to flight-path angles of about  $-20^\circ$  (fig. 55). This delay in the stall would increase the permissible rate of descent to 850 feet per minute (as compared with 300 ft/min for the slat-off condition) for the 25-knot speed (fig. 55) corresponding to the 30/20.7 flap-deflection configuration with which the slat was investigated.

#### CONCLUSIONS

The wind-tunnel investigation of the longitudinal stability, control, and performance characteristics of a 1/5-scale model of a deflected slipstream VTOL airplane indicate the following conclusions:

1. Steady level flight out of the region of ground effect can be accomplished without wing stall being encountered; however, decelerating or descending flight will have to be limited to decelerations of 0.12g or less or descent angles of  $7^\circ$  to  $8^\circ$  or less if stall is to be avoided.
2. The addition of a leading-edge slat increased the limiting descent angle to about  $20^\circ$  (deceleration of about 0.34g).

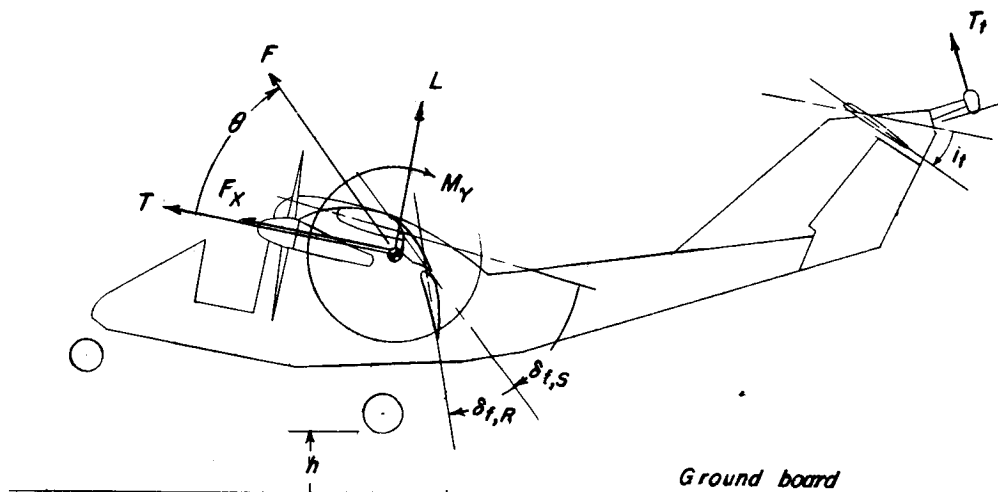
3. A relatively large diving moment is present in the hovering condition out of the ground-effect region. To alleviate this diving moment may require that the center of gravity be moved rearward from the point used in this analysis, that the propeller thrust axis be lowered, that the tail-fan thrust be increased, or that a combination of these changes be provided.

4. In hovering, the presence of the ground deflected the slipstream on to the horizontal tail, so that a large increase in the diving moment occurred, unless the tail was set at an incidence (nosedown) of about  $-37^\circ$ .

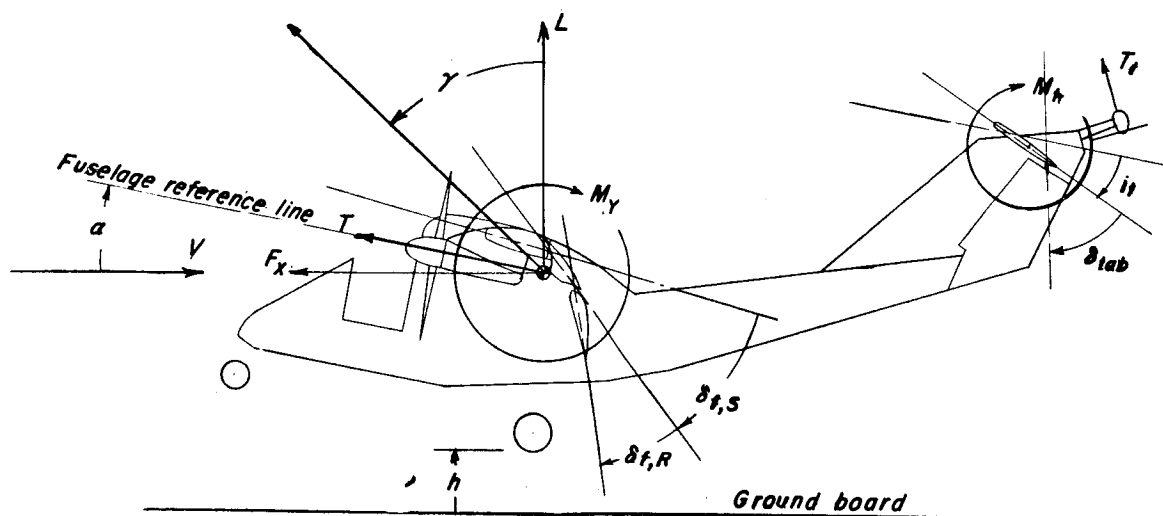
Langley Research Center,  
National Aeronautics and Space Administration,  
Langley Field, Va., January 6, 1960.

## REFERENCES

1. Kuhn, Richard E., and Draper, John W.: Investigation of the Aerodynamic Characteristics of a Model Wing-Propeller Combination and of the Wing and Propeller Separately at Angles of Attack up to  $90^{\circ}$ . NACA Rep. 1263, 1956. (Supersedes NACA TN 3304 by Draper and Kuhn.)
2. Kuhn, Richard E., and Hayes, William C., Jr.: Wind-Tunnel Investigation of Longitudinal Aerodynamic Characteristics of Three Propeller-Driven VTOL Configurations in the Transition Speed Range, Including Effects of Ground Proximity. NASA TN D-55, 1960.
3. Gillis, Clarence L., Polhamus, Edward C., and Gray, Joseph L., Jr.: Charts for Determining Jet-Boundary Corrections for Complete Models in 7- by 10-Foot Closed Rectangular Wind Tunnels. NACA WR L-123, 1945. (Formerly NACA ARR L5G31.)
4. Kuhn, Richard E.: Semiempirical Procedure for Estimating Lift and Drag Characteristics of Propeller-Wing-Flap Configurations for Vertical- and Short-Take-Off-and-Landing Airplanes. NASA MEMO 1-16-59L, 1959.
5. Shenkman, Albert M.: Generalized Performance of Conventional Propellers for VTOL-STOL Aircraft. Rep. No. HS-1829, Hamilton Standard, Div. United Aircraft Corp., Mar. 31, 1958.
6. Kirby, Robert H.: Stability and Control of Propeller-Driven Transport VTOL Airplanes. Proc. Thirteenth Annual National Forum, Am. Helicopter Soc., Inc., May 8-11, 1957, pp. 43-50.
7. Tosti, Louis P.: Transition-Flight Investigation of a Four-Engine-Transport Vertical-Take-Off Airplane Model Utilizing a Large Flap and Extensible Vanes for Redirecting the Propeller Slipstream. NACA TN 4131, 1957.
8. Kuhn, Richard E., and Hayes, William C., Jr.: Wind-Tunnel Investigation of Effect of Propeller Slipstreams on Aerodynamic Characteristics of a Wing Equipped with a 50-Percent-Chord Sliding Flap and a 30-Percent-Chord Slotted Flap. NACA TN 3918, 1957.



(a) Static tests.



(b) Forward-speed tests.

Figure 1.- Conventions used to define positive sense of forces, moments, and angles.

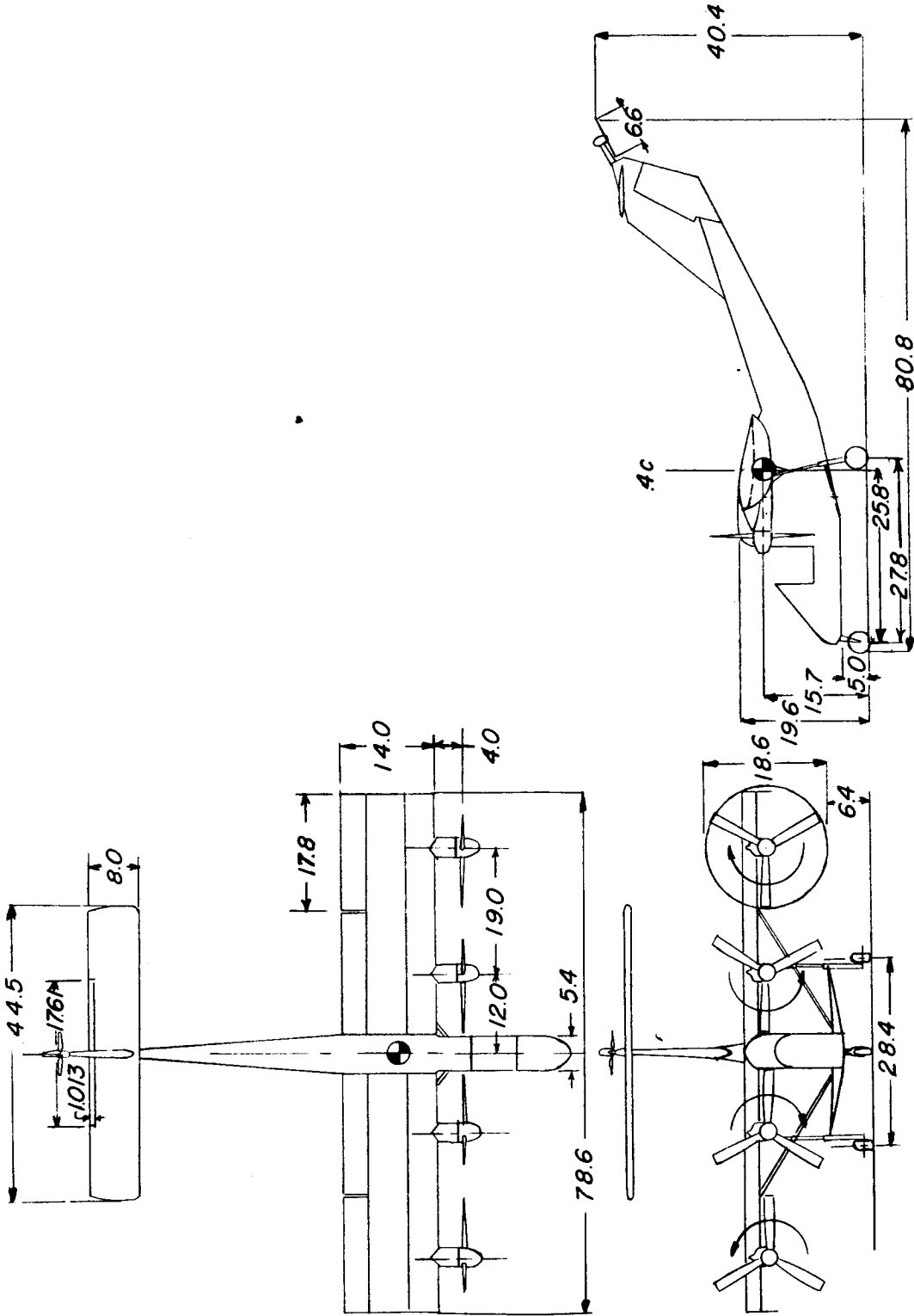
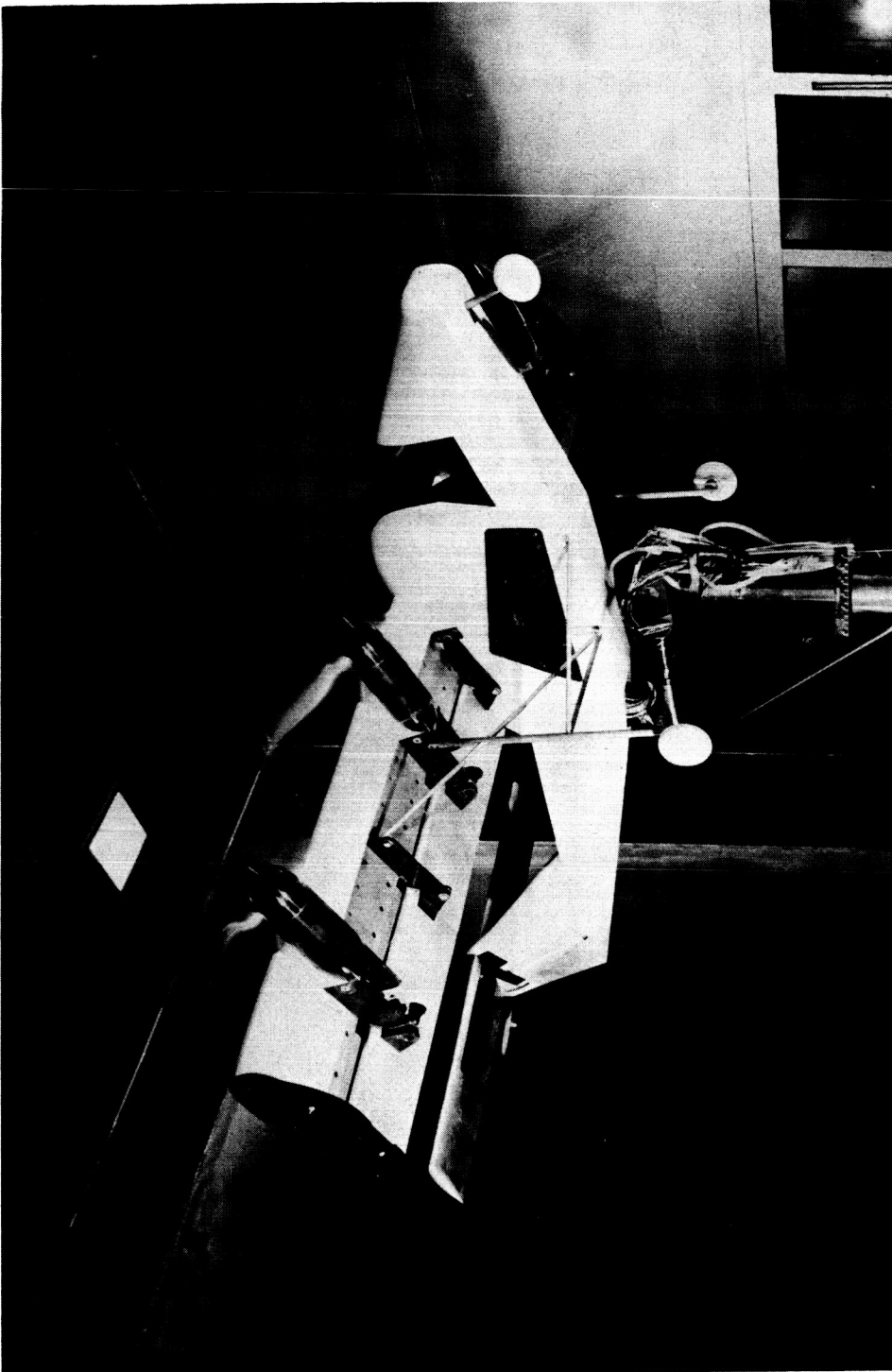


Figure 2.- Three-view drawing of 1/5-scale model. Dimensions are in inches.



(a) Three-quarter front view of model (flaps retracted). L-58-2886

Figure 3.- Photographs of the model installed in the 17-foot test section of the Langley 300-MPH  
7- by 10-foot tunnel.

L-735



L-58-3277

(b) Model in low position with ground board.

Figure 3.- Concluded.

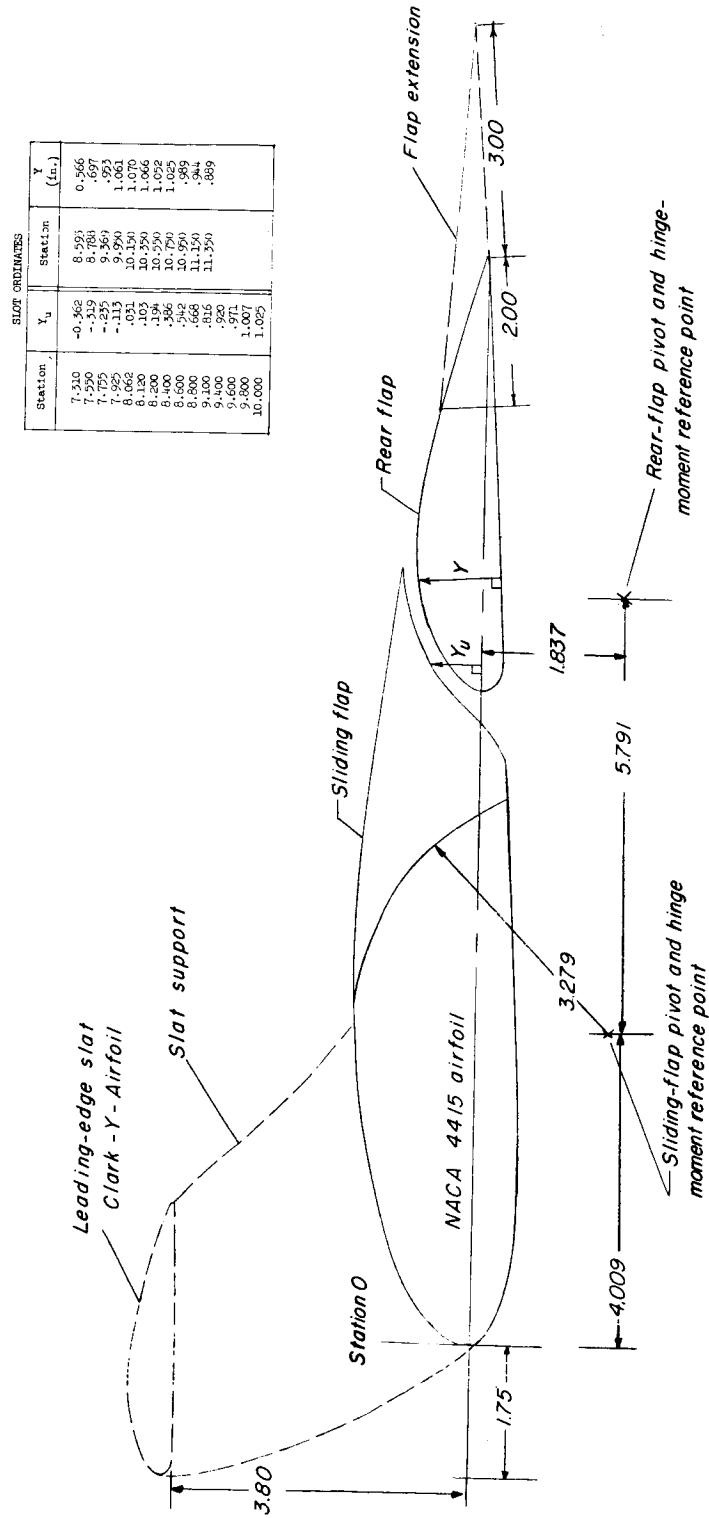
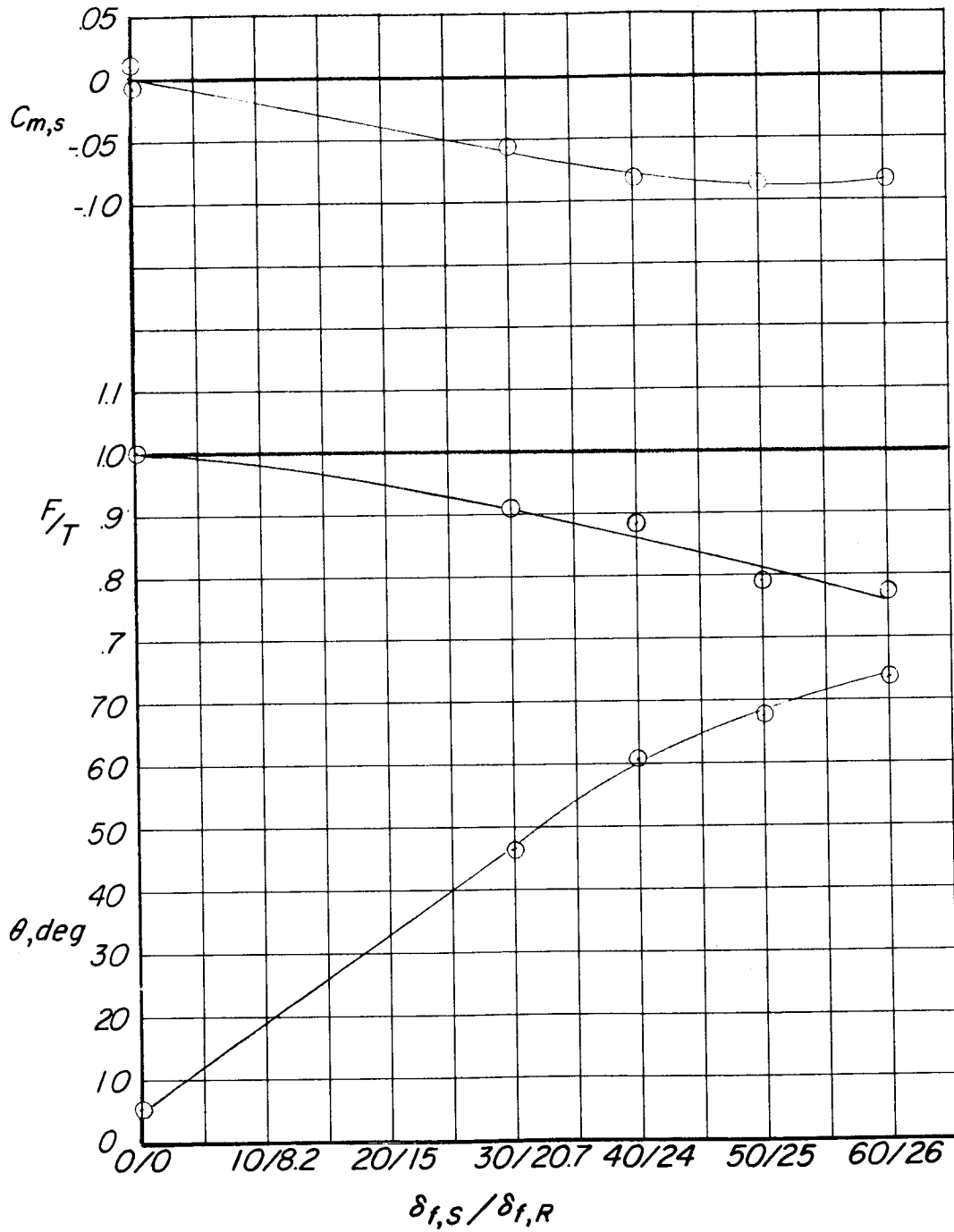


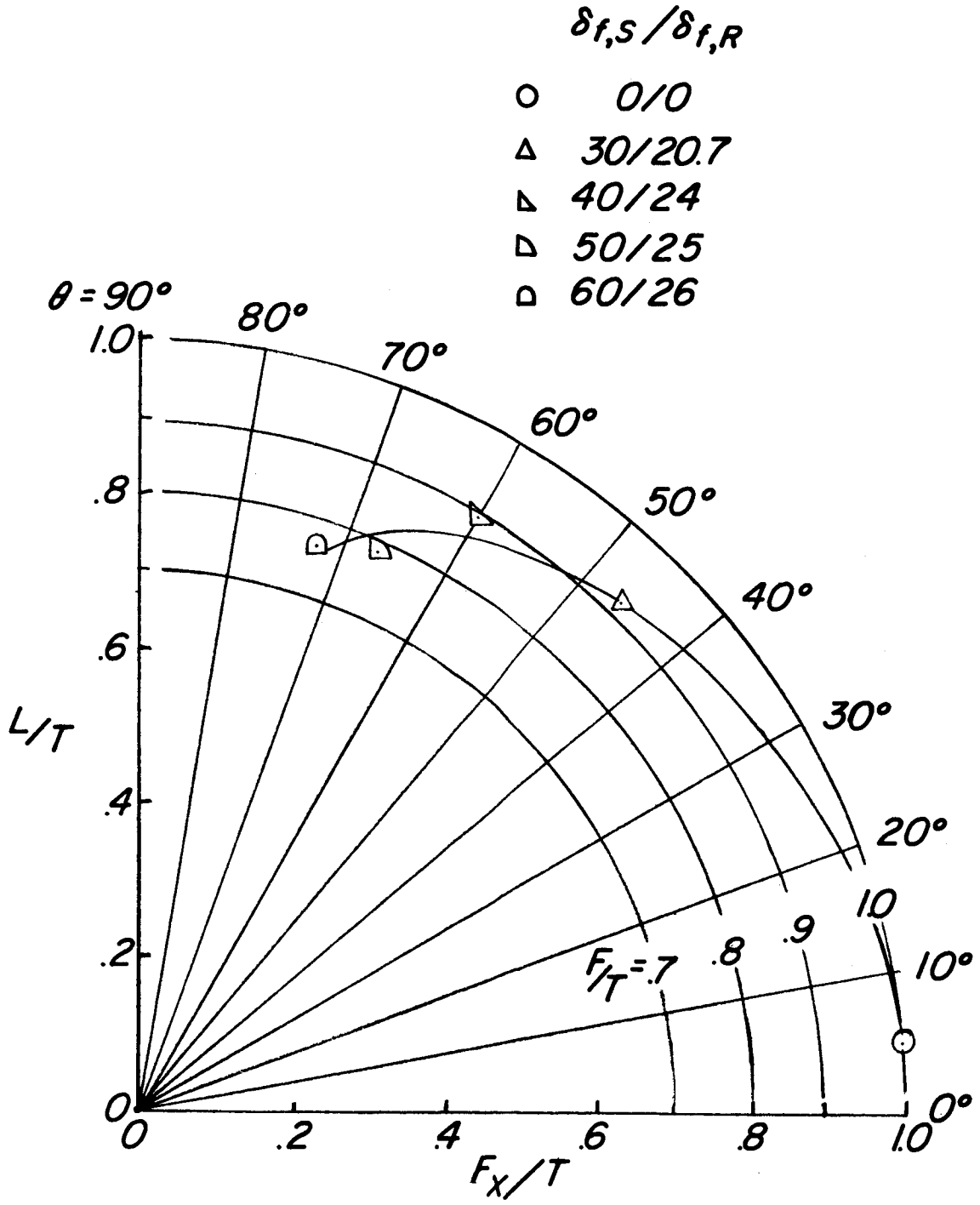
Figure 4.- Drawing of wing profile, leading-edge slat, and flap-chord extension. All dimensions are in inches.



(a) Pitching moment, thrust-recovery factor, and turning angle.

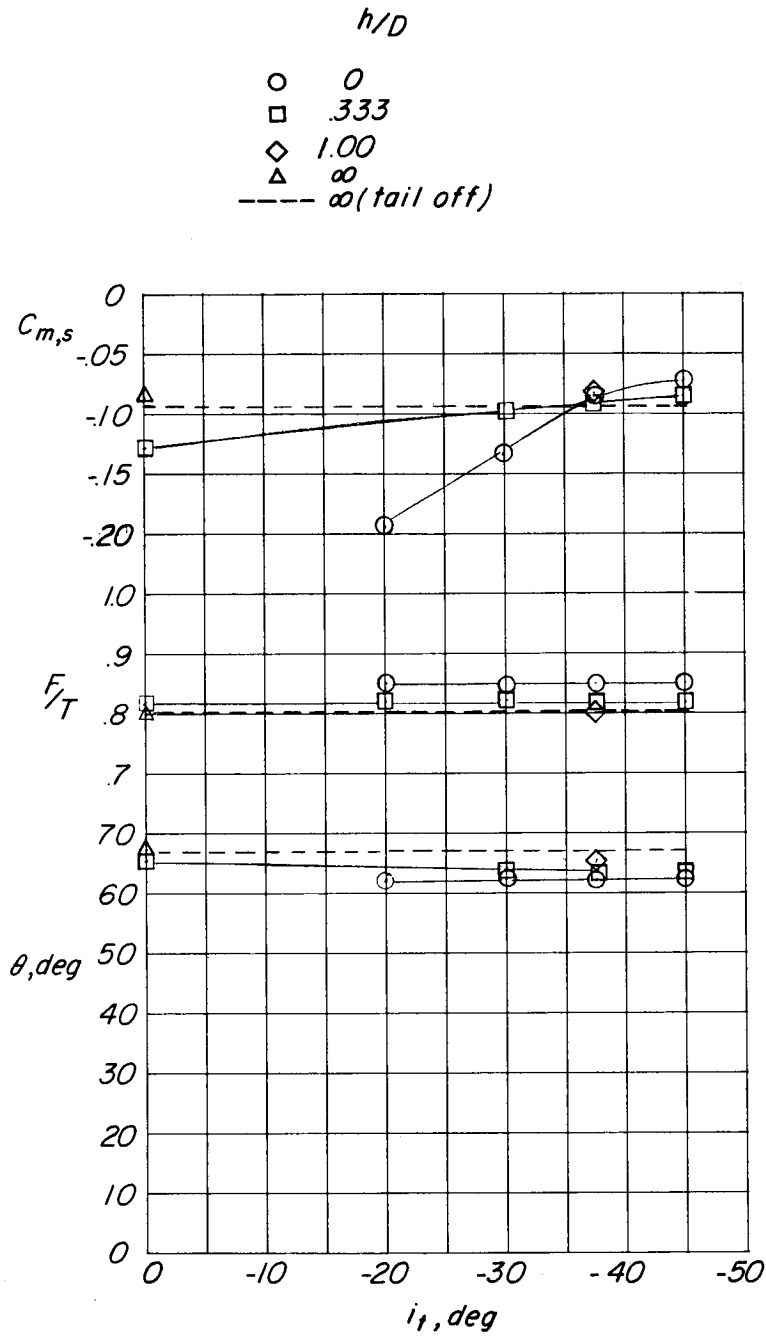
Figure 5.- Static slipstream deflection characteristics.

L-735



(b) Turning-effectiveness summary.

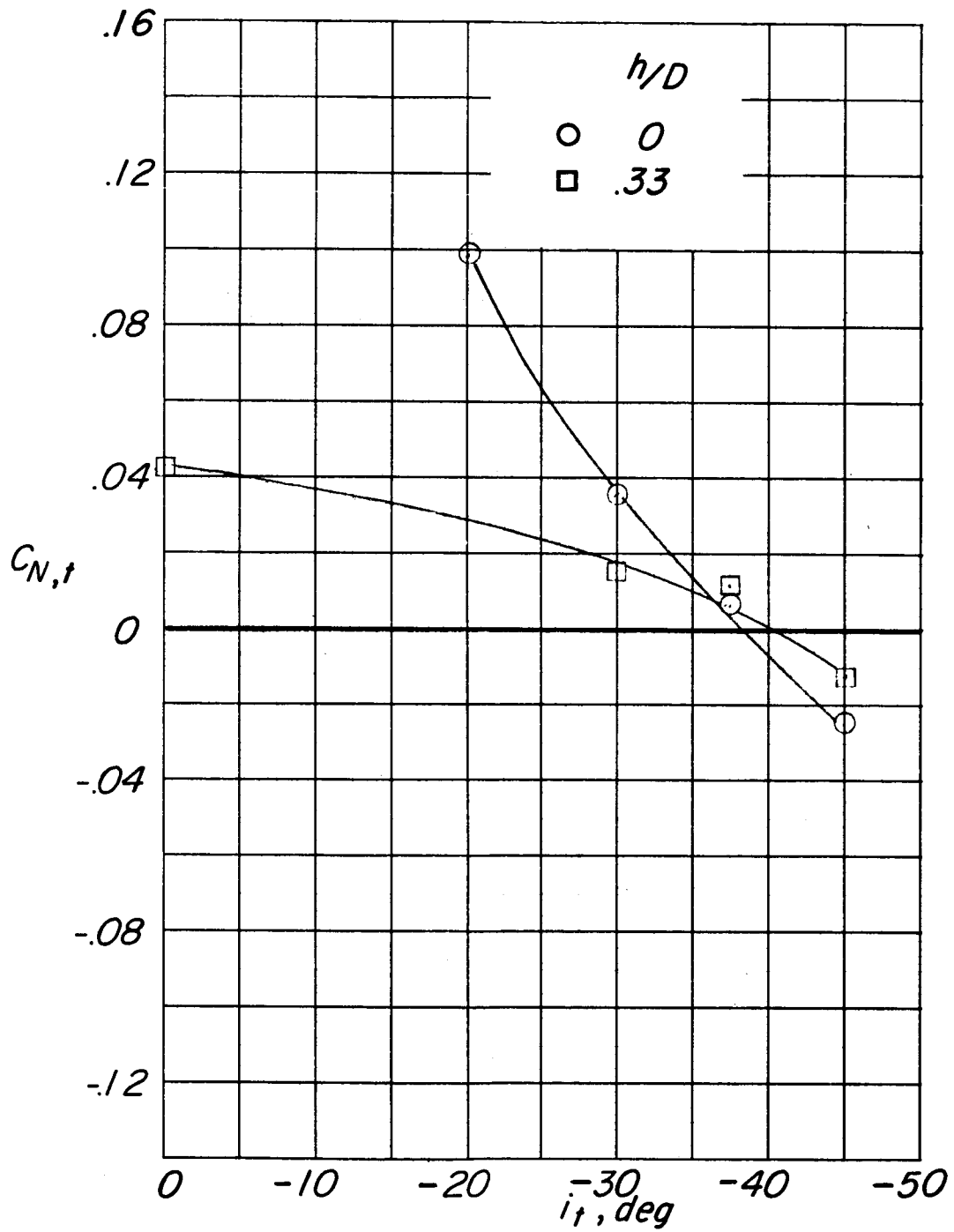
Figure 5.- Concluded.



L-735

(a) Pitching-moment coefficient, thrust-recovery factor, and turning angle.

Figure 6.- Effect of ground proximity on horizontal-tail effectiveness with model at  $25^\circ$  noseup attitude and  $\delta_{f,S}/\delta_{f,R} = 50/25$ .



(b) Tail normal-force coefficient.

Figure 6.- Concluded.

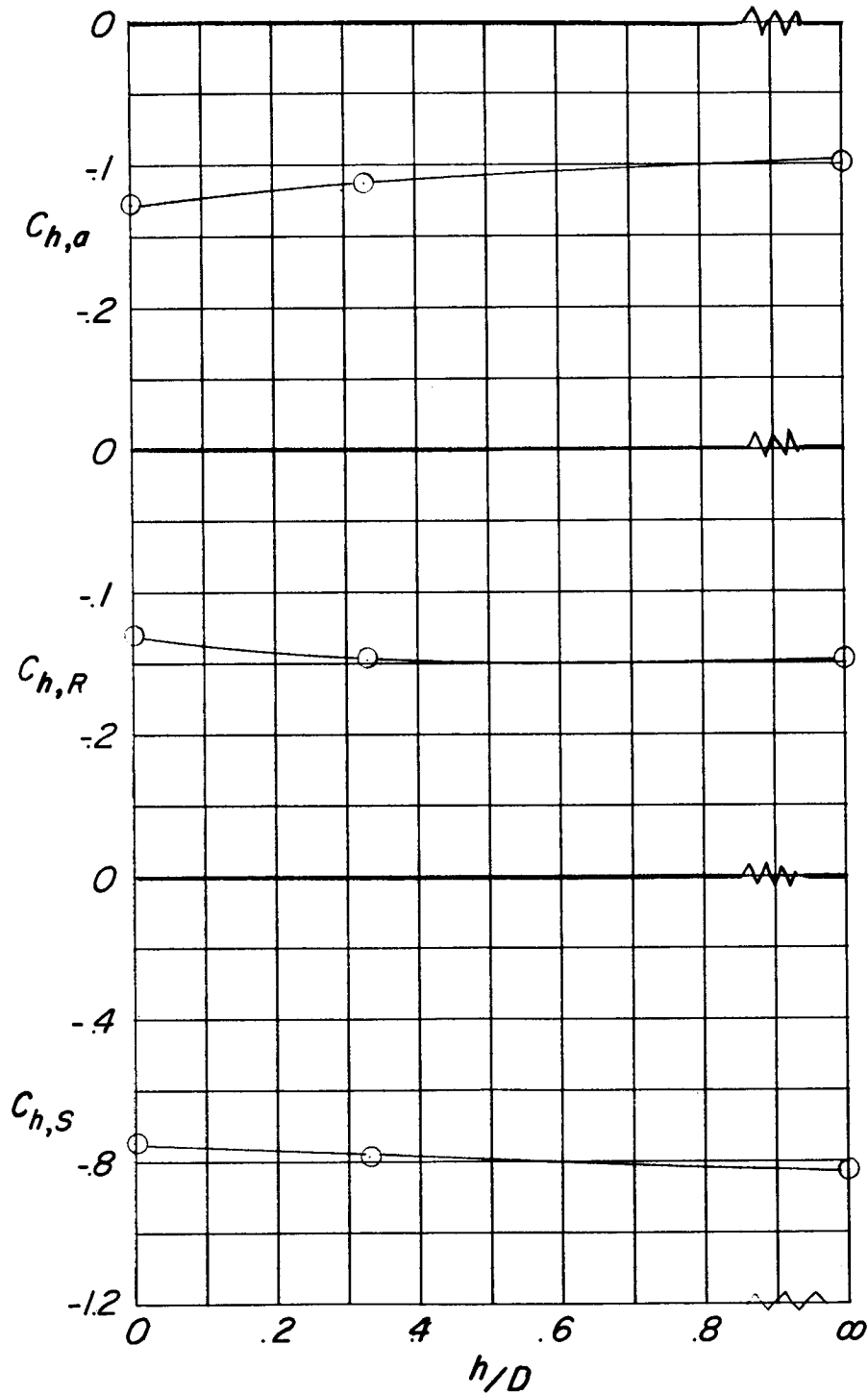


Figure 7.- Effect of ground proximity on flap hinge moment in hovering with model at  $25^\circ$  noseup attitude and  $\delta_{f,S}/\delta_{f,R} = 50/25$ .

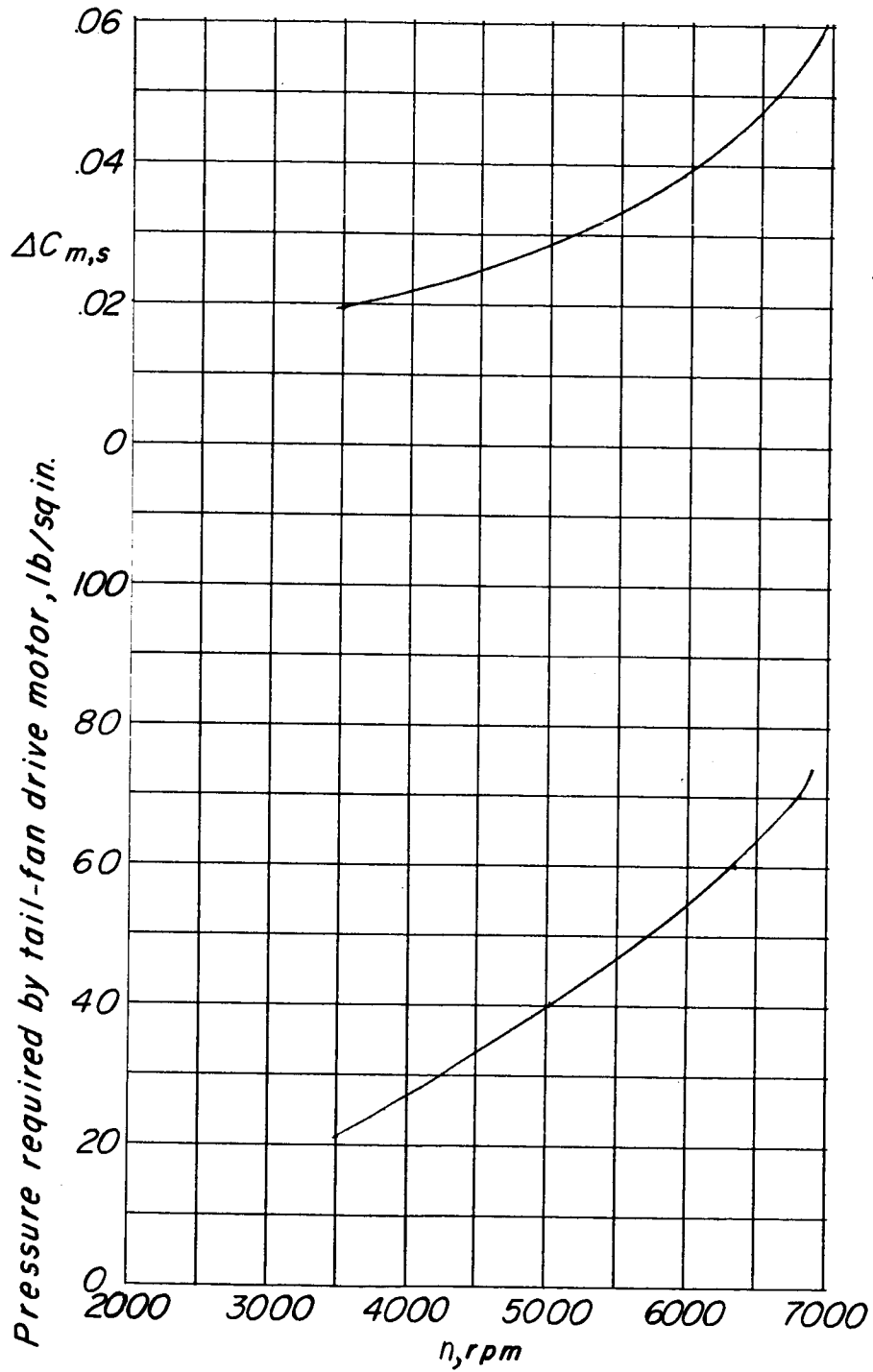
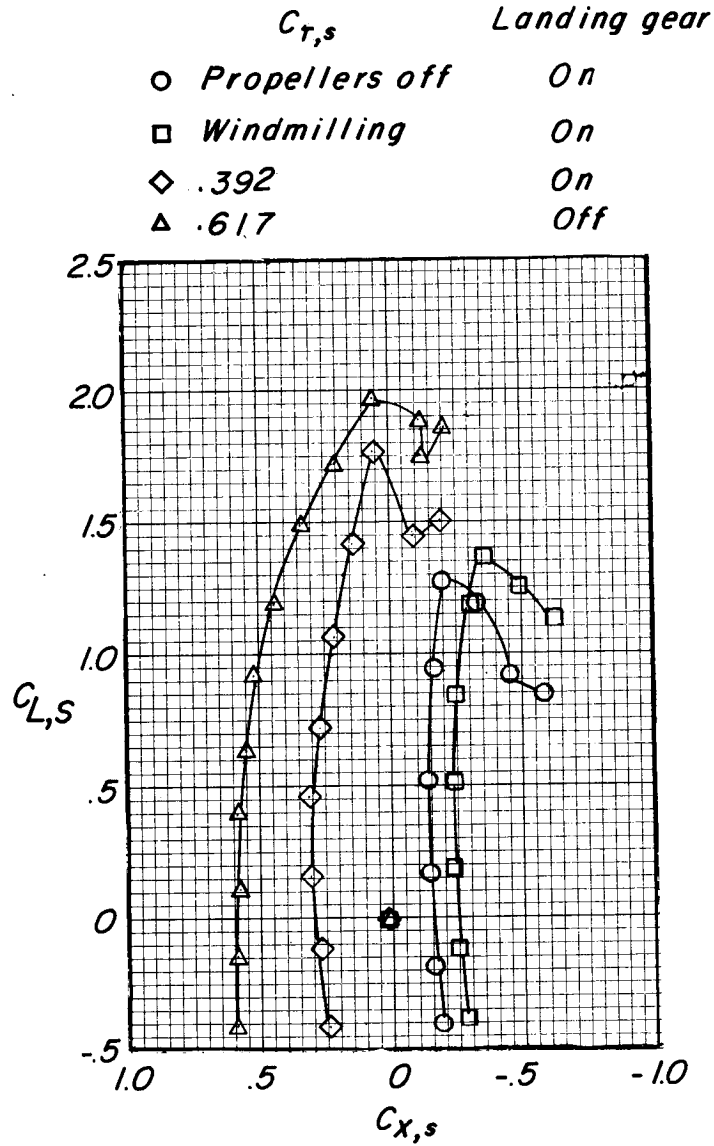
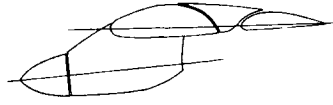


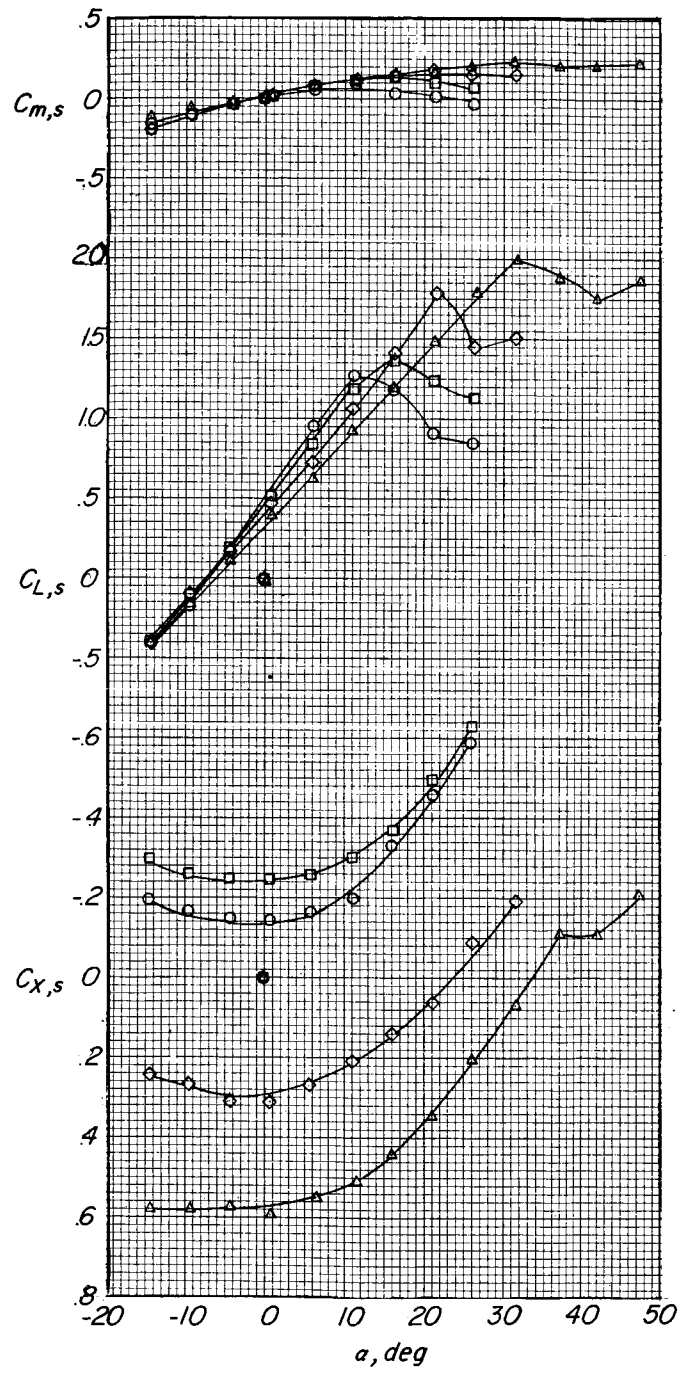
Figure 8.- Model tail-fan effectiveness and pressure required out of ground-effect region. Propellers not running;  $i_t = 0^\circ$ .



(a) Lift coefficient as function of longitudinal-force coefficient.

Figure 9.- Effect of thrust coefficient. Tail off;  $\delta_{f,S}/\delta_{f,R} = 0/0$ .

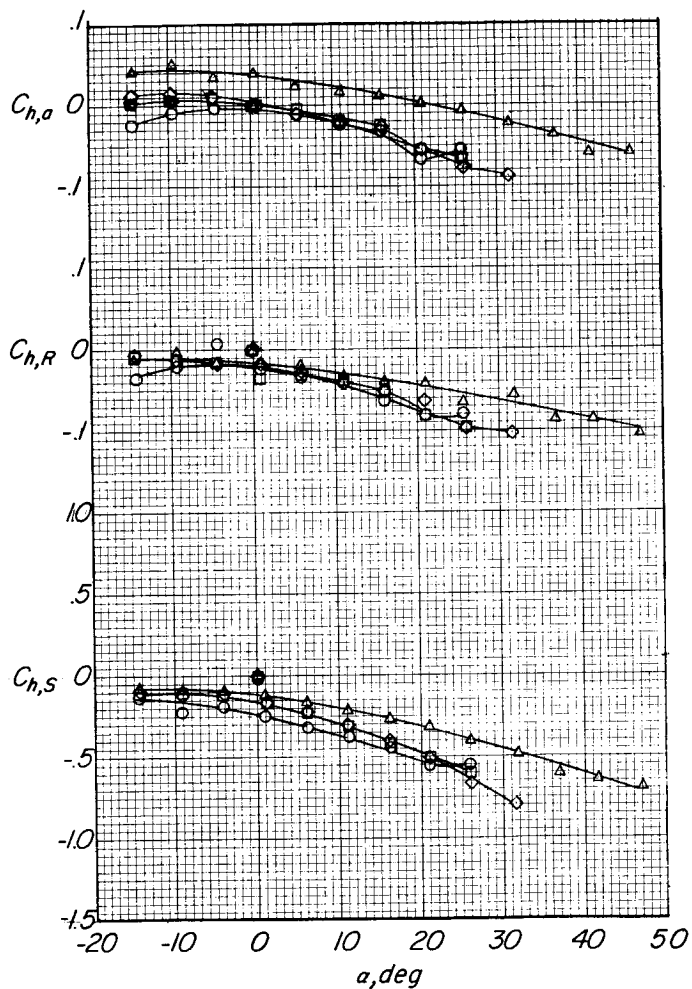
L-735



$C_{T,s}$	Landing gear
○ Propellers off	On
□ Windmilling	On
◇ .392	On
△ .617	Off

(b) Pitching-moment, lift, and longitudinal-force coefficients.

Figure 9.- Continued.



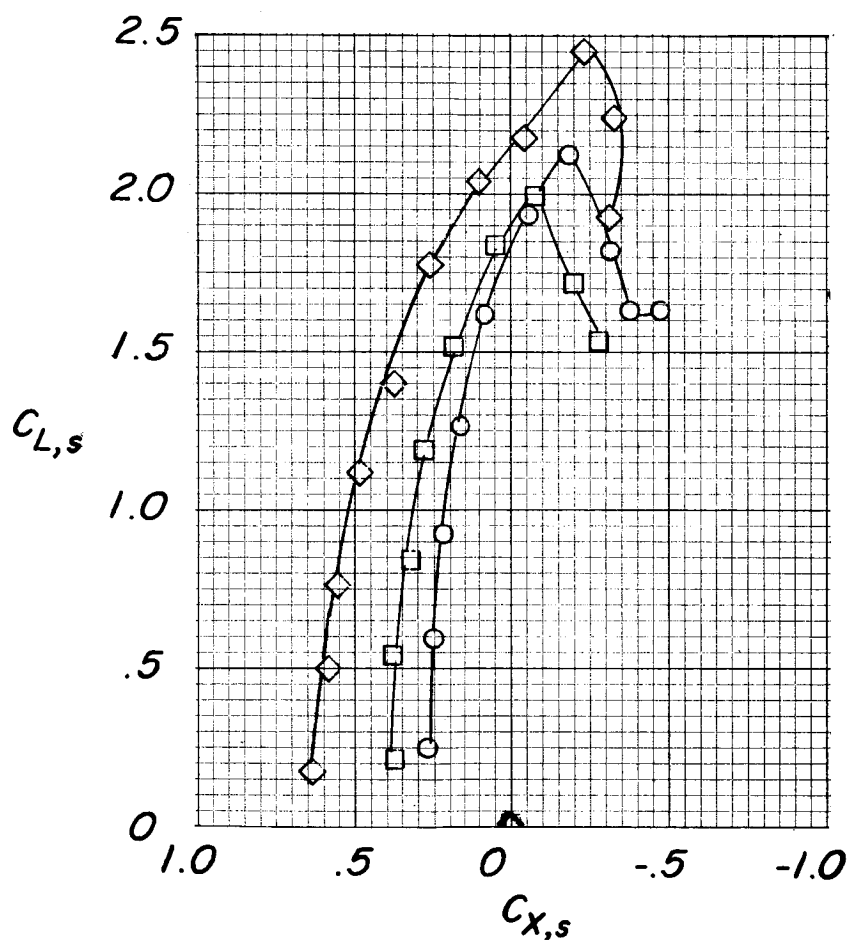
$C_{T,s}$	Landing gear
○ Propellers off	On
□ Windmilling	On
◇ .392	On
△ .617	Off

(c) Flap and aileron hinge-moment coefficients.

Figure 9.- Concluded.

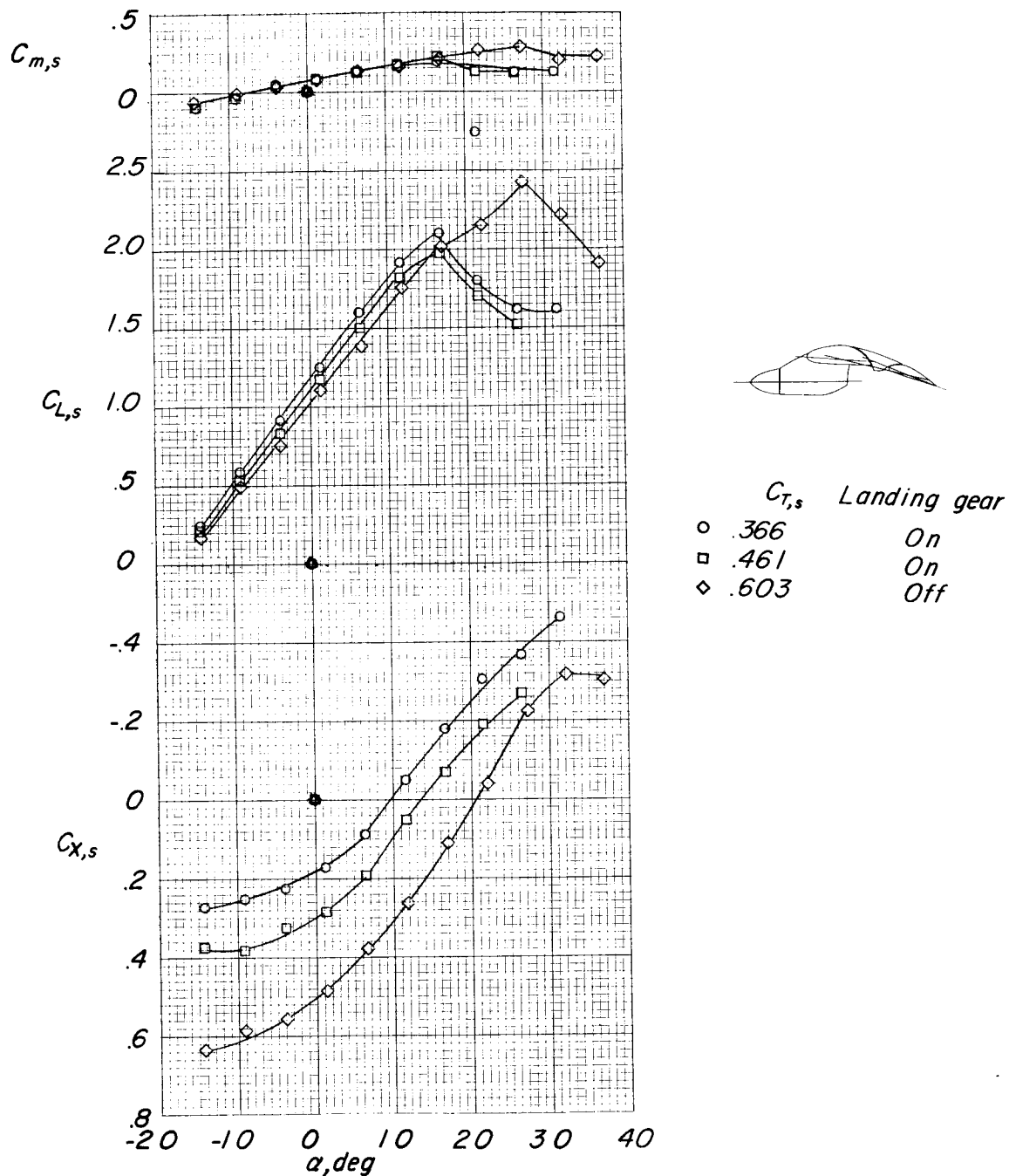


$C_{T,s}$	Landing gear
○ .366	On
□ .461	On
◇ .603	Off



(a) Lift coefficient as function of longitudinal-force coefficient.

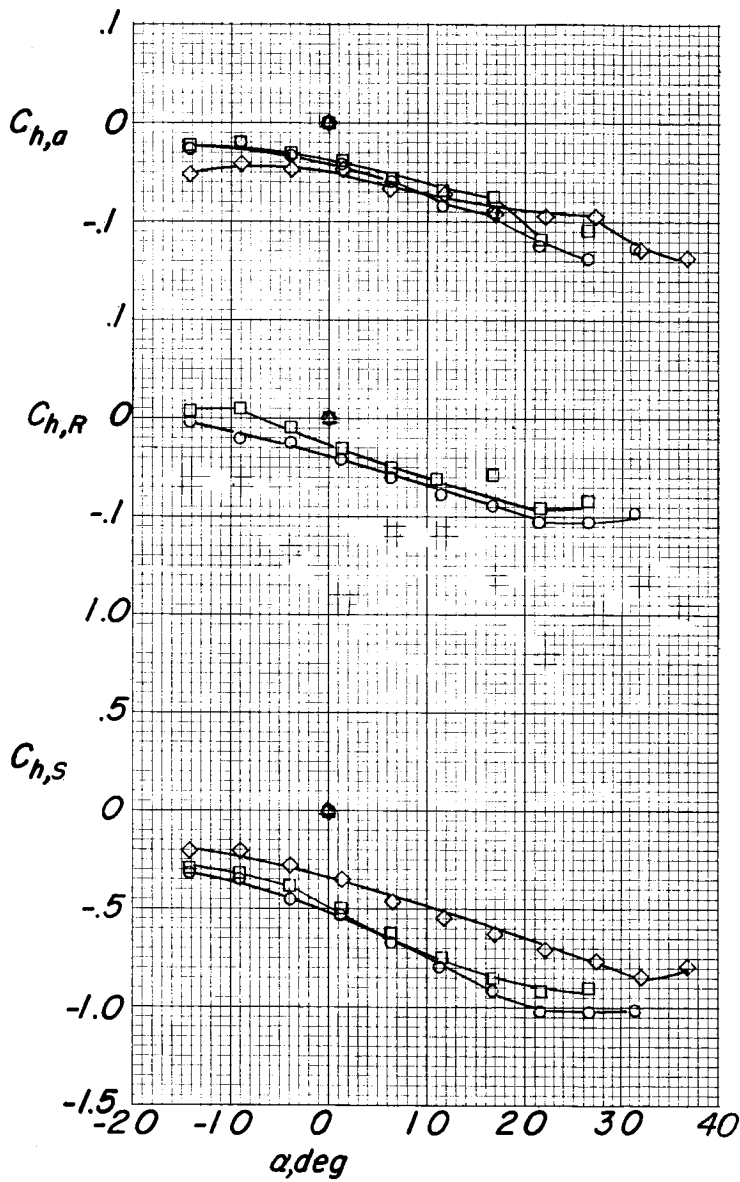
Figure 10.- Effect of thrust coefficient. Tail off;  $\delta_{f,S}/\delta_{f,R} = 10/8.2$ .



(b) Pitching-moment, lift, and longitudinal-force coefficients.

Figure 10.- Continued.

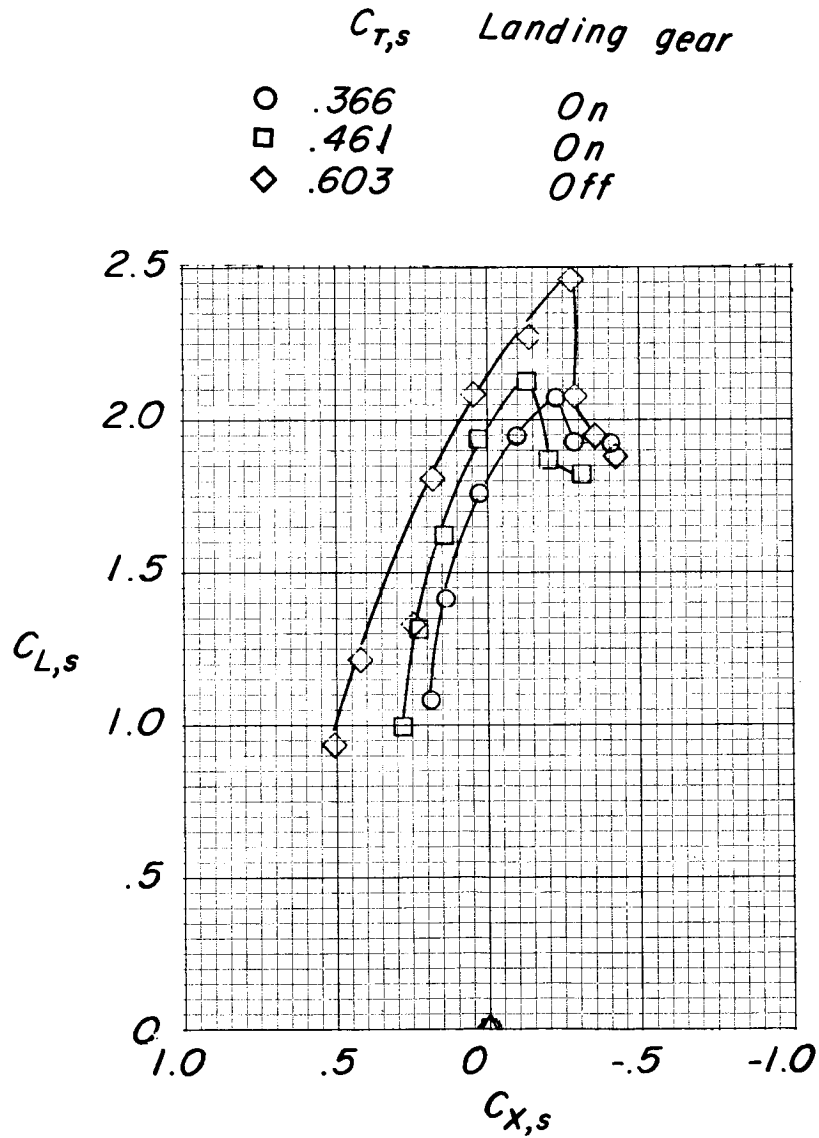
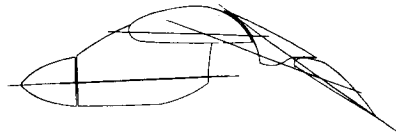
I-735



$C_{T,s}$	Landing gear
○ .366	On
□ .461	On
◇ .603	Off

(c) Flap and aileron hinge-moment coefficients.

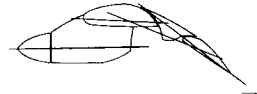
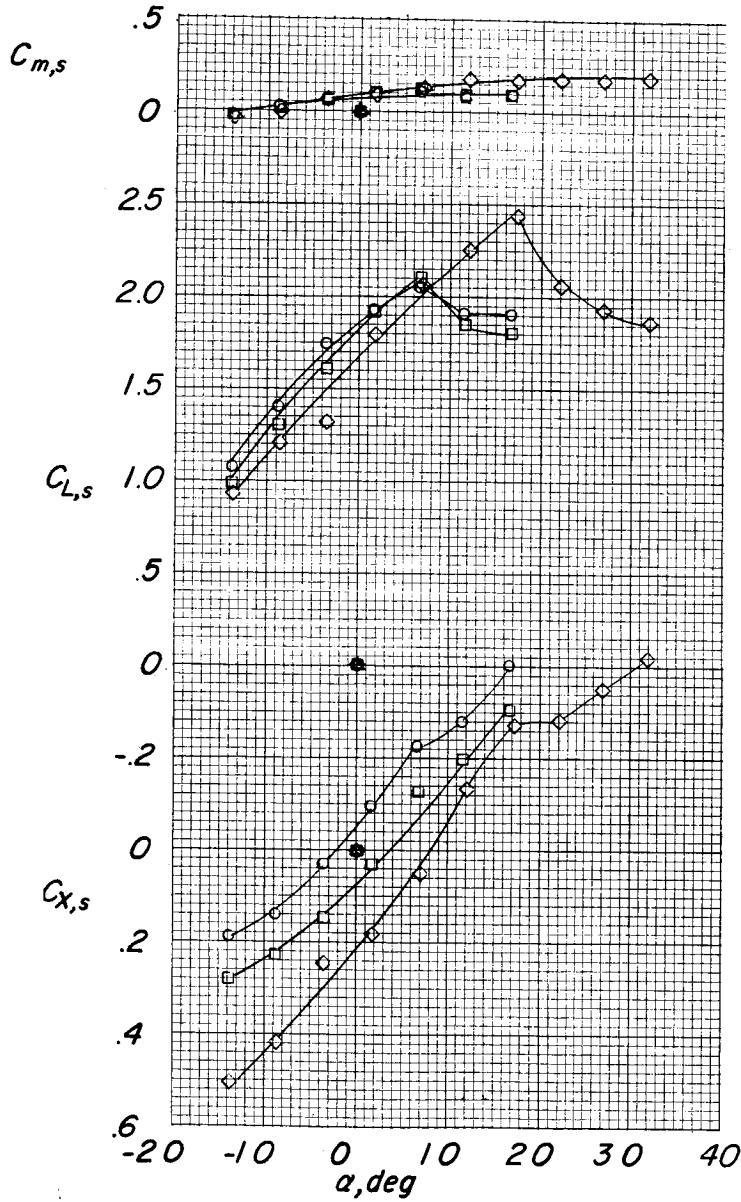
Figure 10.- Concluded.



(a) Lift coefficient as function of longitudinal-force coefficient.

Figure 11.- Effect of thrust coefficient. Tail off;  $\delta_{f,S}/\delta_{f,R} = 20/15$ .

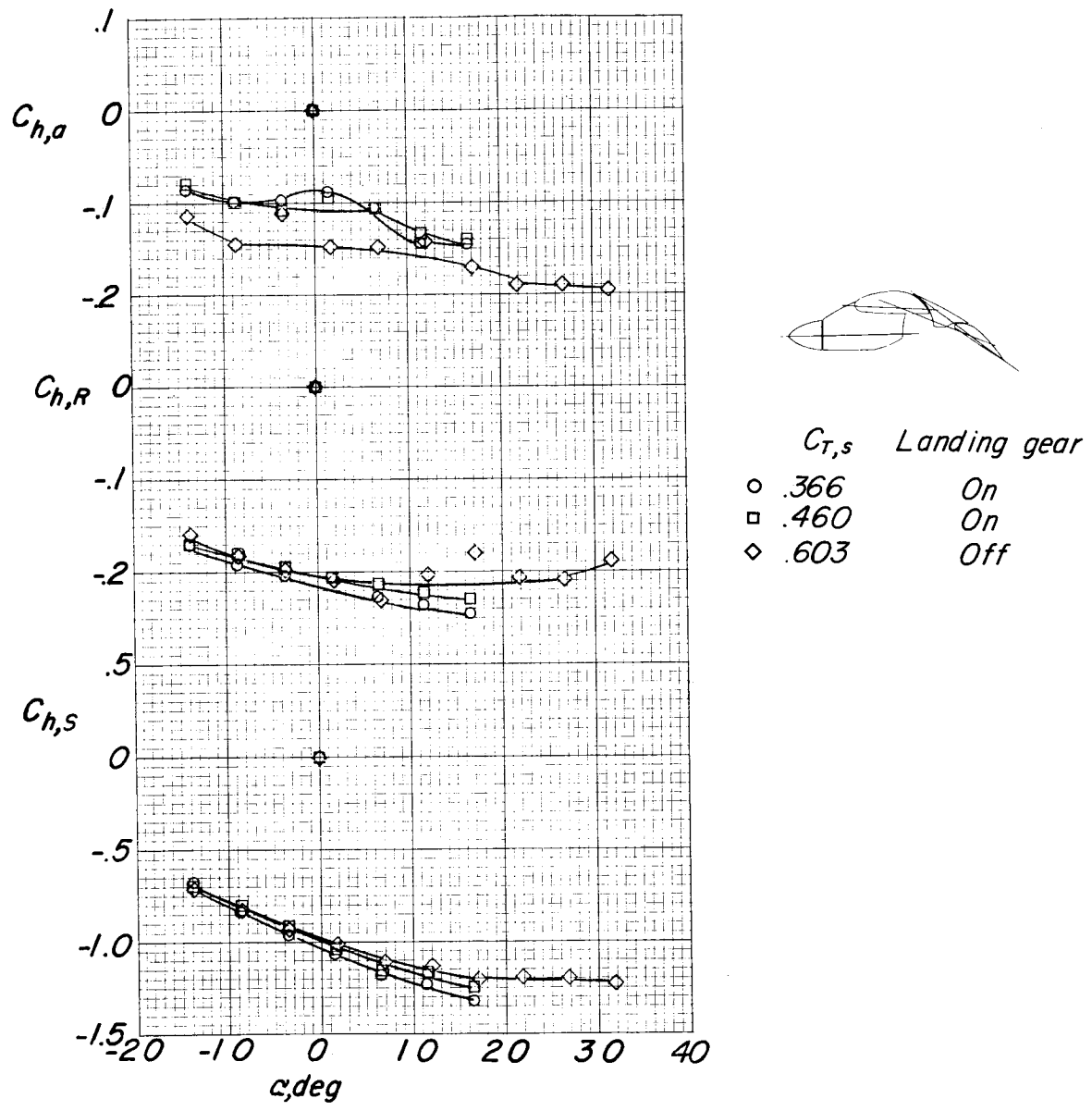
I-735



$C_{T,s}$	Landing gear
○ .366	On
□ .460	On
◇ .603	Off

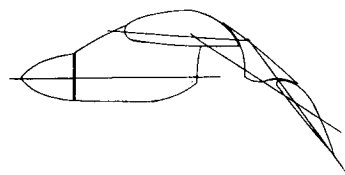
(b) Pitching-moment, lift, and longitudinal-force coefficients.

Figure 11.- Continued.



(c) Flap and aileron hinge-moment coefficients.

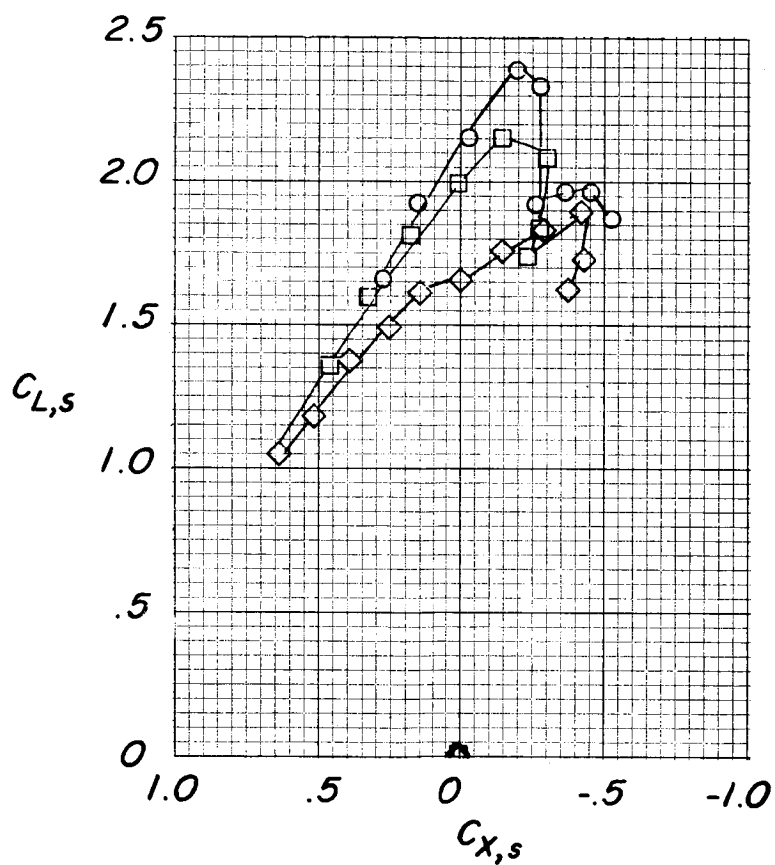
Figure 11.- Concluded.


 $C_{T,s}$ 

○ .603

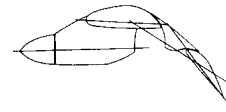
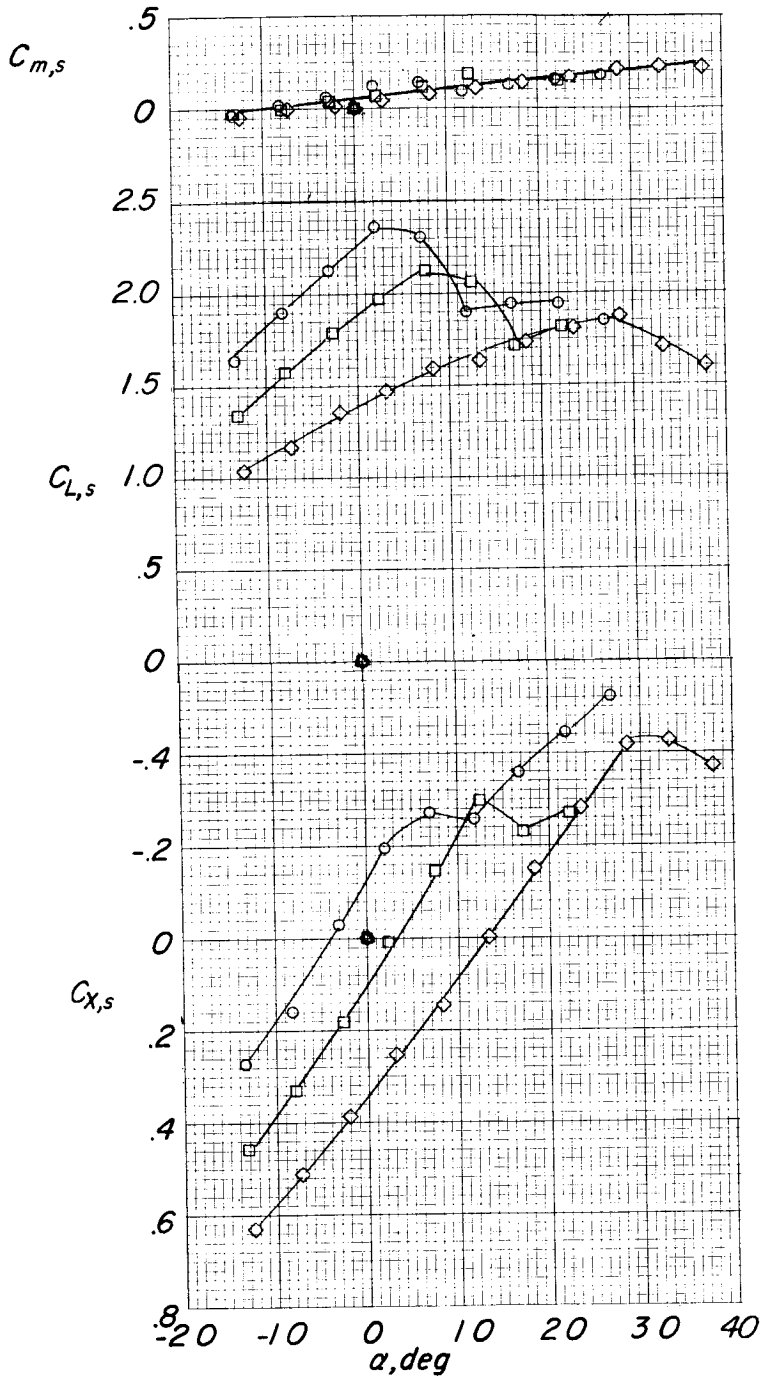
□ .744

◇ .882



(a) Lift coefficient as function of longitudinal-force coefficient.

Figure 12.- Effect of thrust coefficient. Landing gear off; tail off;  
 $\delta_{f,S}/\delta_{f,R} = 30/20.7$ .



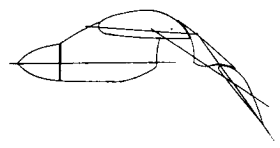
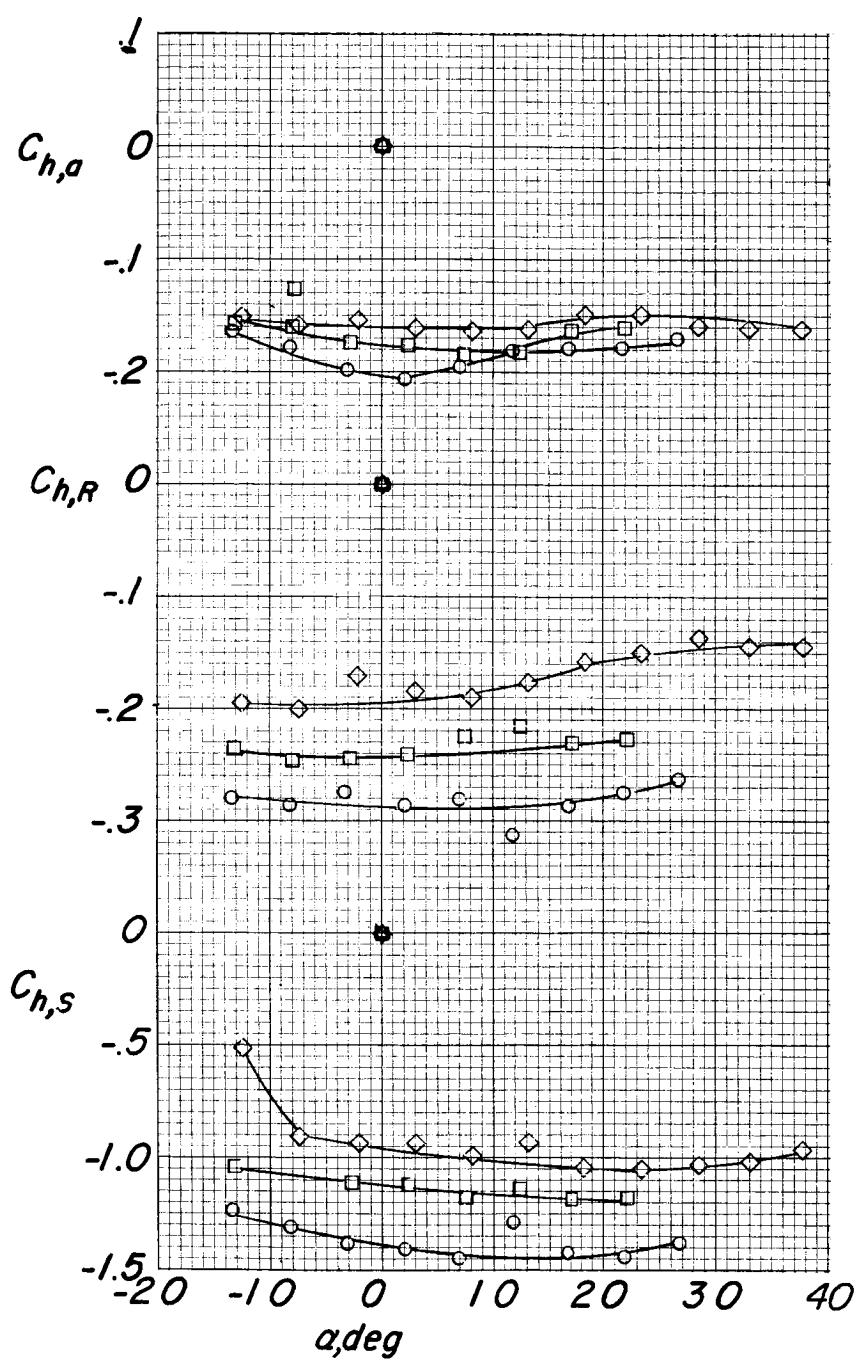
- $C_{T,s}$
- .603
  - .744
  - ◇ .882

(b) Pitching-moment, lift, and longitudinal-force coefficients.

Figure 12.- Continued.

L-735

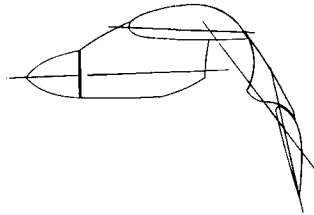
L-735



- $C_{T,s}$
- .603
  - .744
  - ◇ .882

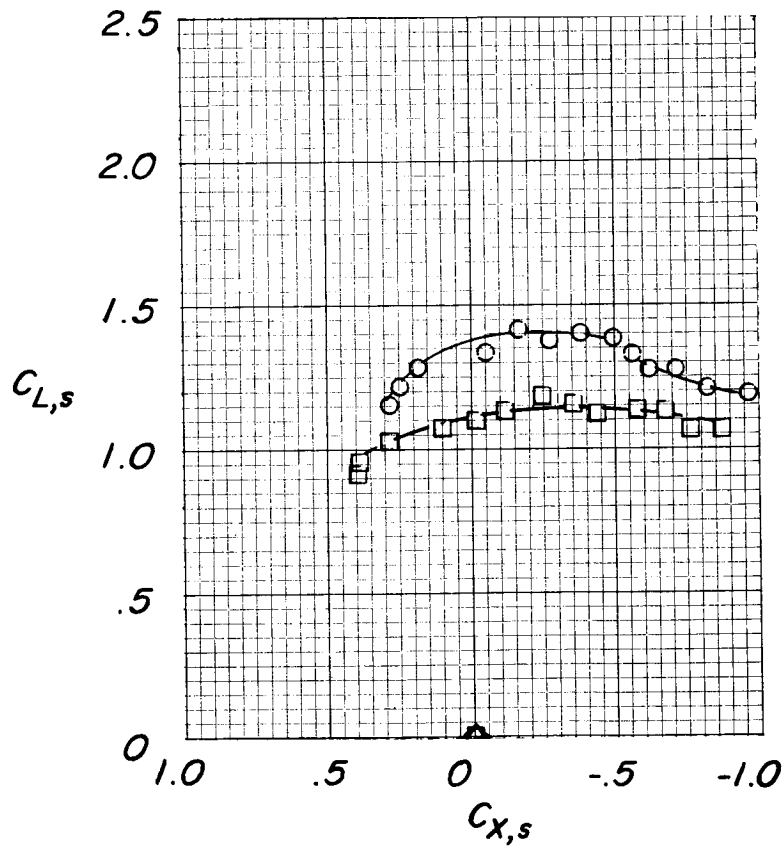
(c) Flap and aileron hinge-moment coefficients.

Figure 12.- Concluded.


 $C_{T,s}$ 

○ .944

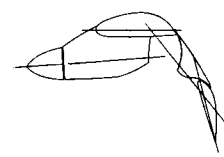
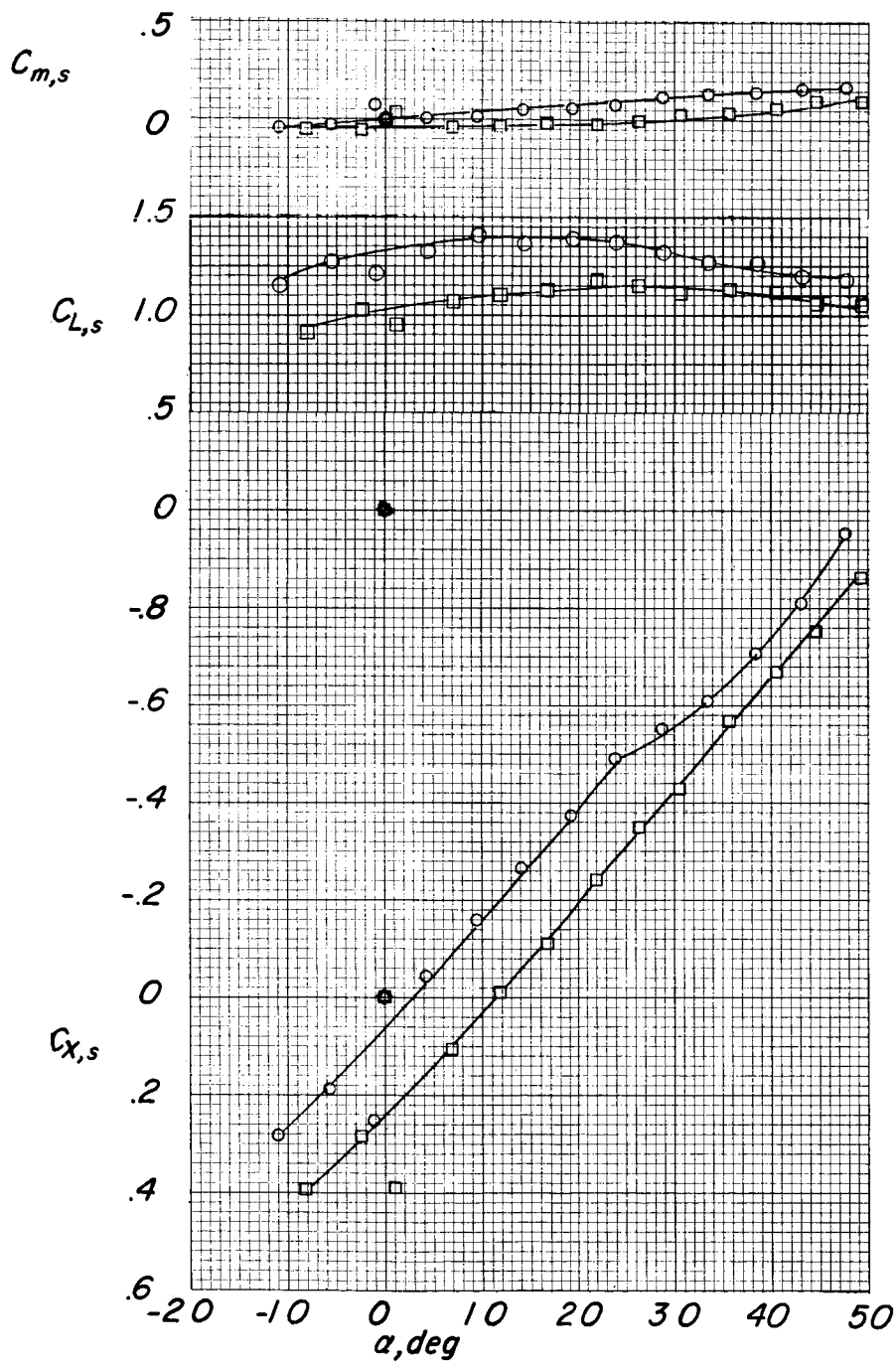
□ .980



(a) Lift coefficient as function of longitudinal-force coefficient.

Figure 13.- Effect of thrust coefficient. Landing gear off; tail off;  
 $\delta_{f,s}/\delta_{f,R} = 50/25$ .

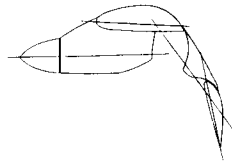
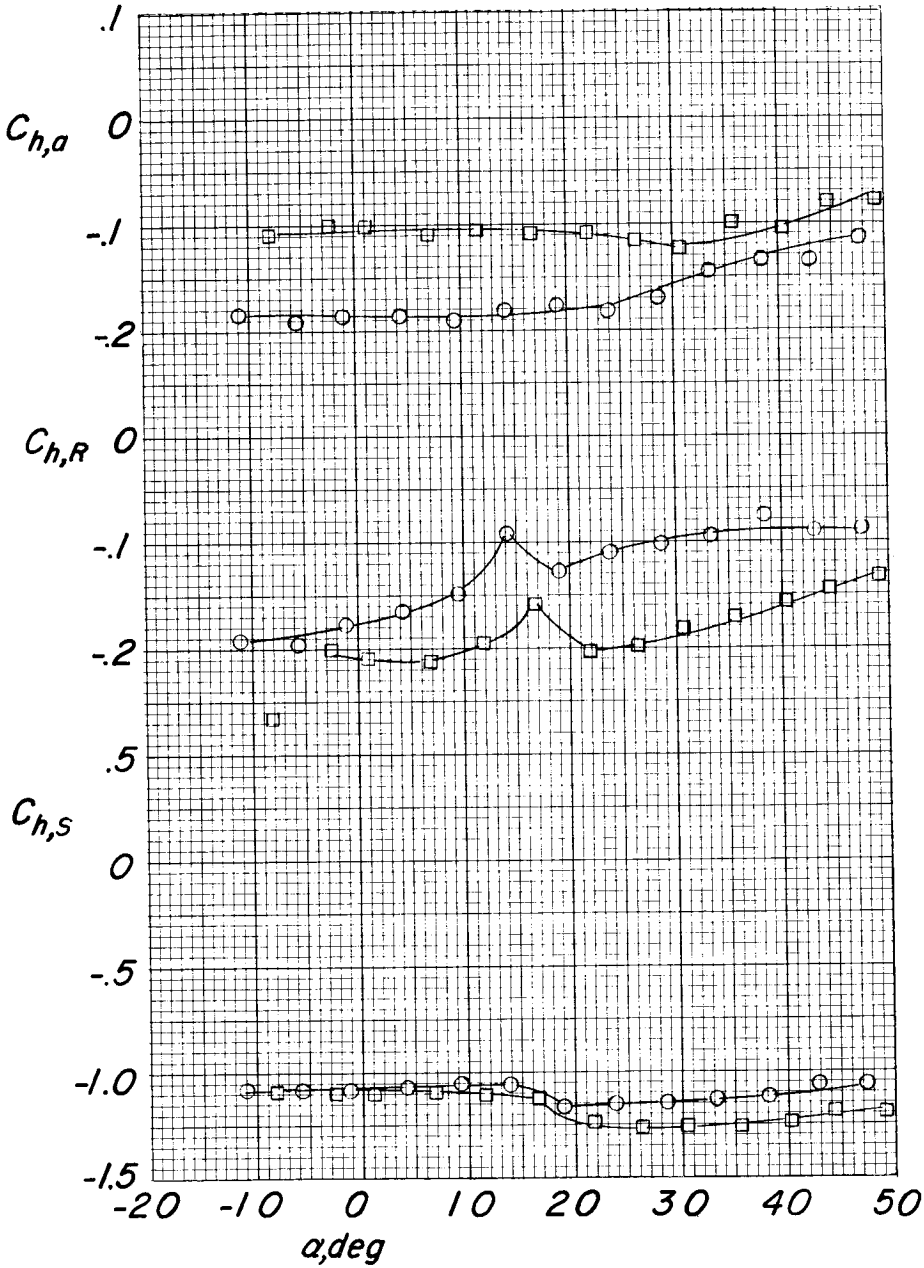
I-735



$C_{T,s}$   
 ○ .944  
 □ .980

(b) Pitching-moment, lift, and longitudinal-force coefficients.

Figure 13.- Continued.



$C_{T,s}$   
 ○ .944  
 □ .980

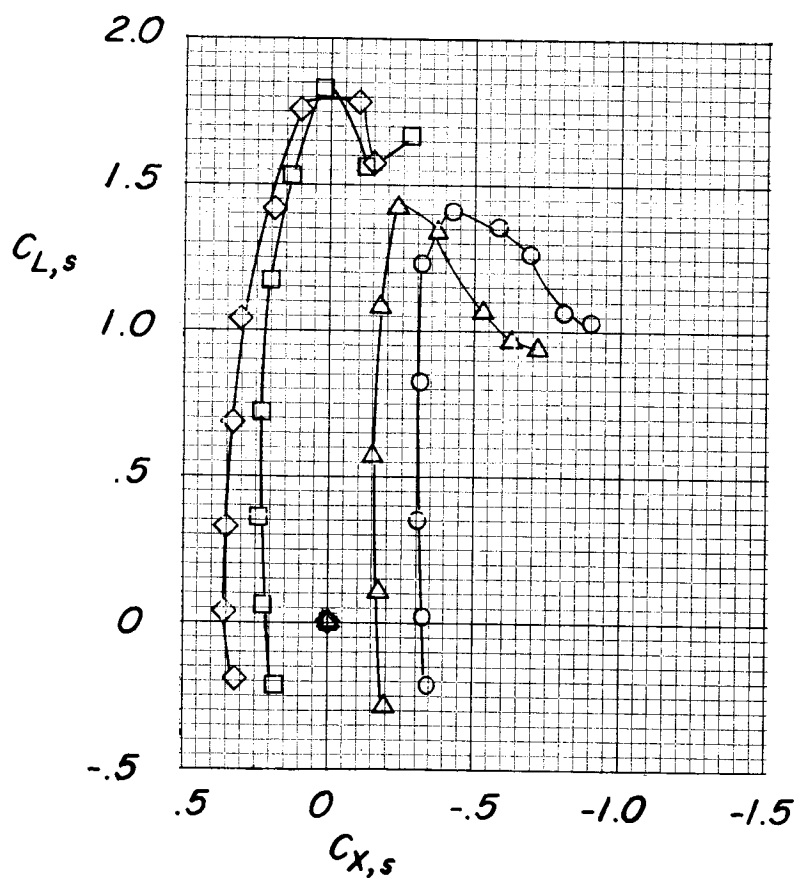
L-735

(c) Flap and aileron hinge-moment coefficients.

Figure 13.- Concluded.



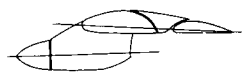
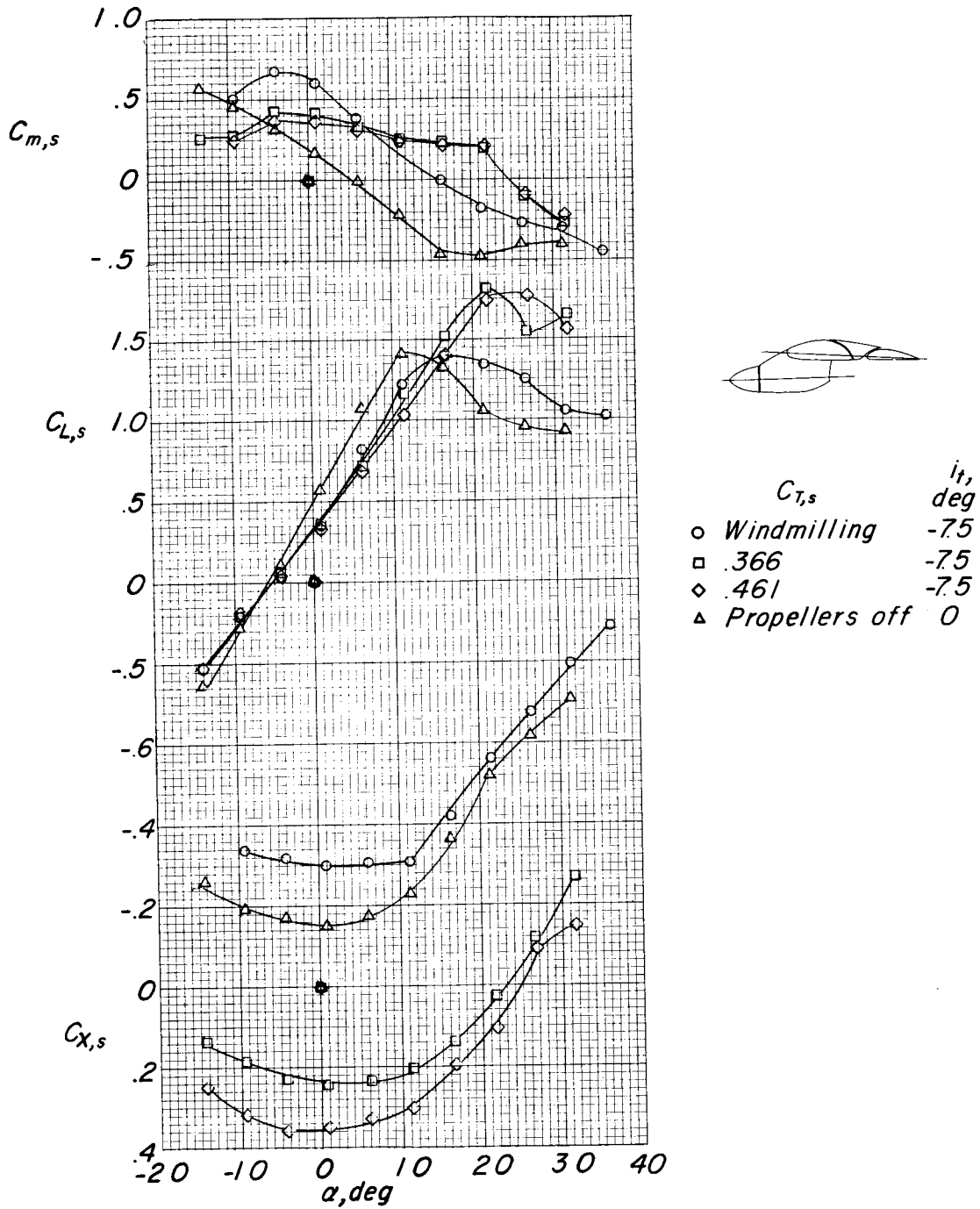
$C_{T,s}$	$i_t,$ deg
○ Windmilling	-7.5
□ .366	-7.5
◇ .461	-7.5
△ Propellers off	0



(a) Lift coefficient as function of longitudinal-force coefficient.

Figure 14.- Effect of thrust coefficient.  $\delta_{f,S}/\delta_{f,R} = 0/0$ .

L-735

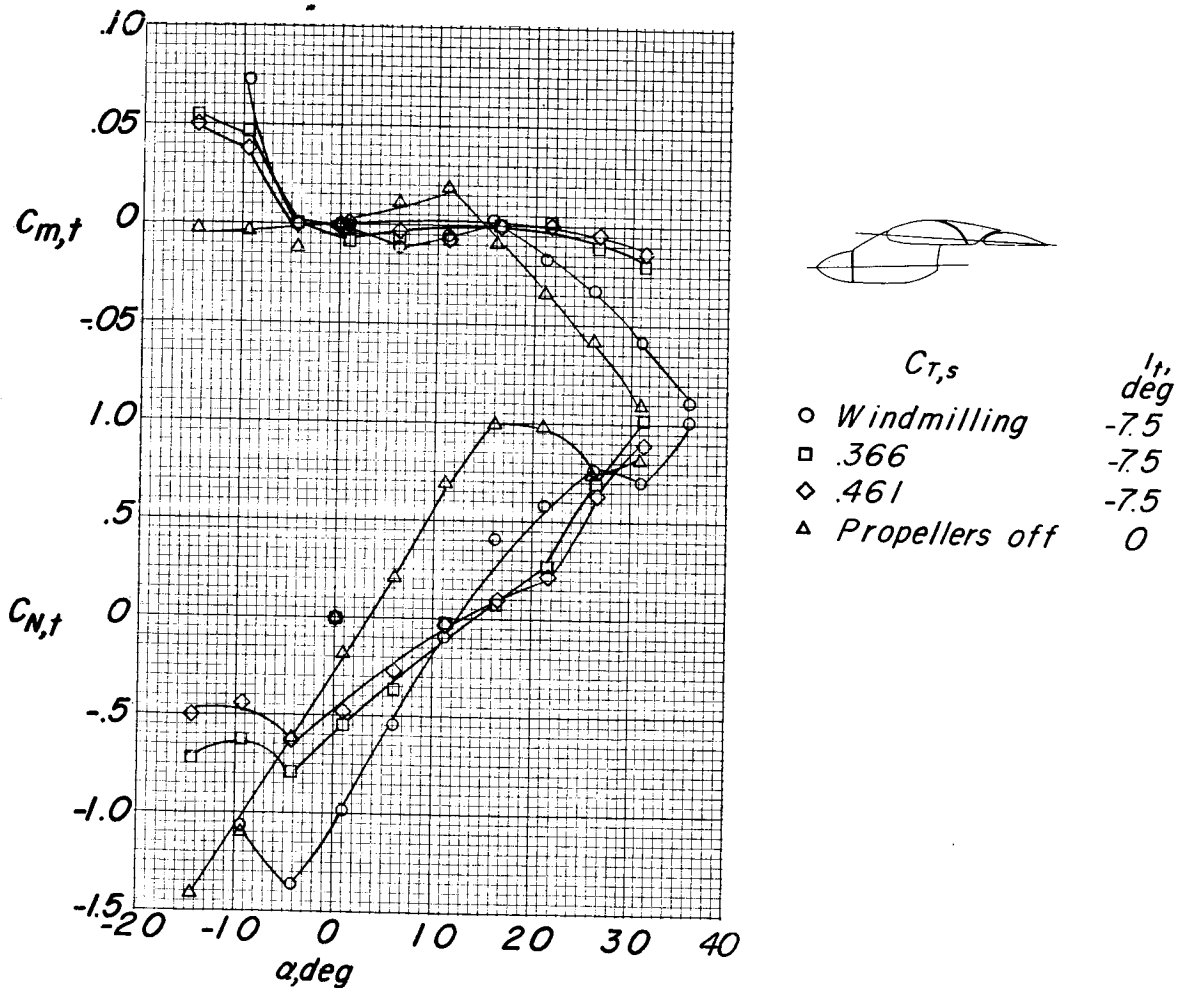


L-735

(b) Pitching-moment, lift, and longitudinal-force coefficients.

Figure 14.- Continued.

L-135

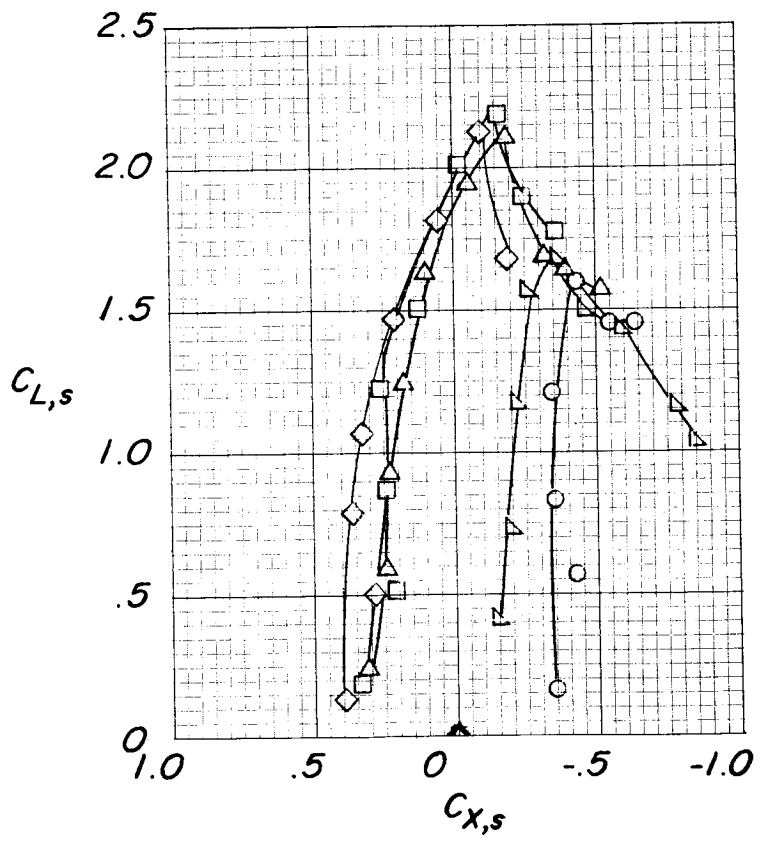


(c) Horizontal-tail pitching-moment and normal-force coefficients.

Figure 14.- Concluded.



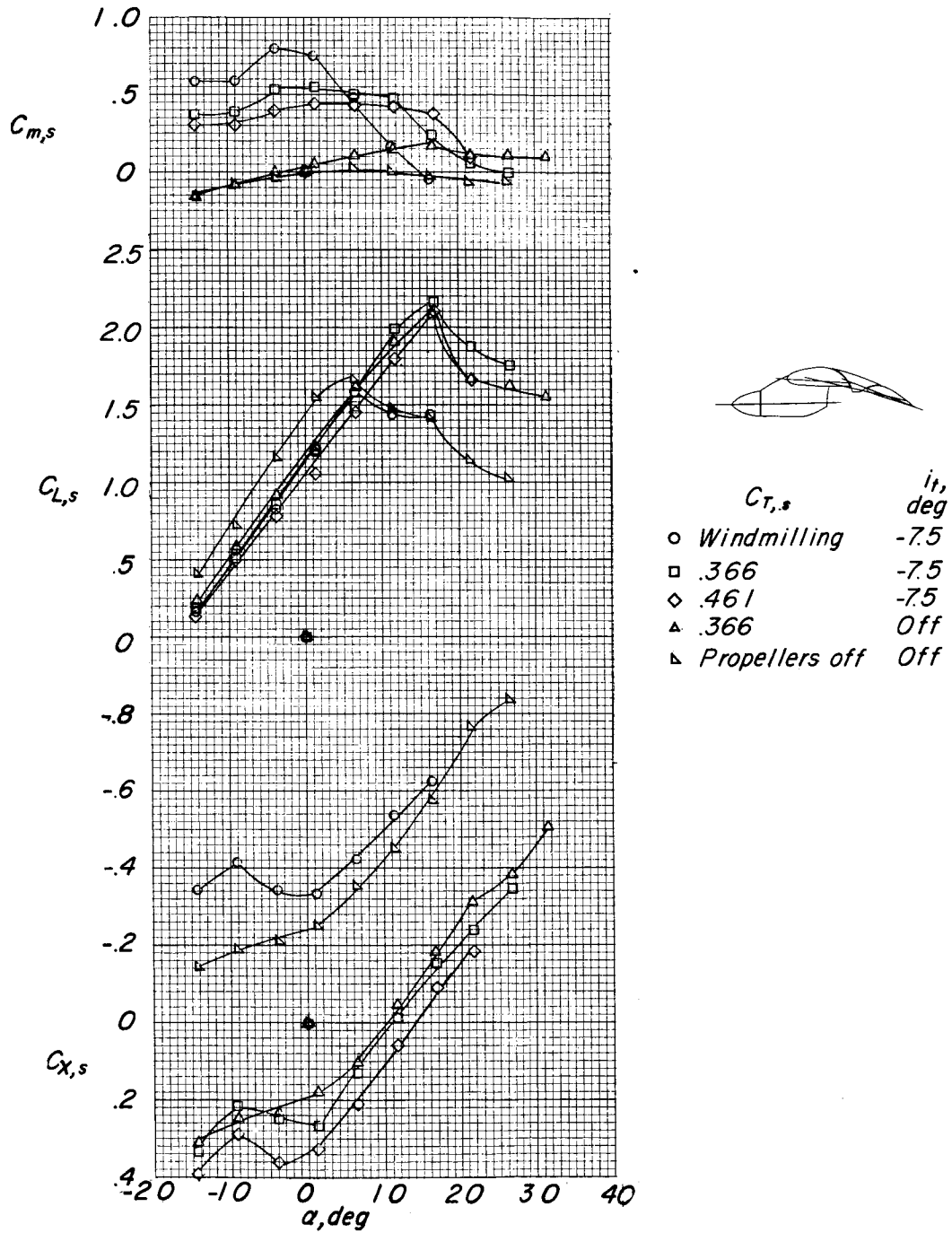
	$C_{T,s}$	$i_t,$ deg.
○	Windmilling	-7.5
□	.366	-7.5
◇	.461	-7.5
△	.366	Off
▾	Propellers off	Off



(a) Lift coefficient as function of longitudinal-force coefficient.

Figure 15.- Effect of thrust coefficient.  $\delta_{f,S}/\delta_{f,R} = 10/8.2$ .

I-735

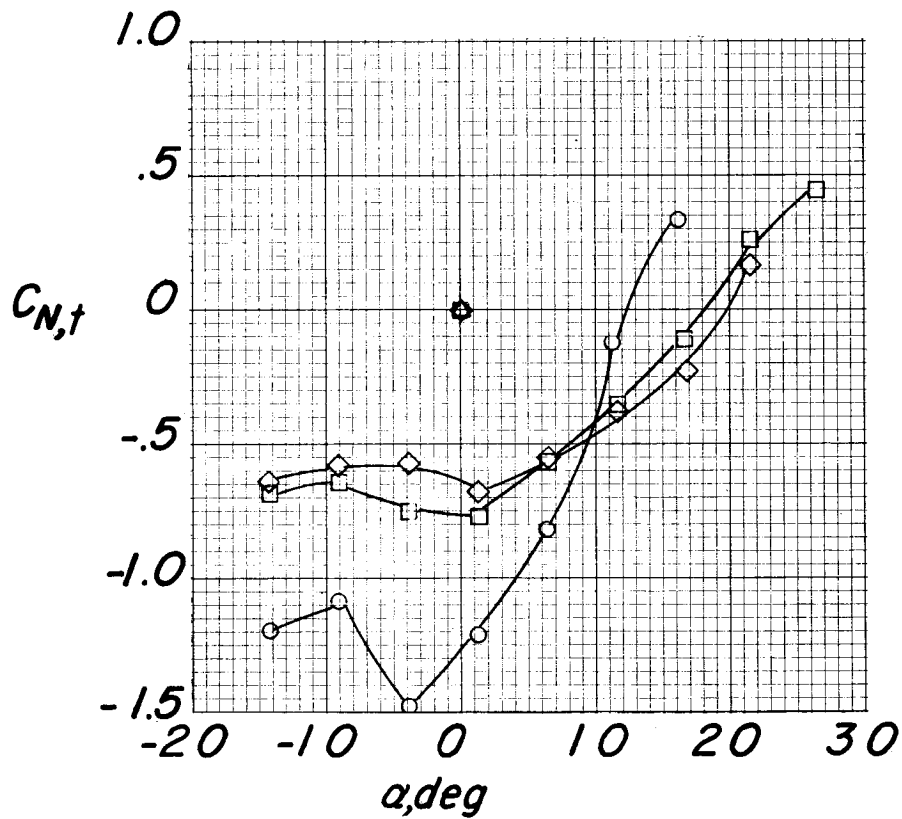


(b) Pitching-moment, lift, and longitudinal-force coefficients.

Figure 15.- Continued.



	$C_{T,s}$	$i_{T,}$ deg
○	Windmilling	-7.5
□	.366	-7.5
◇	.461	-7.5
△	.366	Off
▽	Propellers off	Off



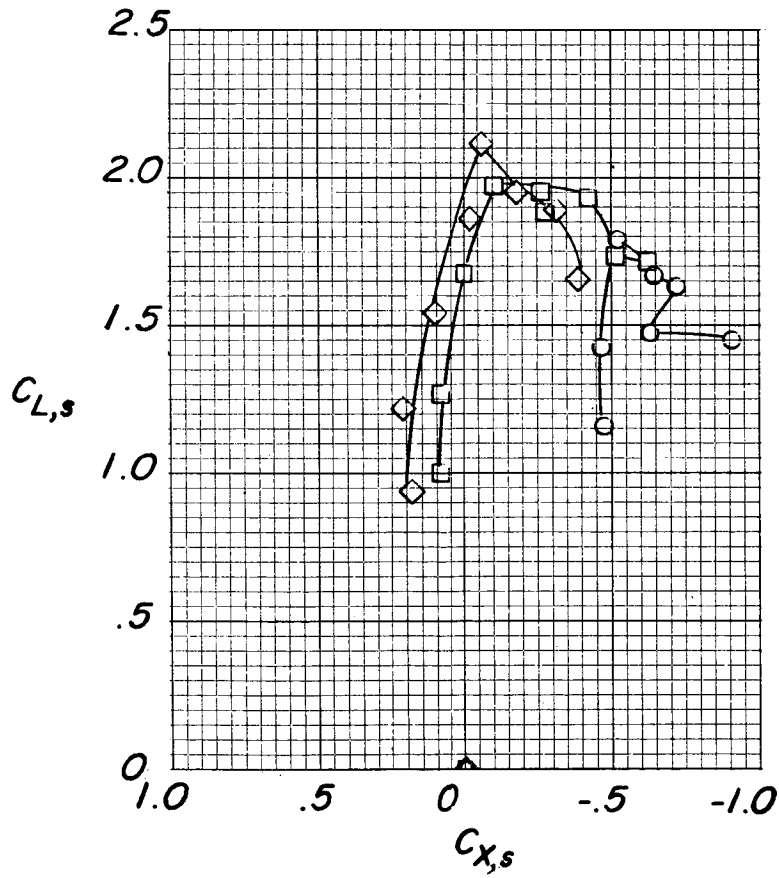
(c) Horizontal-tail normal-force coefficient.

Figure 15.- Concluded.



$C_{T,s}$

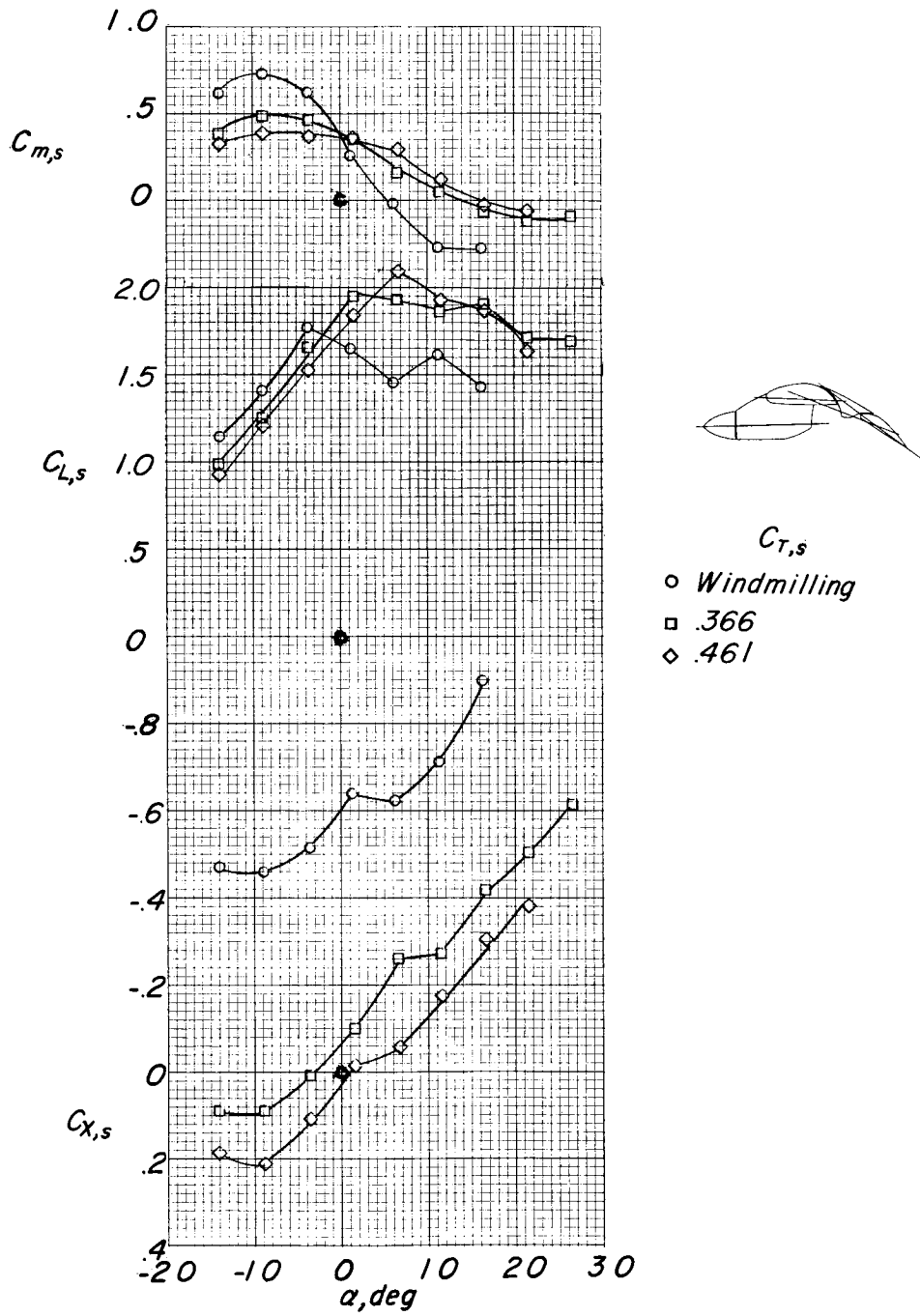
○ Windmilling  
 □ .366  
 ◇ .461



(a) Lift coefficient as function of longitudinal-force coefficient.

Figure 16.- Effect of thrust coefficient.  $i_t = 0^\circ$ ;  $\delta_{f,s}/\delta_{f,R} = 20/15$ .

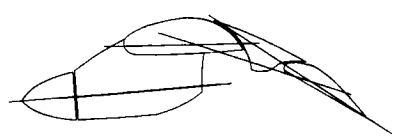
L-735



(b) Pitching-moment, lift, and longitudinal-force coefficients.

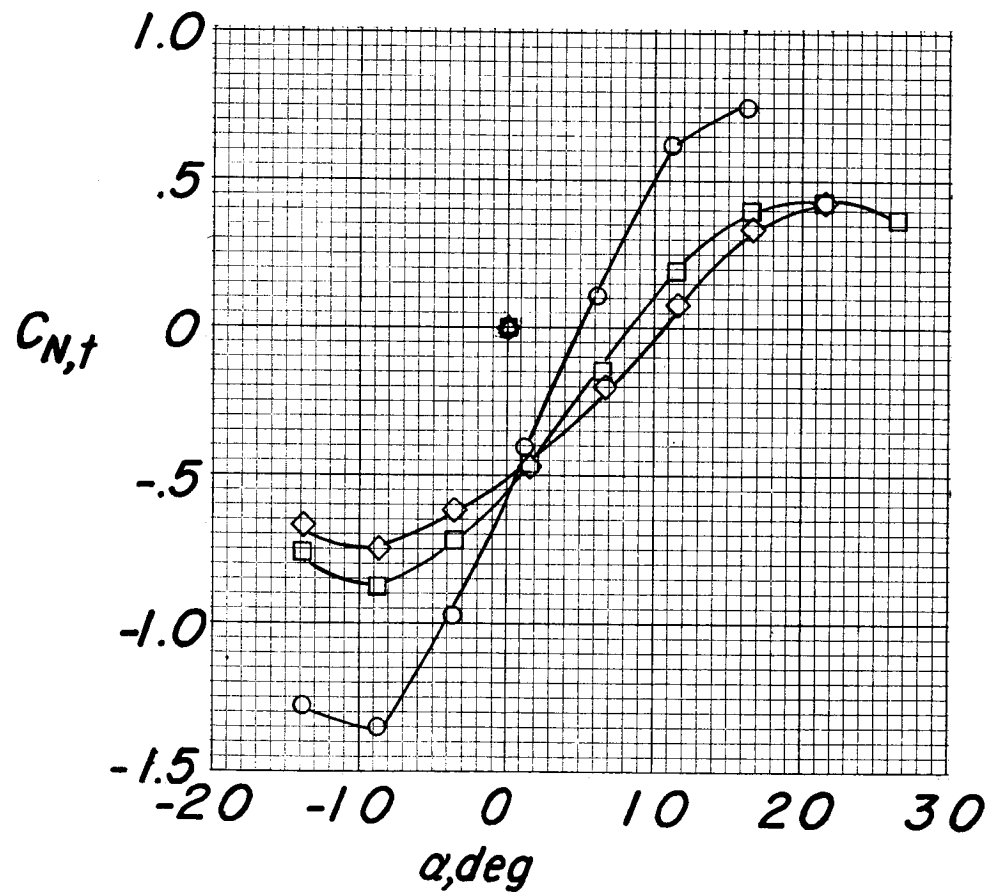
Figure 16.- Continued.

L-735



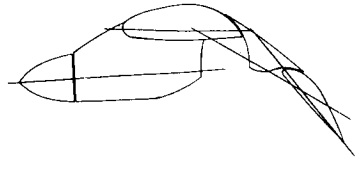
$C_{T,s}$

- Windmilling
- .366
- ◇ .461

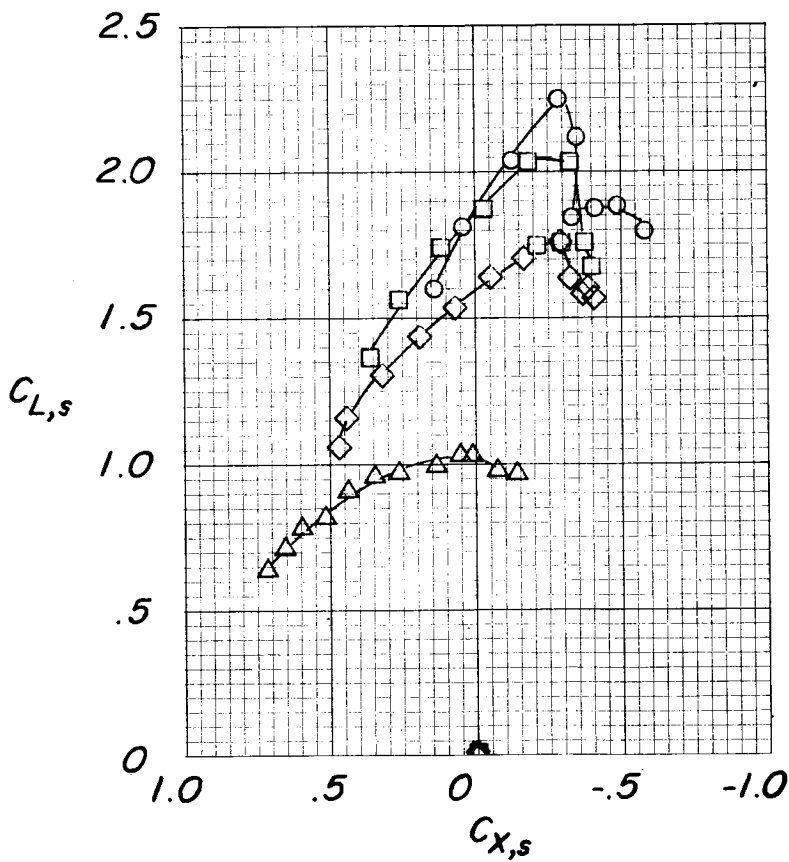


(c) Horizontal-tail normal-force coefficient.

Figure 16.- Concluded.

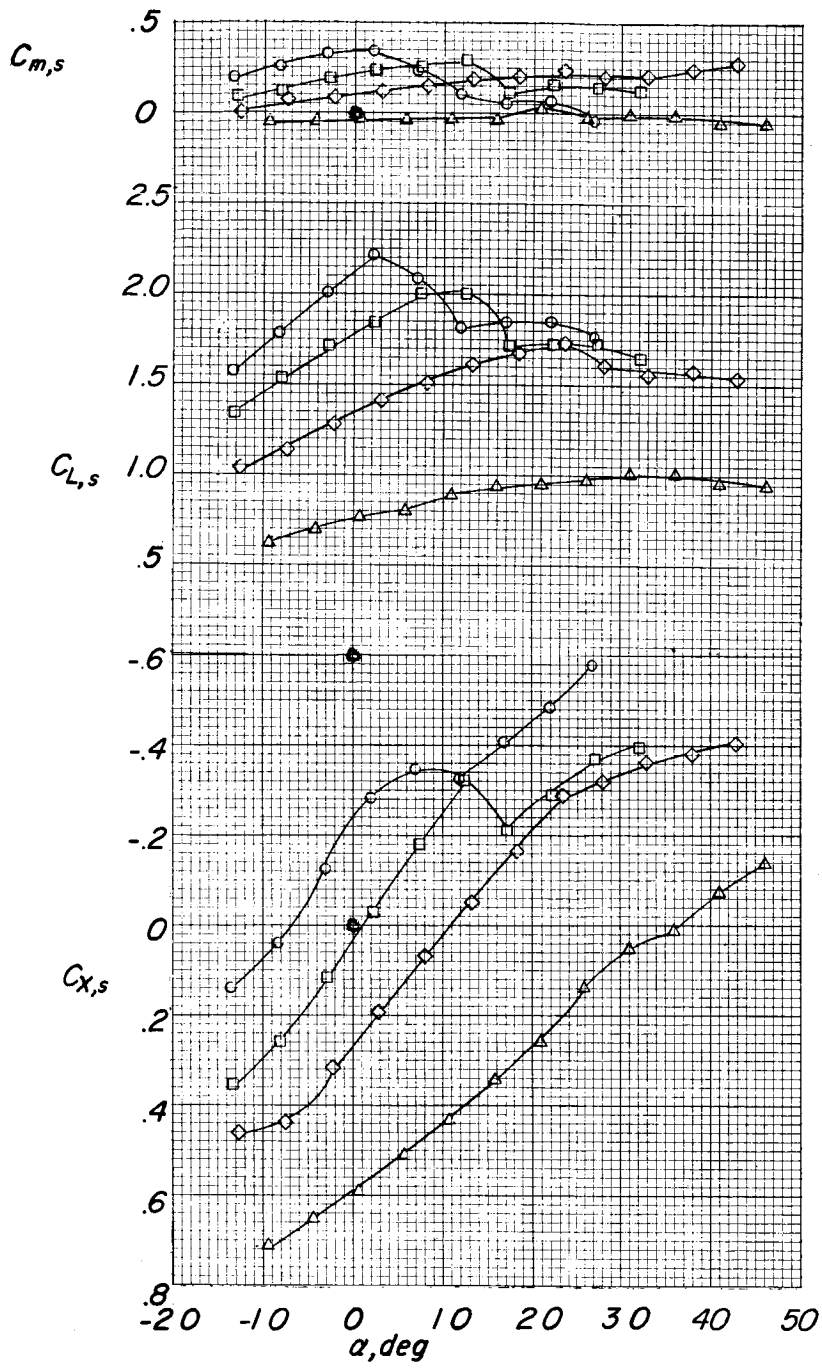


- $C_{T,s}$
- .603
  - .744
  - ◇ .882
  - △ .995



(a) Lift coefficient as function of longitudinal-force coefficient.

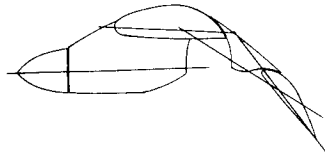
Figure 17.- Effect of thrust coefficient.  $i_t = 0^\circ$ ;  $\delta_{f,S}/\delta_{f,R} = 30/20.7$ .



(b) Pitching-moment, lift, and longitudinal-force coefficients.

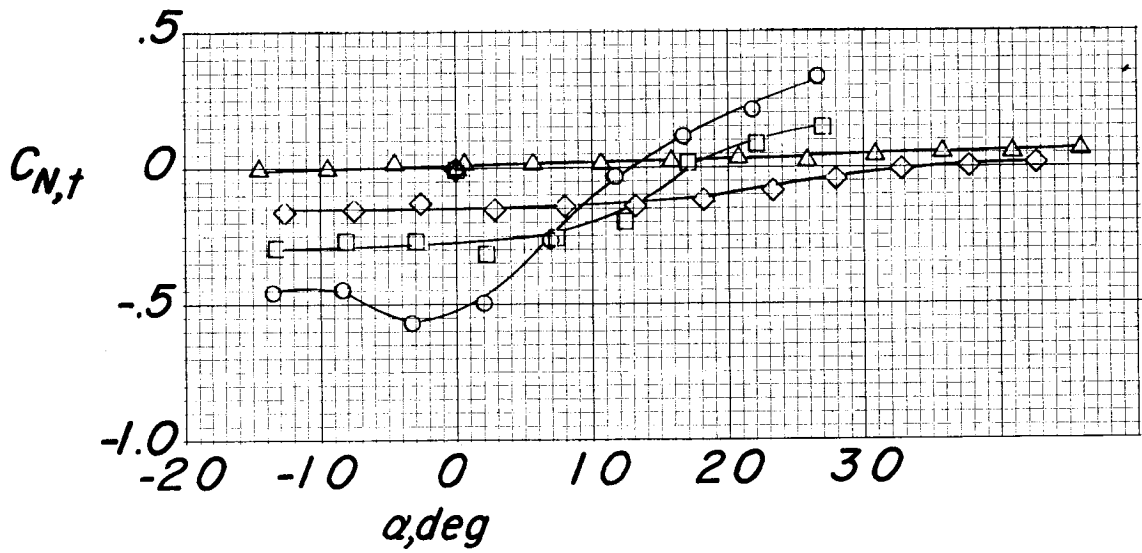
Figure 17.- Continued.

L-735



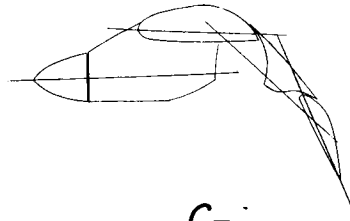
$C_{T,s}$

- .603
- .744
- ◇ .882
- △ .995



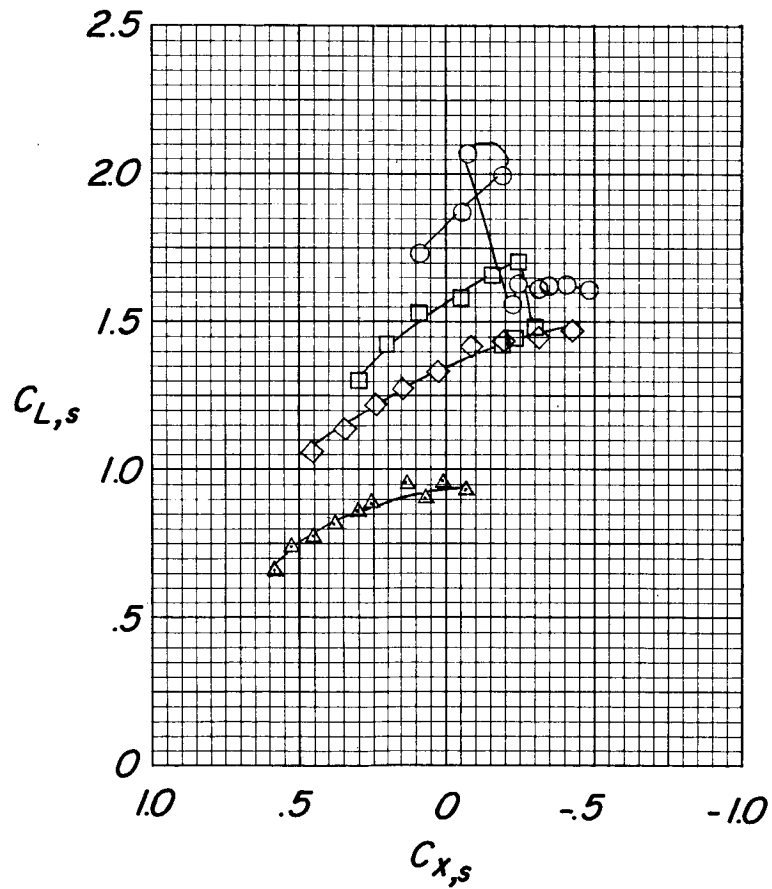
(c) Horizontal-tail normal-force coefficient.

Figure 17.- Concluded.



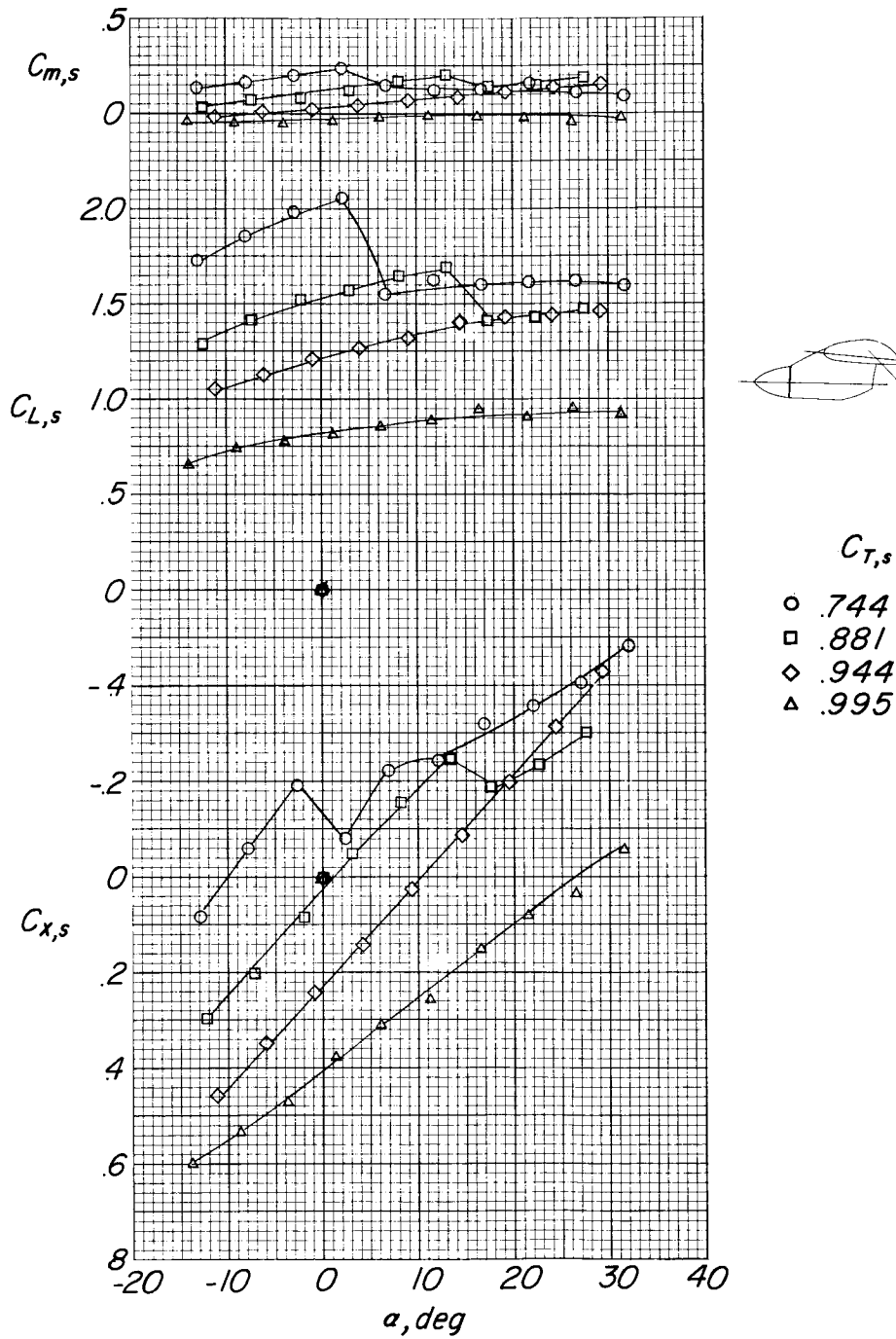
$C_{T,s}$

- .744
- .881
- ◇ .944
- △ .995



(a) Lift coefficient as function of longitudinal-force coefficient.

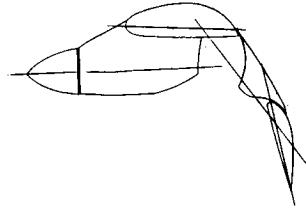
Figure 18.- Effect of thrust coefficient.  $i_t = 0^\circ$ ;  $\delta_{f,s}/\delta_{f,R} = 40/24$ .



L-735

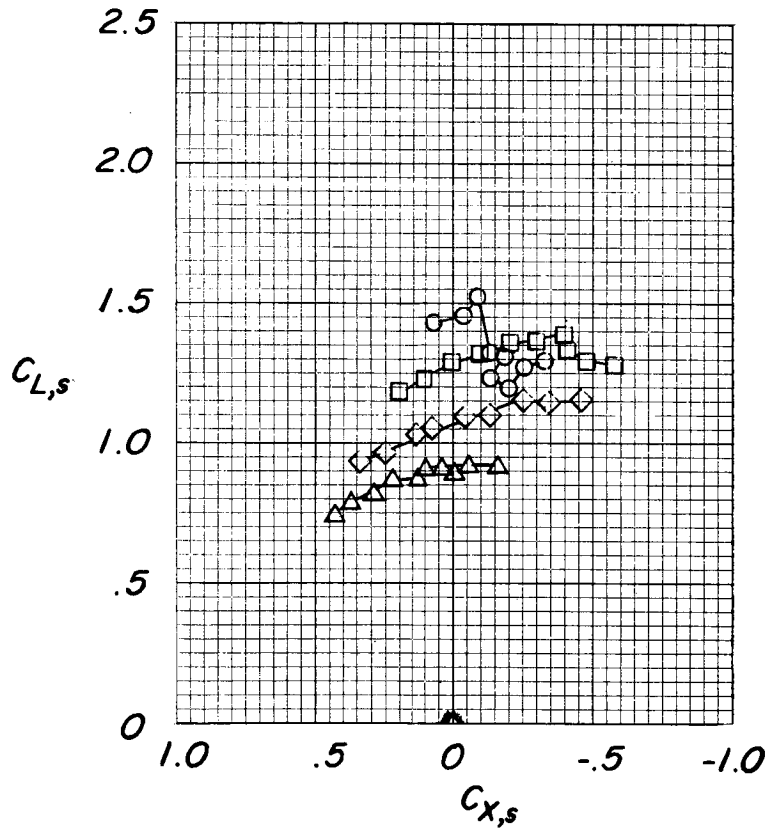
(b) Pitching-moment, lift, and longitudinal-force coefficients.

Figure 18.- Concluded.



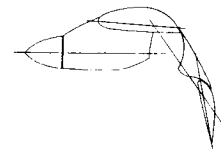
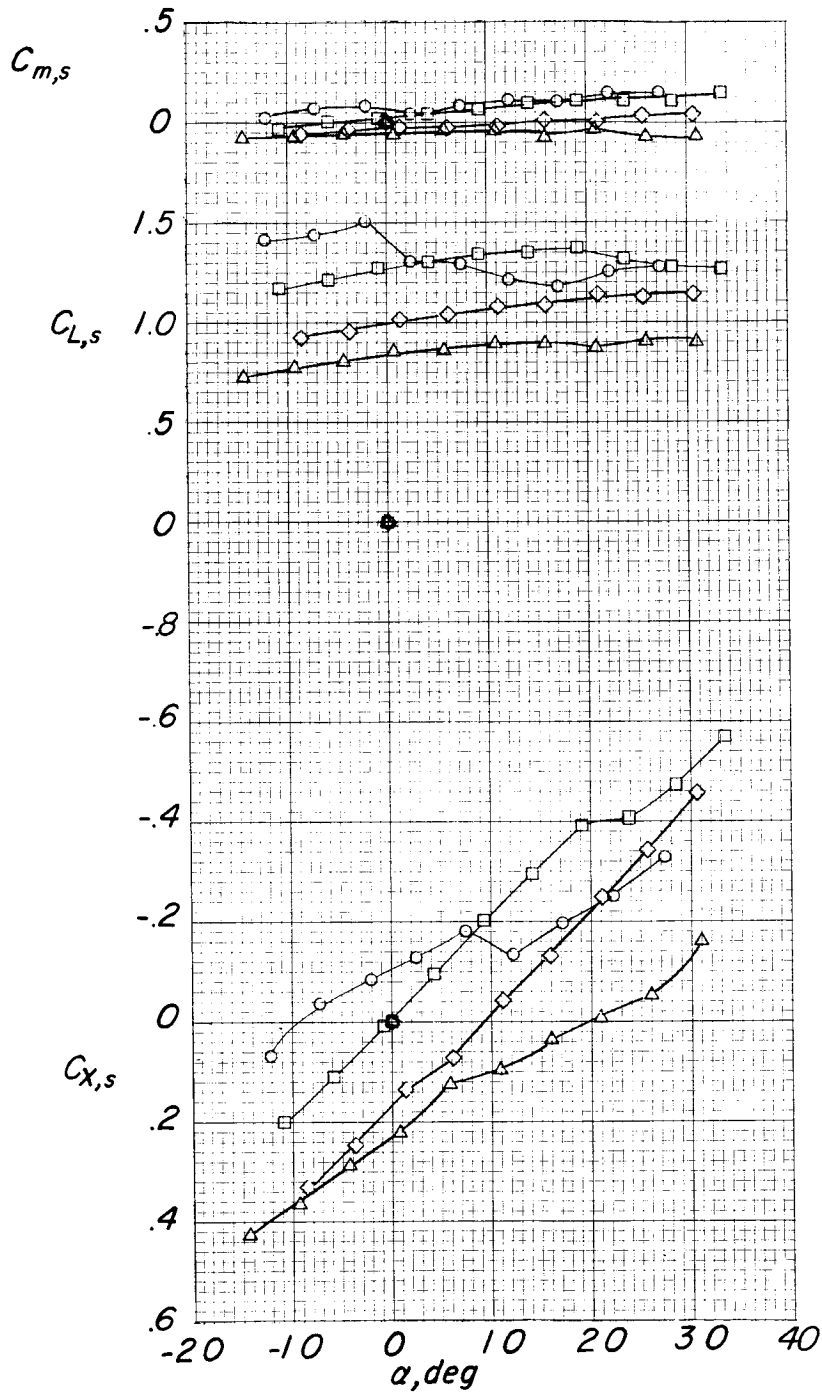
L-735

- $C_{T,s}$
- .882
  - .944
  - ◇ .978
  - △ .995



(a) Lift coefficient as function of longitudinal-force coefficient.

Figure 19.- Effect of thrust coefficient.  $i_t = 0^\circ$ ;  $\delta_{f,S}/\delta_{f,R} = 50/25$ .

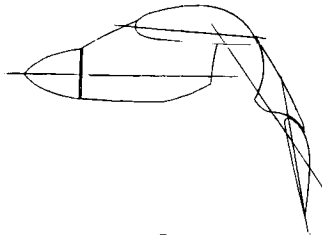


- $C_{T,s}$
- .882
  - .944
  - ◇ .978
  - △ .995

L-735

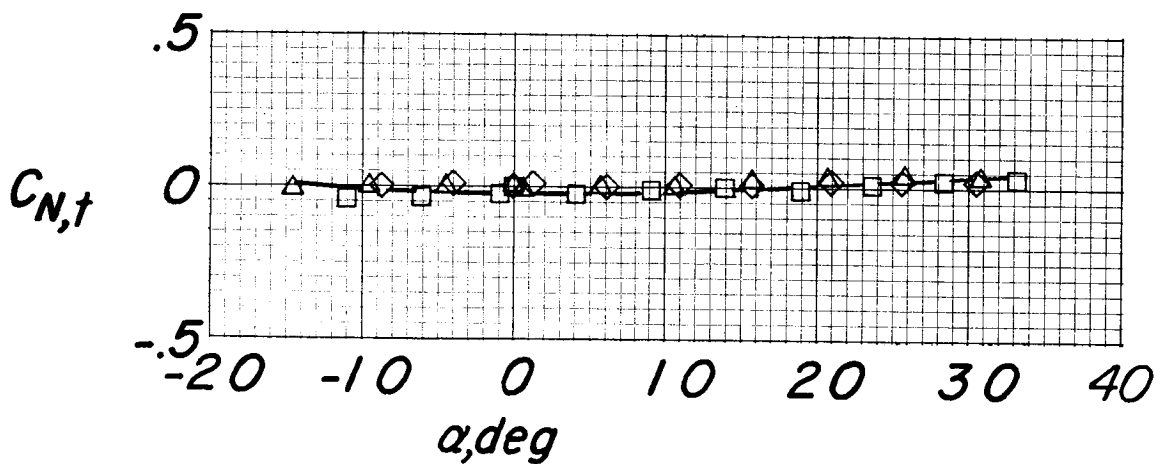
(b) Pitching-moment, lift, and longitudinal-force coefficients.

Figure 19.- Continued.



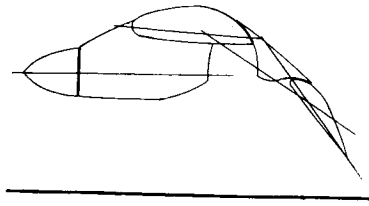
$C_{T,s}$

- .882
- .944
- ◇ .978
- △ .995

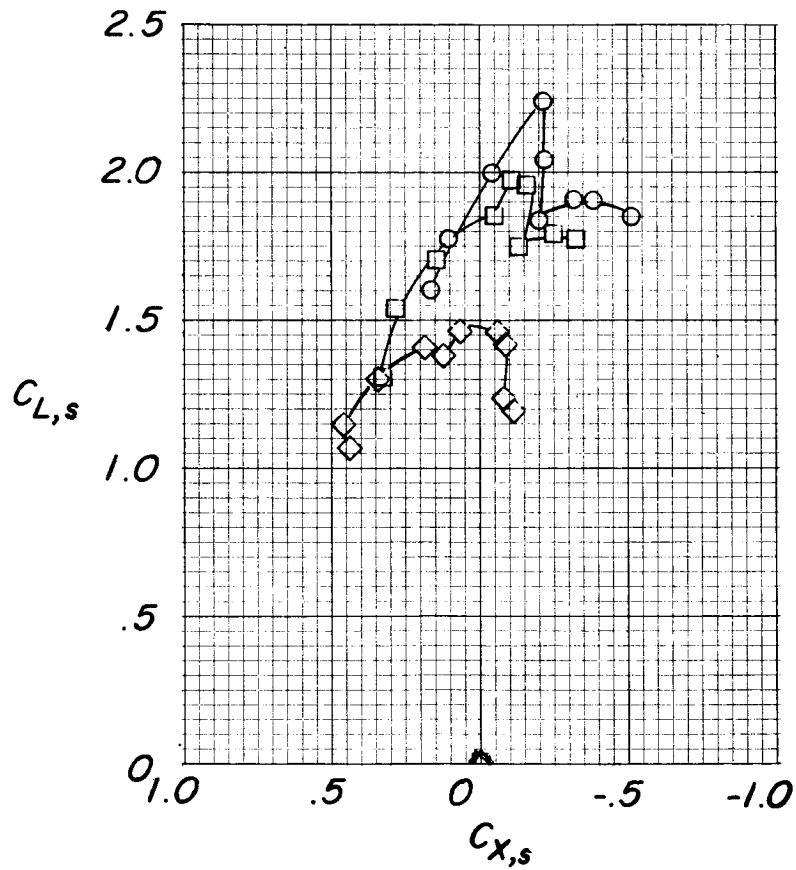


(c) Horizontal-tail normal-force coefficient.

Figure 19.- Concluded.


 $C_{T,s}$ 
 $\circ$  .605

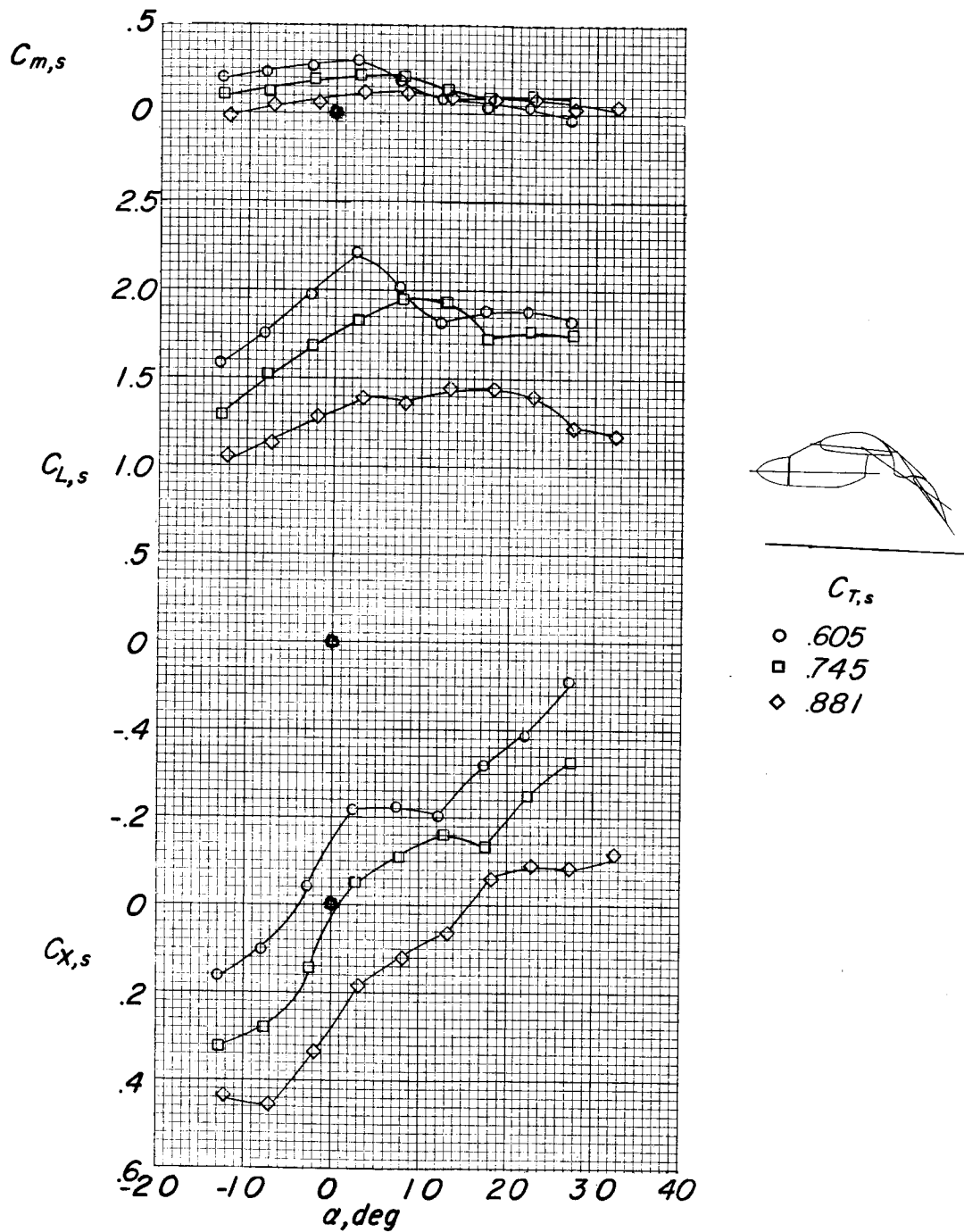
 $\square$  .745

 $\diamond$  .881


(a) Lift coefficient as function of longitudinal-force coefficient.

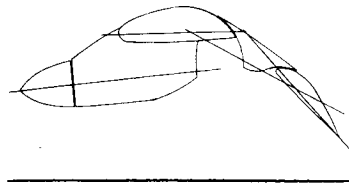
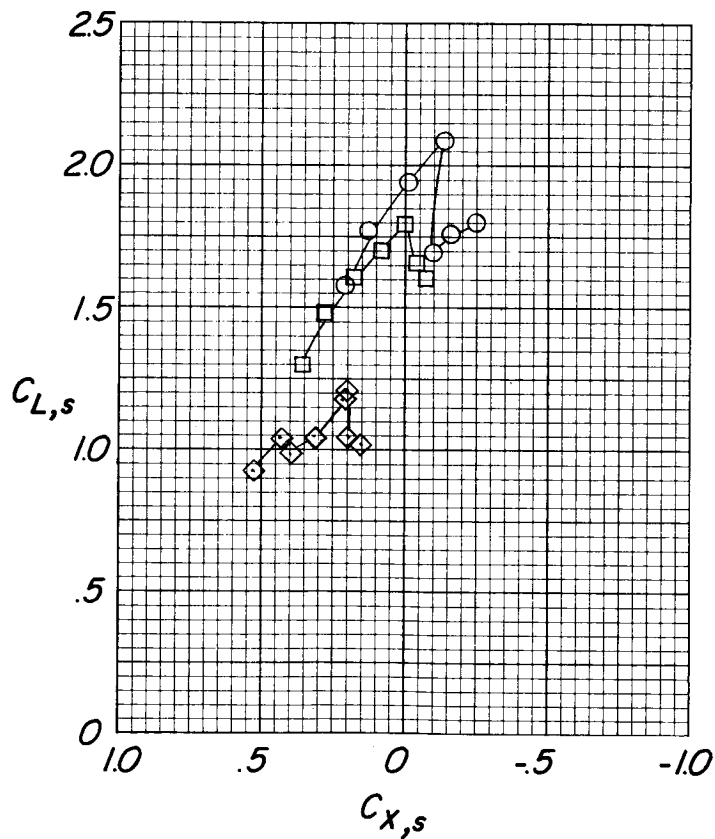
Figure 20.- Effect of thrust coefficient in region of ground effect.

$i_t = 0^0$ ;  $\delta_{f,S}/\delta_{f,R} = 30/20.7$ ;  $h/D = 1.00$ .



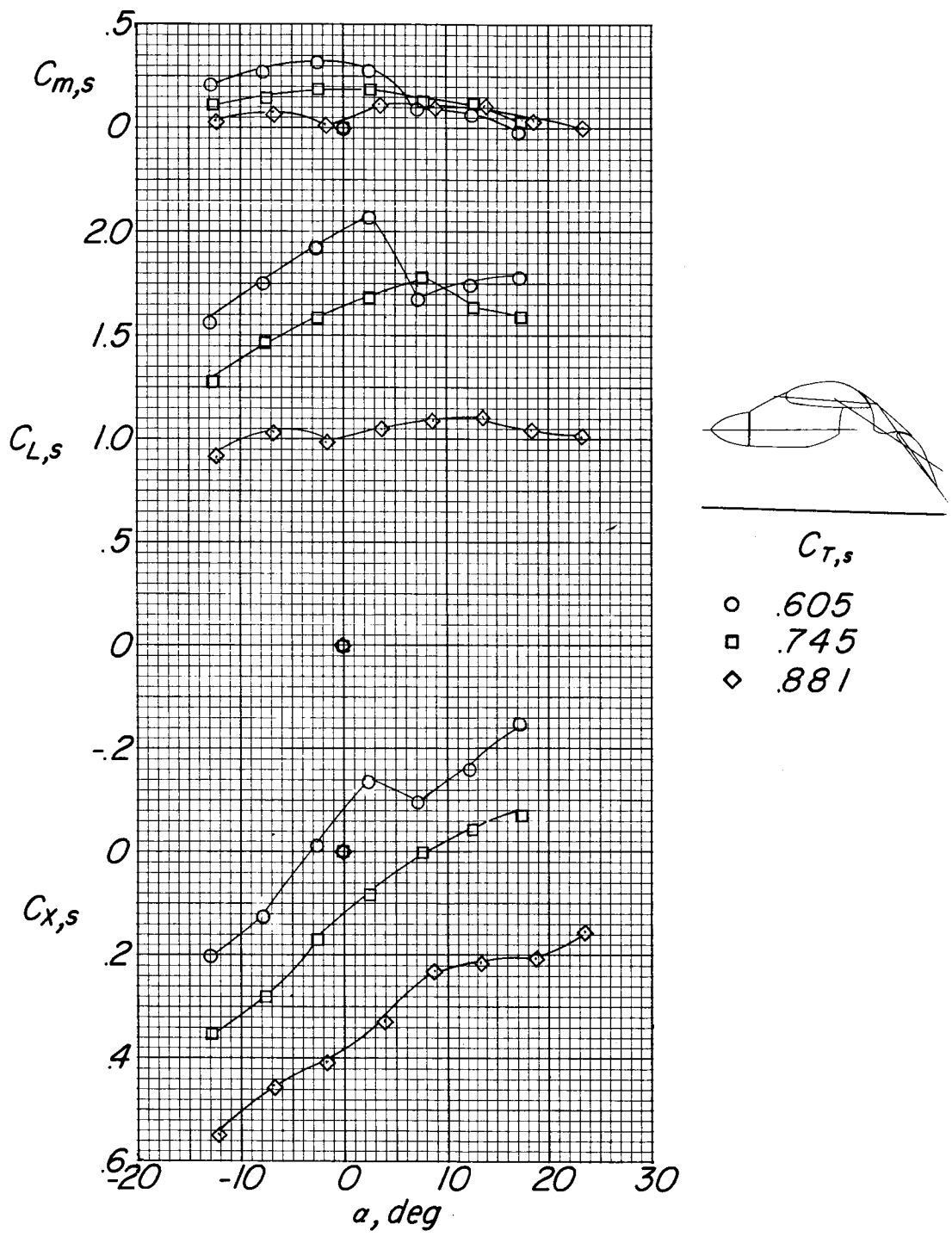
(b) Pitching-moment, lift, and longitudinal-force coefficients.

Figure 20.- Concluded.

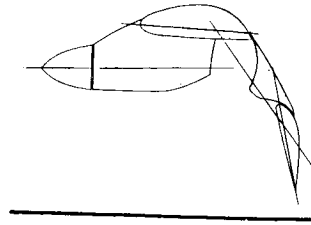

 $C_{T,s}$ 
 $\circ .605$ 
 $\square .745$ 
 $\diamond .881$ 


(a) Lift coefficient as function of longitudinal-force coefficient.

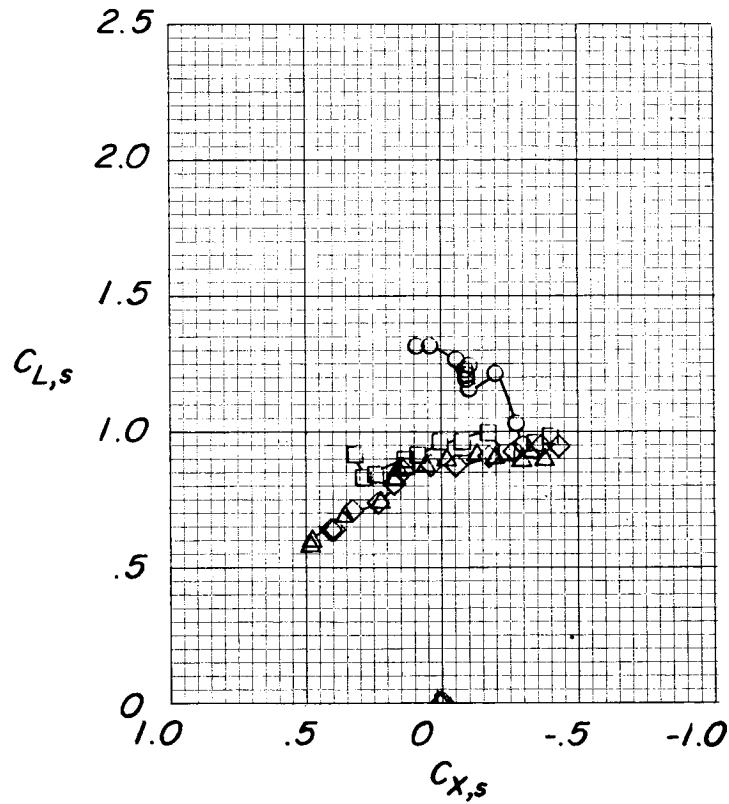
Figure 21.- Effect of thrust coefficient in region of ground effect.  
 $i_t = 0^\circ$ ;  $\delta_{f,s}/\delta_{f,R} = 30/20.7$ ;  $h/D = 0.33$ .



(b) Pitching-moment, lift, and longitudinal-force coefficients.


 $C_{T,s}$ 

○	.881
□	.943
◇	.978
△	.995

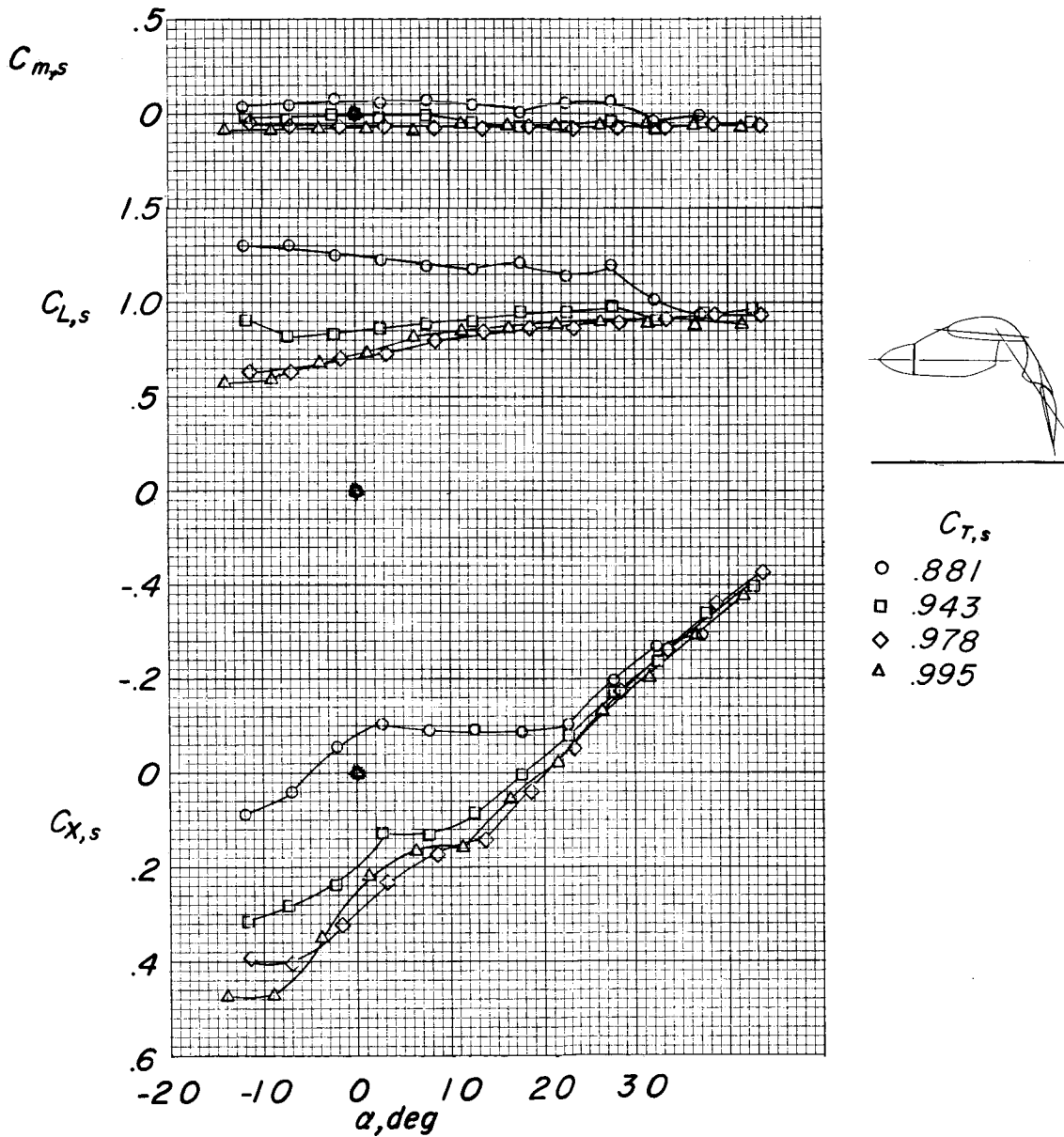


(a) Lift coefficient as function of longitudinal-force coefficient.

Figure 22.- Effect of thrust coefficient in region of ground effect.

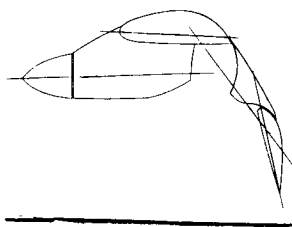
$$i_t = 0^\circ; \delta_{f,S}/\delta_{f,R} = 50/25; h/D = 1.00.$$

L-735

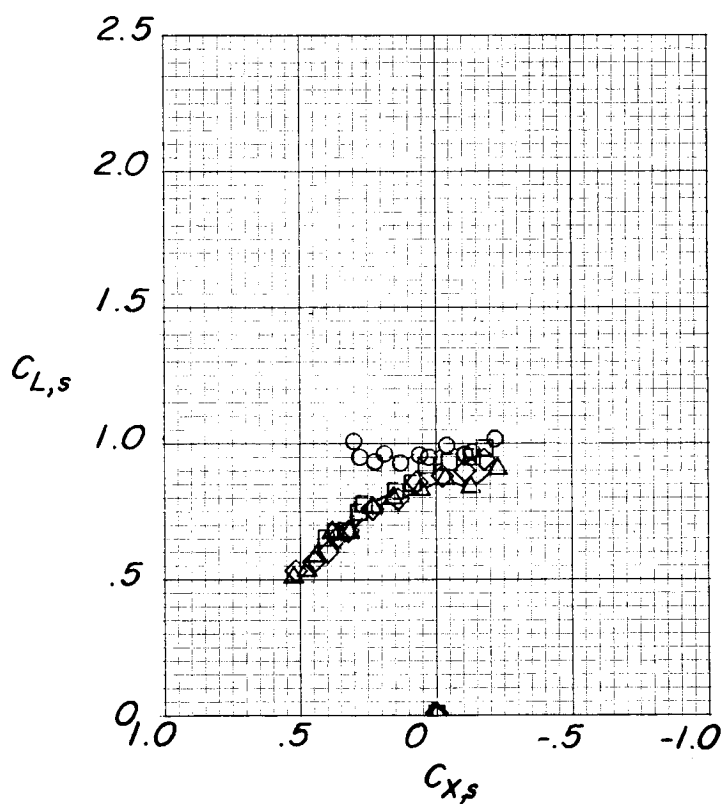


(b) Pitching-moment, lift, and longitudinal-force coefficients.

Figure 22.- Concluded.


 $C_{T,S}$ 

- .881
- .943
- ◇ .978
- △ .995

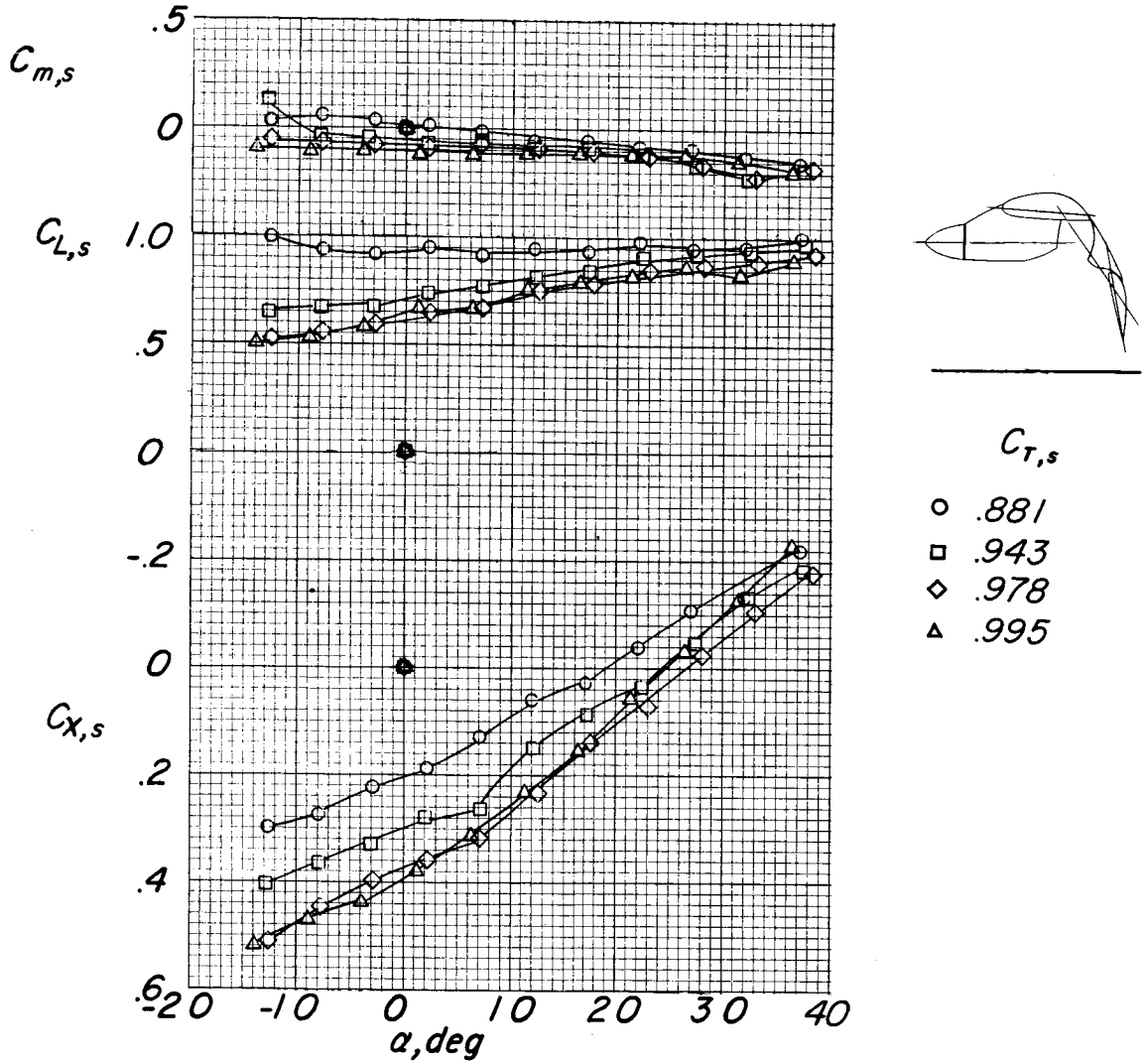


(a) Lift coefficient as function of longitudinal-force coefficient.

Figure 23.- Effect of thrust coefficient in region of ground effect.

$$i_t = 0^\circ; \delta_{f,S}/\delta_{f,R} = 50/25; h/D = 0.33.$$

I-735

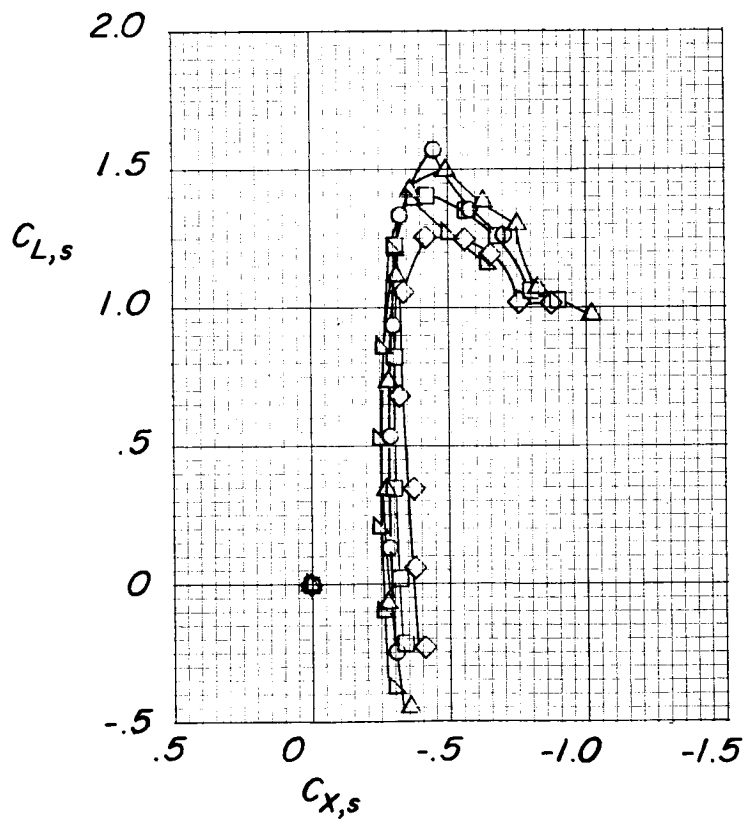


(b) Pitching-moment, lift, and longitudinal-force coefficients.

Figure 23.- Concluded.



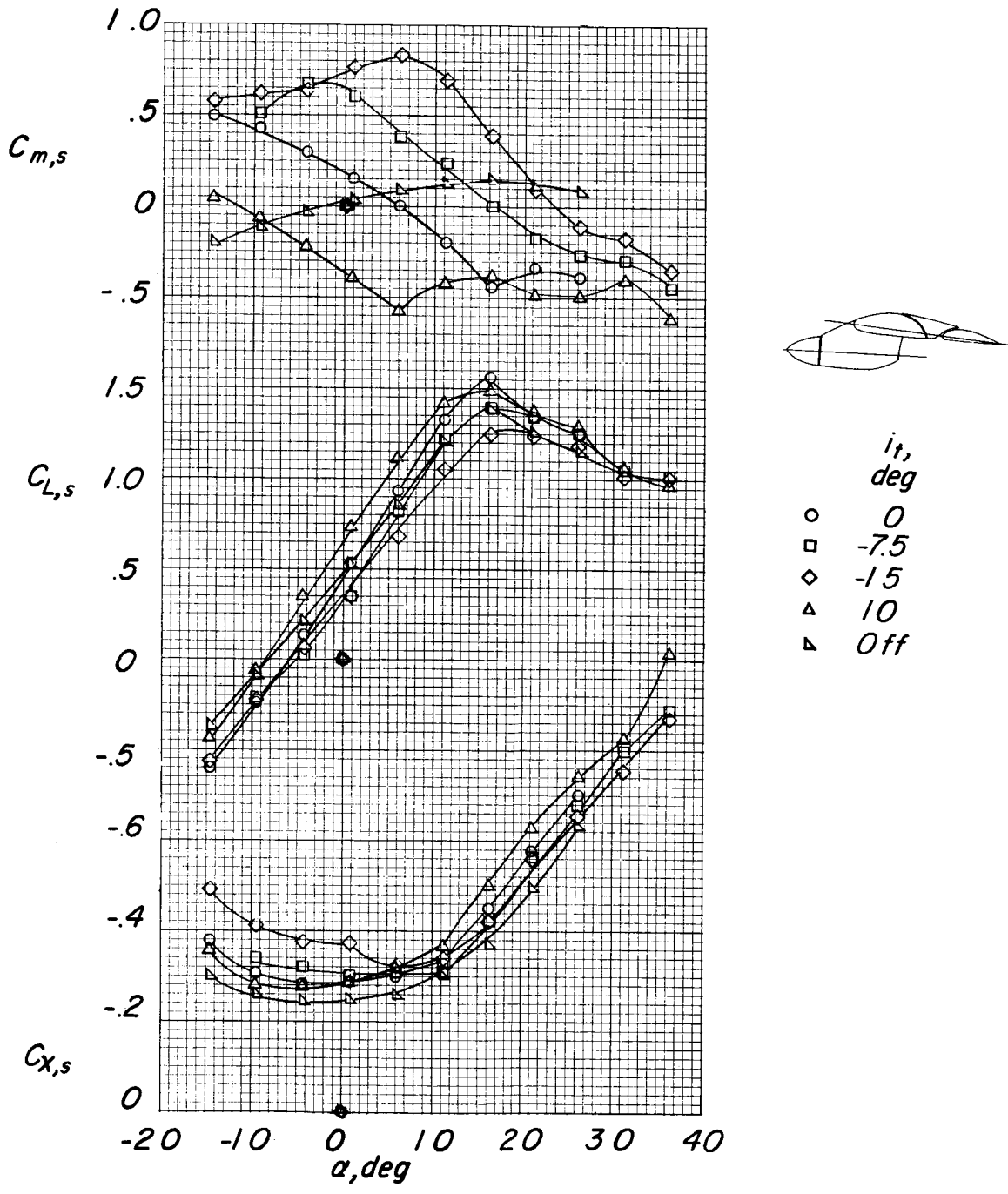
	$i_t,$ <i>deg</i>
○	0
□	-75
◇	-15
△	10
▽	Off



(a) Lift coefficient as function of longitudinal-force coefficient.

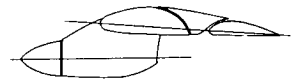
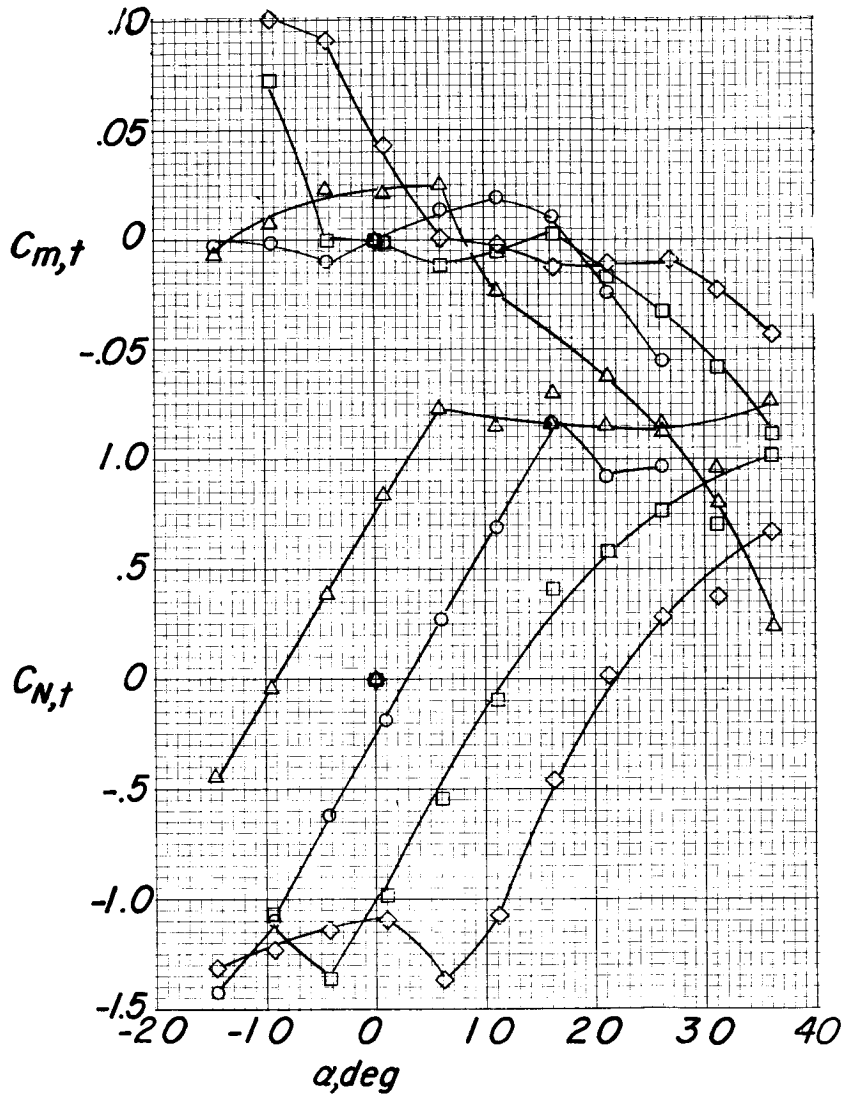
Figure 24.- Effect of tail incidence. Propellers windmilling;  
 $\delta_{f,S}/\delta_{f,R} = 0/0$ .

L-755



(b) Pitching-moment, lift, and longitudinal-force coefficients.

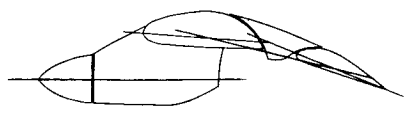
Figure 24.- Continued.



- $i_t$ , deg
- 0
  - -7.5
  - ◇ -15
  - ▲ 10
  - ▼ Off

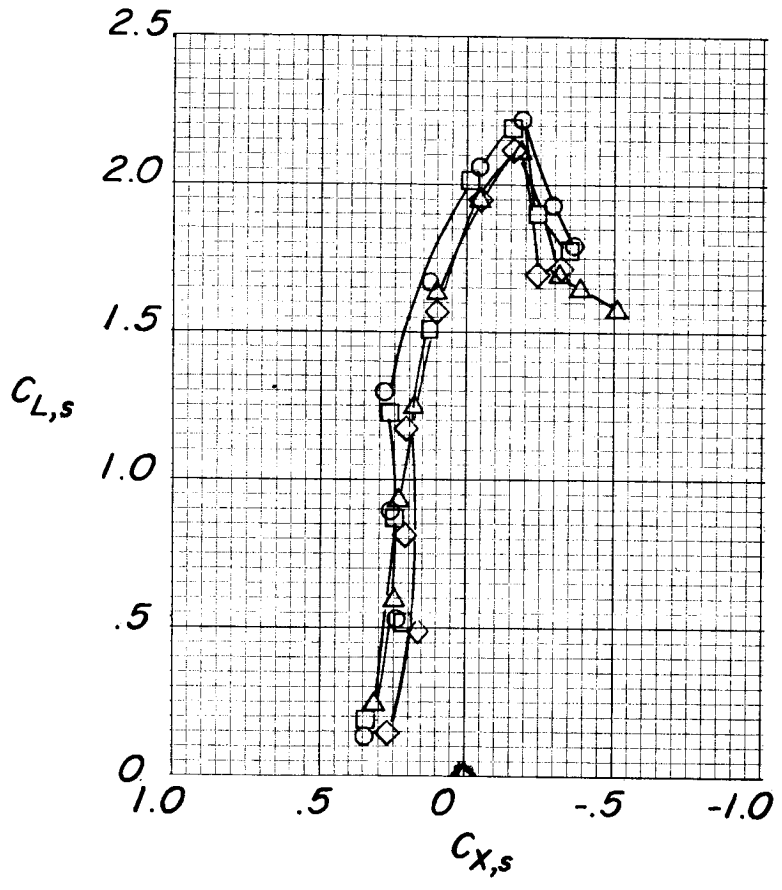
(c) Horizontal-tail pitching-moment and normal-force coefficients.

Figure 24.- Concluded.



$i_t,$   
deg

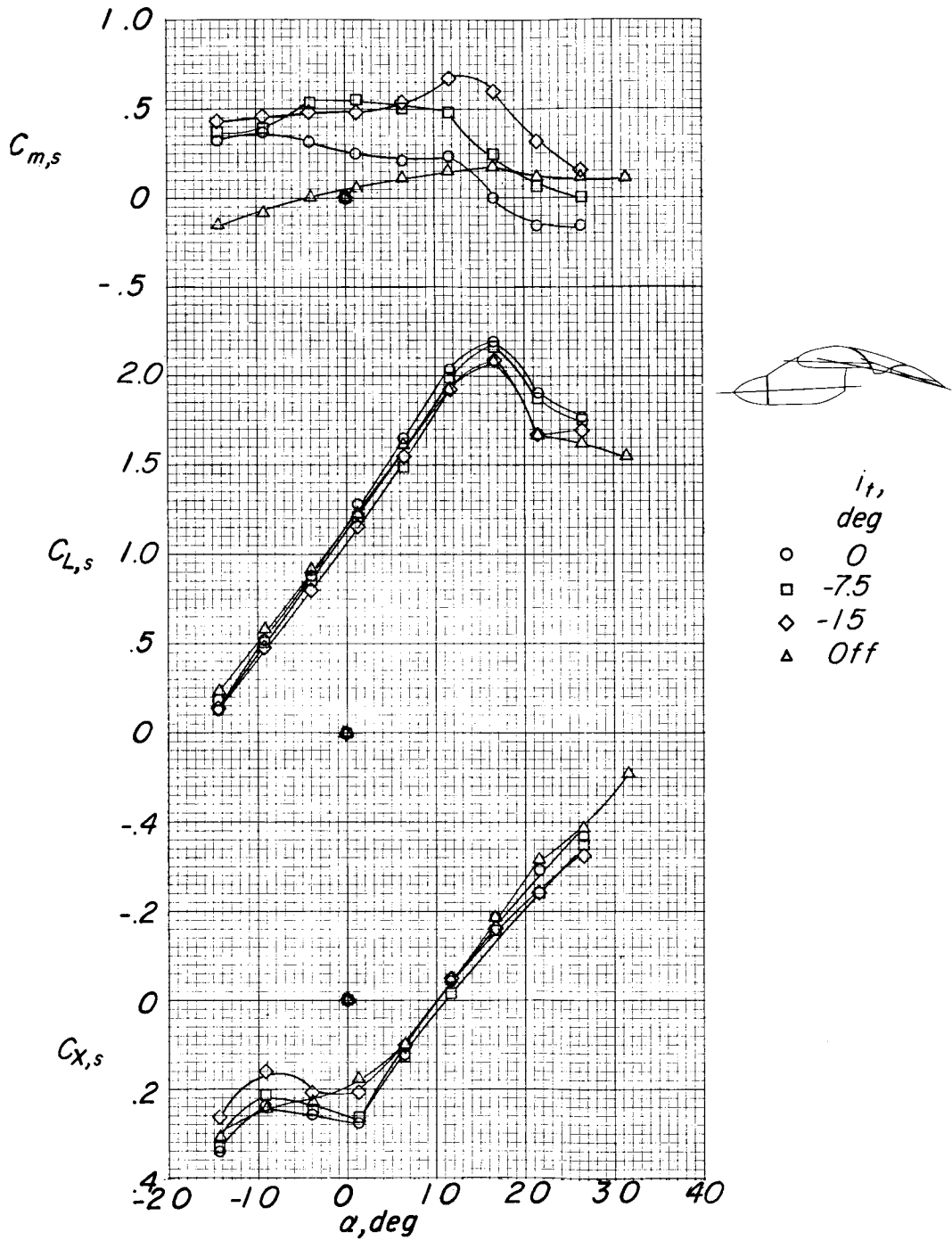
- 0
- -7.5
- ◇ -15
- △ Off



(a) Lift coefficient as function of longitudinal-force coefficient.

Figure 25.- Effect of tail incidence.  $C_{T,s} = 0.366$ ;  $\delta_{f,s}/\delta_{f,R} = 10/8.2$ .

L-735



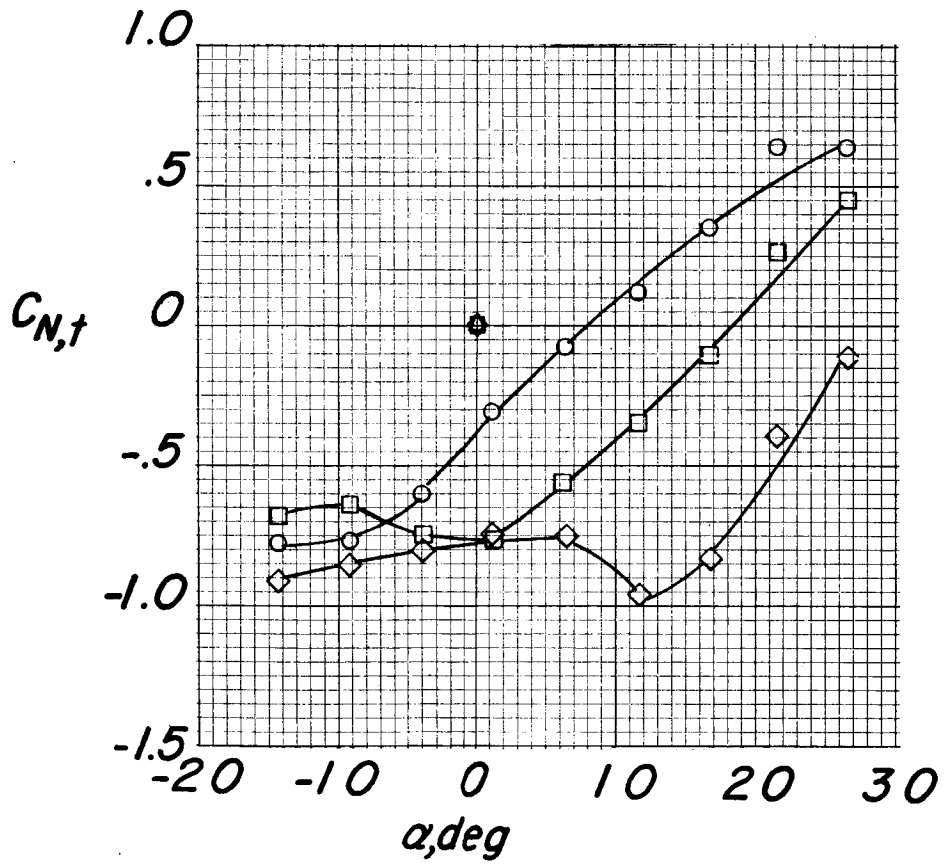
(b) Pitching-moment, lift, and longitudinal-force coefficients.

Figure 25.- Continued.



*i<sub>t</sub>*,  
deg

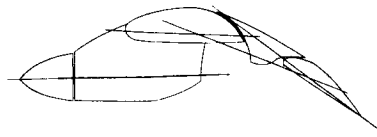
- 0
- -7.5
- ◇ -15
- △ Off



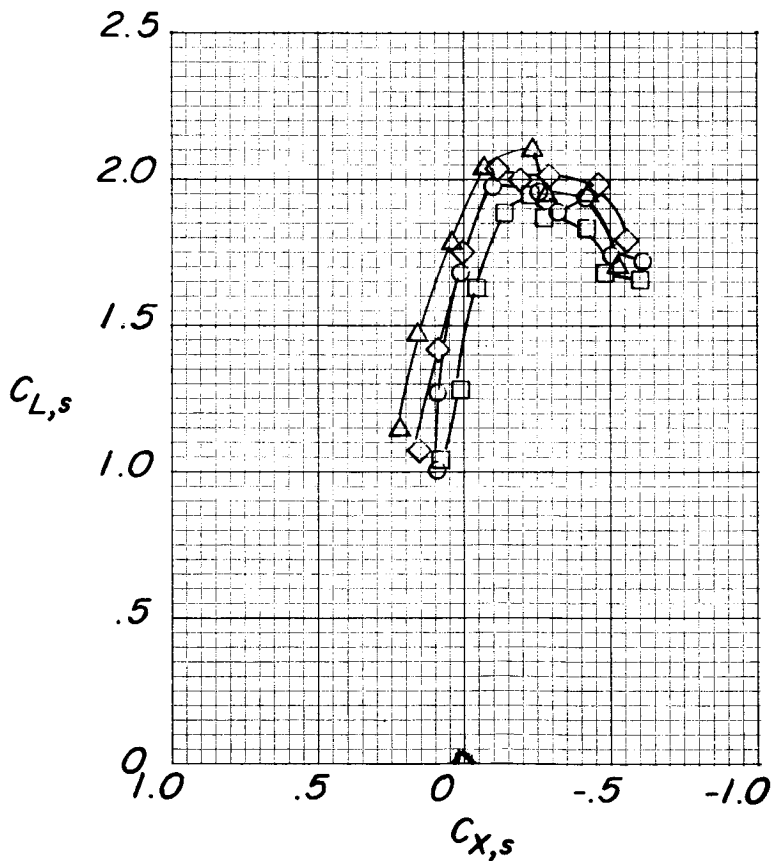
(c) Horizontal-tail normal-force coefficient.

Figure 25.- Concluded.

L-735

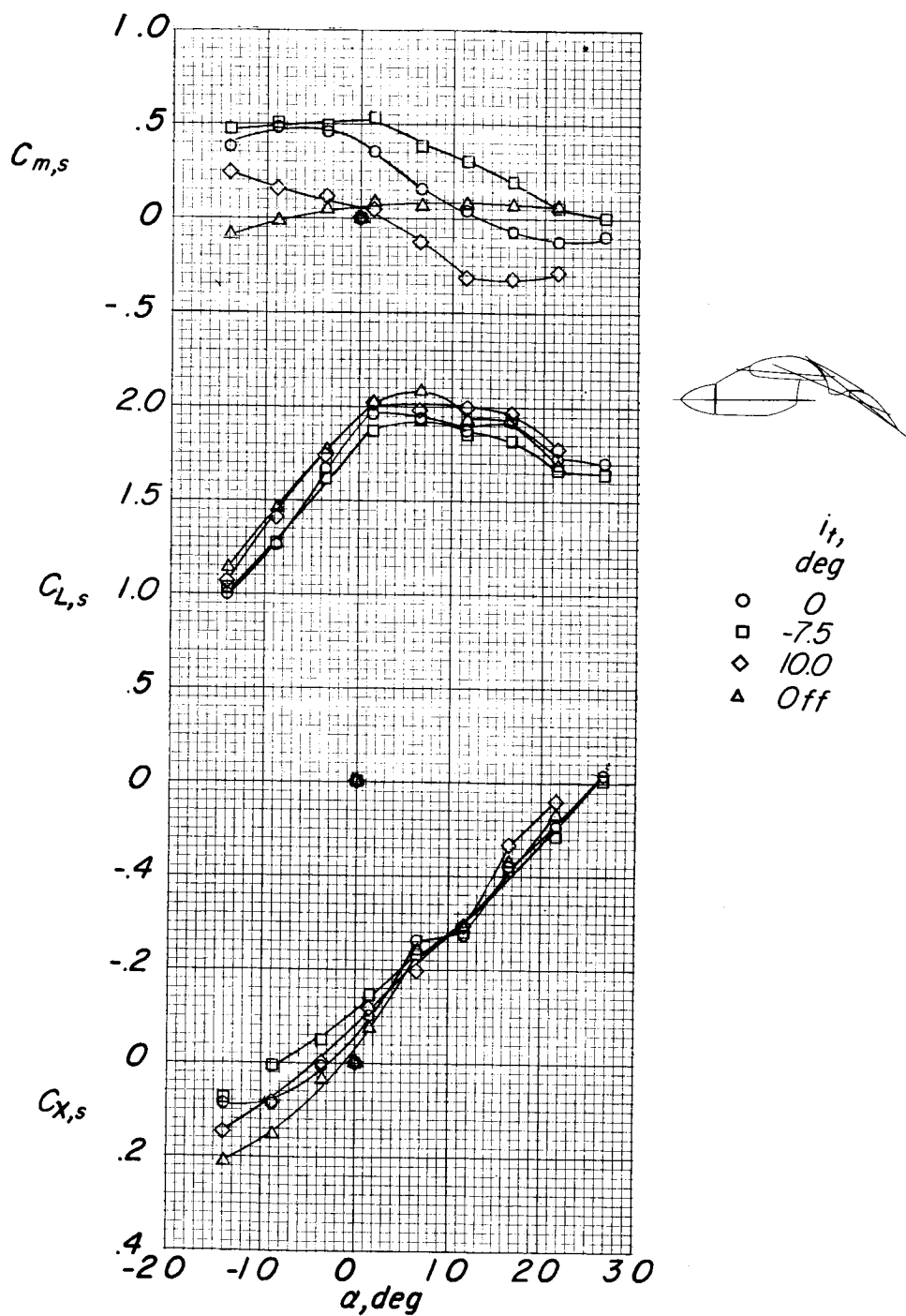


	$i_t,$ deg
○	0
□	-7.5
◇	10.0
△	Off



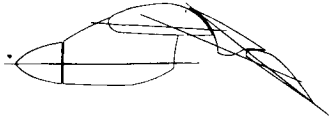
(a) Lift coefficient as function of longitudinal-force coefficient.

Figure 26.- Effect of tail incidence.  $C_{T,s} = 0.366$ ;  $\delta_{f,S}/\delta_{f,R} = 20/15$ .

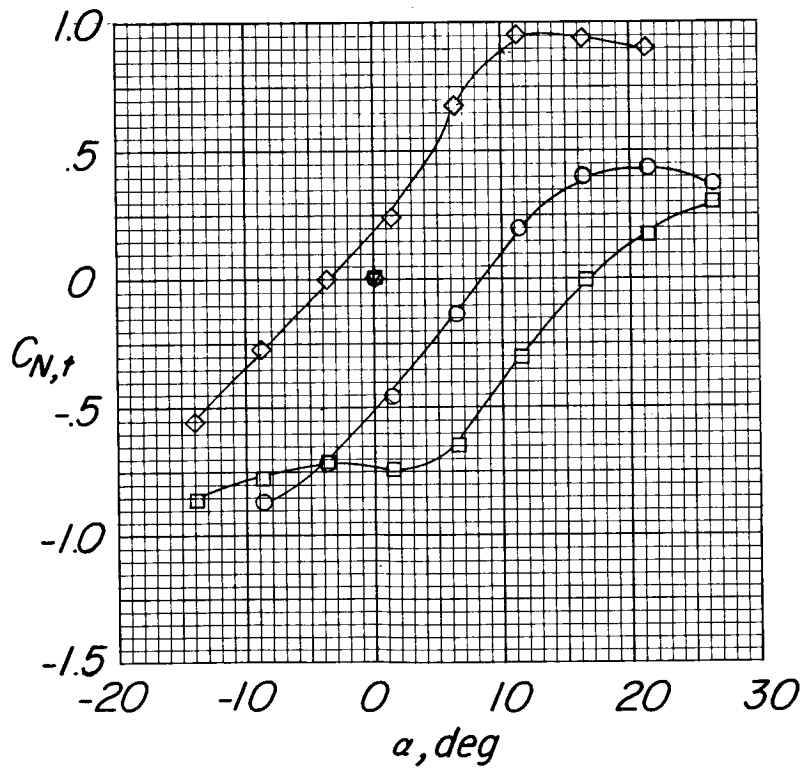


(b) Pitching-moment, lift, and longitudinal-force coefficients.

Figure 26.- Continued.

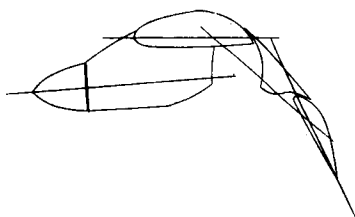


$i_T$ ,  
 deg  
 ○ 0  
 □ -7.5  
 ◇ 10.0  
 △ Off

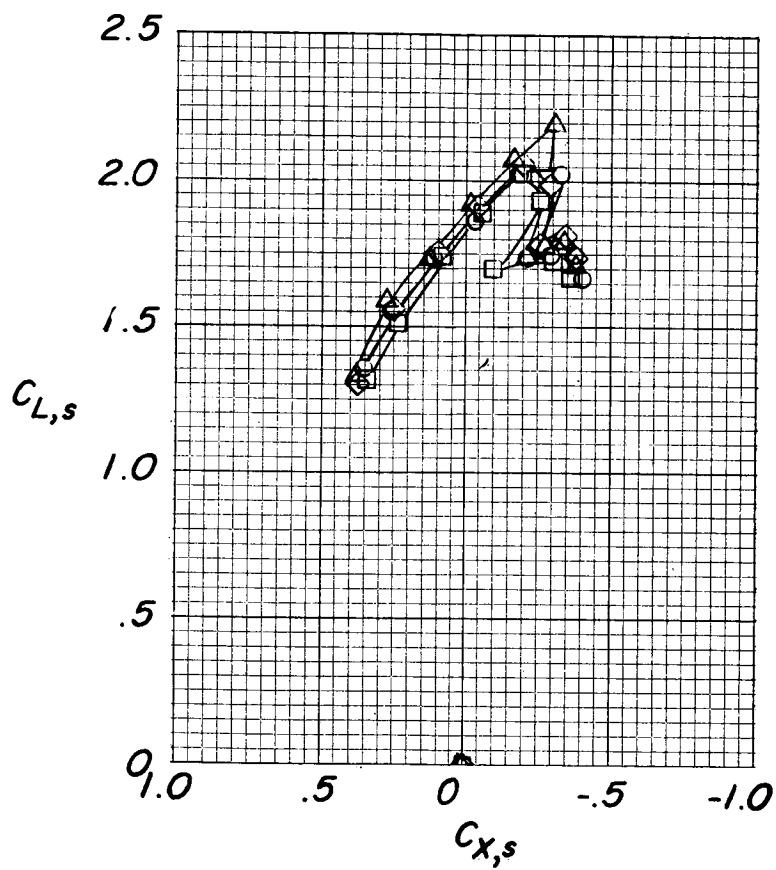


(c) Horizontal-tail normal-force coefficient.

Figure 26.- Concluded.

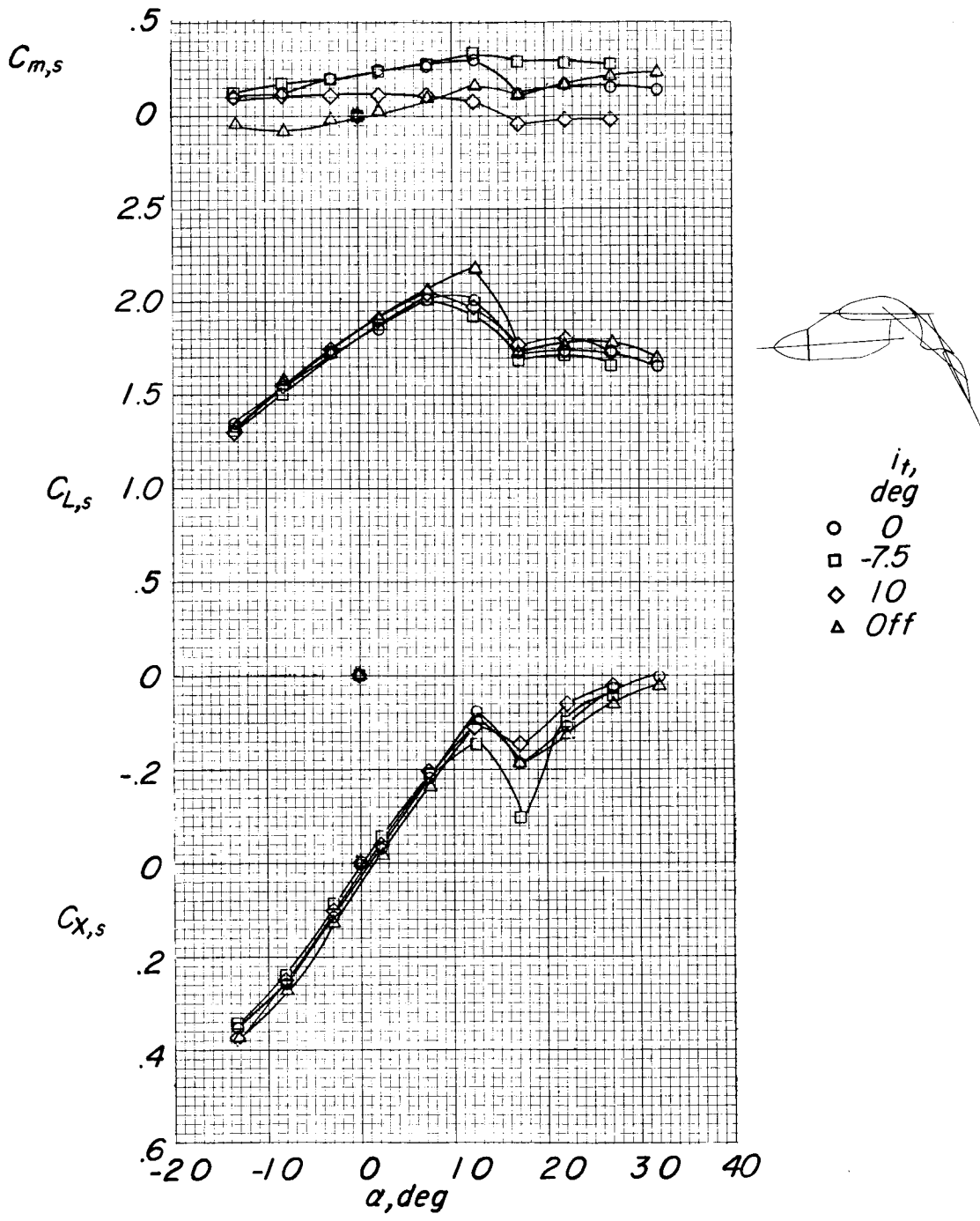


	$i_t$ deg
○	0
□	-7.5
◇	10
△	Off



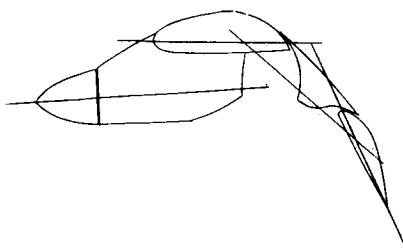
(a) Lift coefficient as function of longitudinal-force coefficient.

Figure 27.- Effect of tail incidence.  $C_{T,s} = 0.744$ ;  $\delta_{f,S}/\delta_{f,R} = 30/20.7$ .



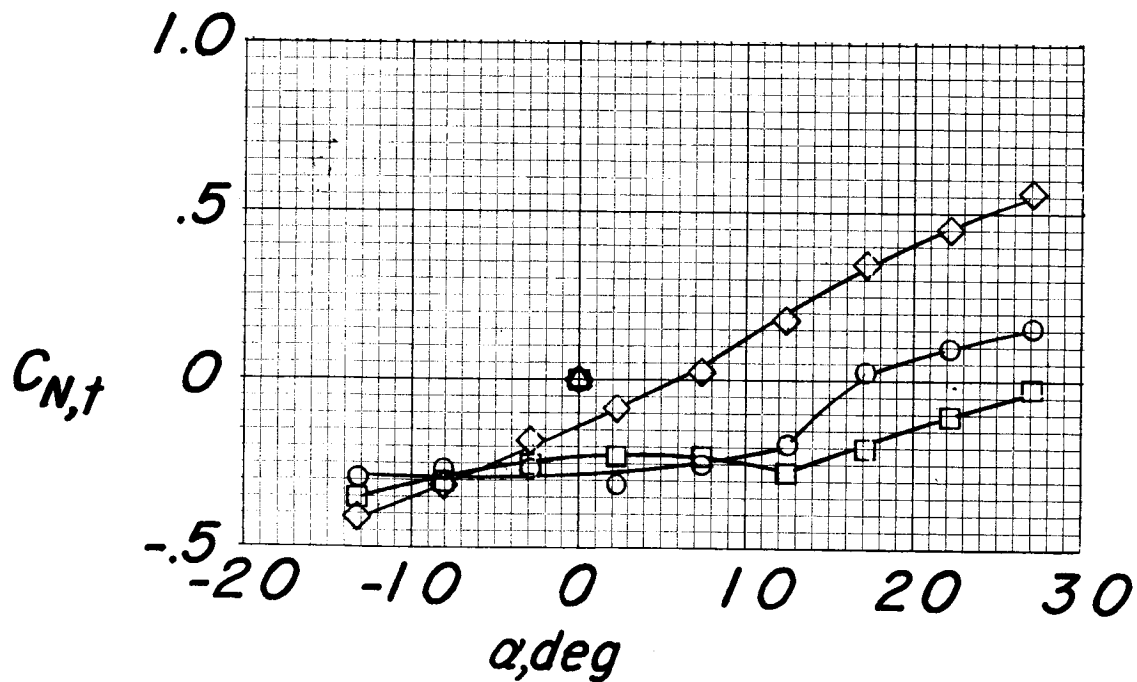
(b) Pitching-moment, lift, and longitudinal-force coefficients.

Figure 27.- Continued.



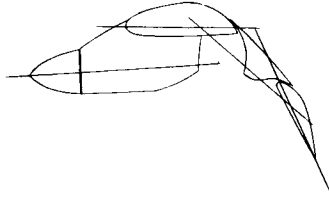
$i_t,$   
 $deg$

○ 0  
 □ -7.5  
 ◇ 10  
 △ Off



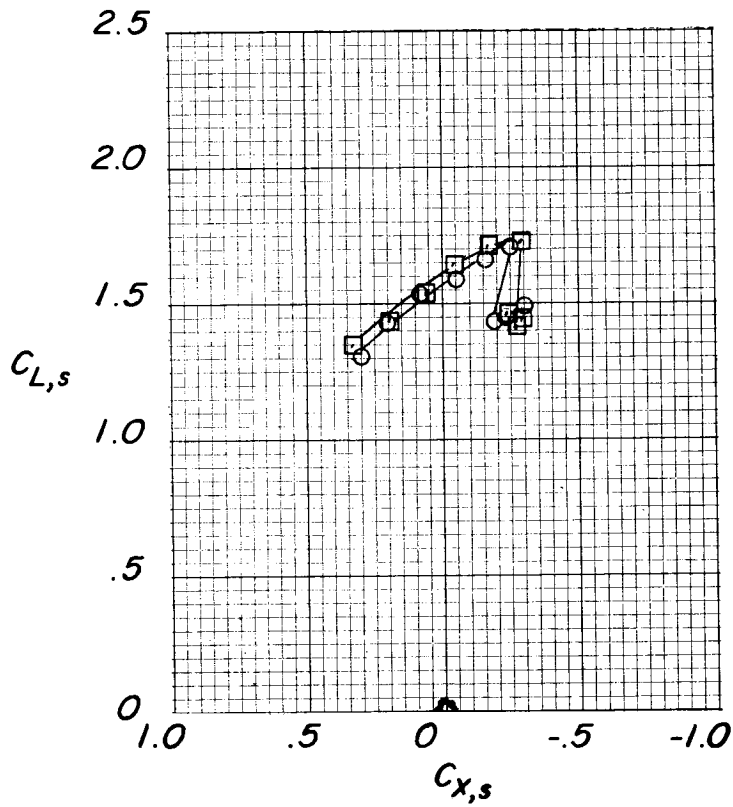
(c) Horizontal-tail normal-force coefficient.

Figure 27.- Concluded.



*i<sub>t</sub>*,  
deg

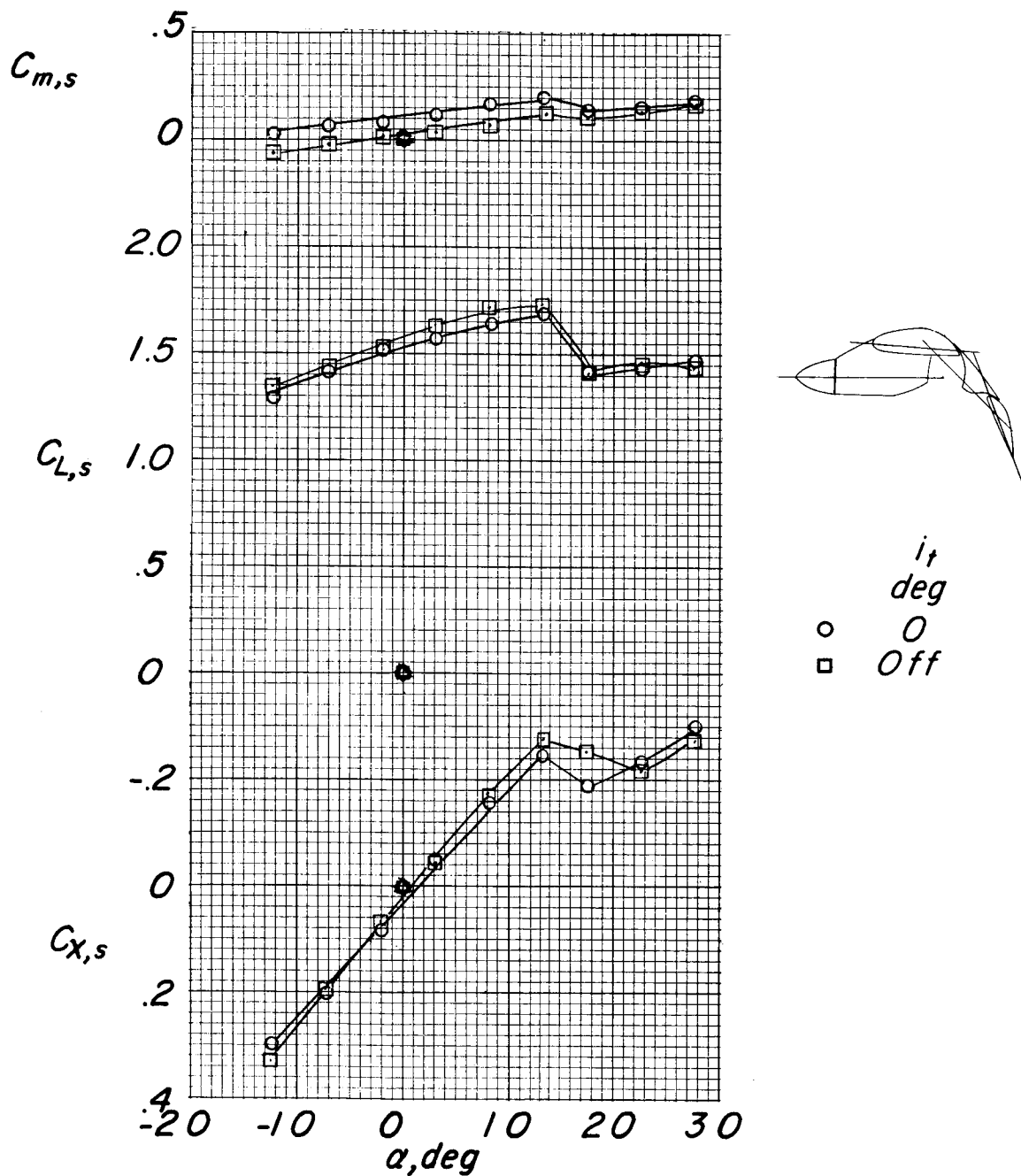
○ 0  
□ Off



(a) Lift coefficient as function of longitudinal-force coefficient.

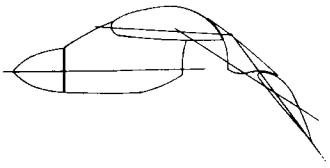
Figure 28.- Effect of tail incidence.  $C_{T,s} = 0.882$ ;  $\delta_{f,S}/\delta_{f,R} = 40/24$ .

I-735

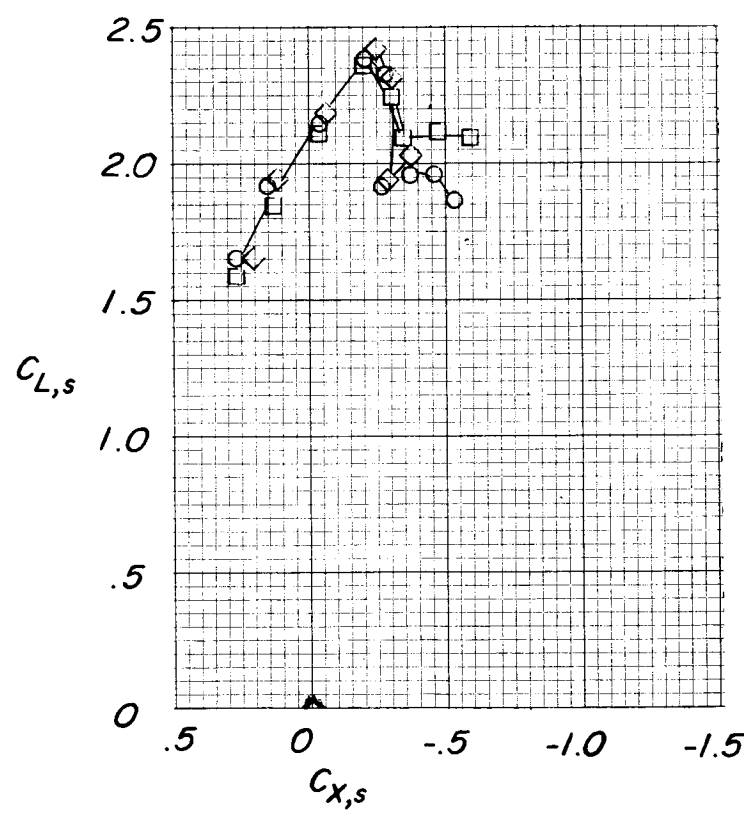


(b) Pitching-moment, lift, and longitudinal-force coefficients.

Figure 28.- Concluded.



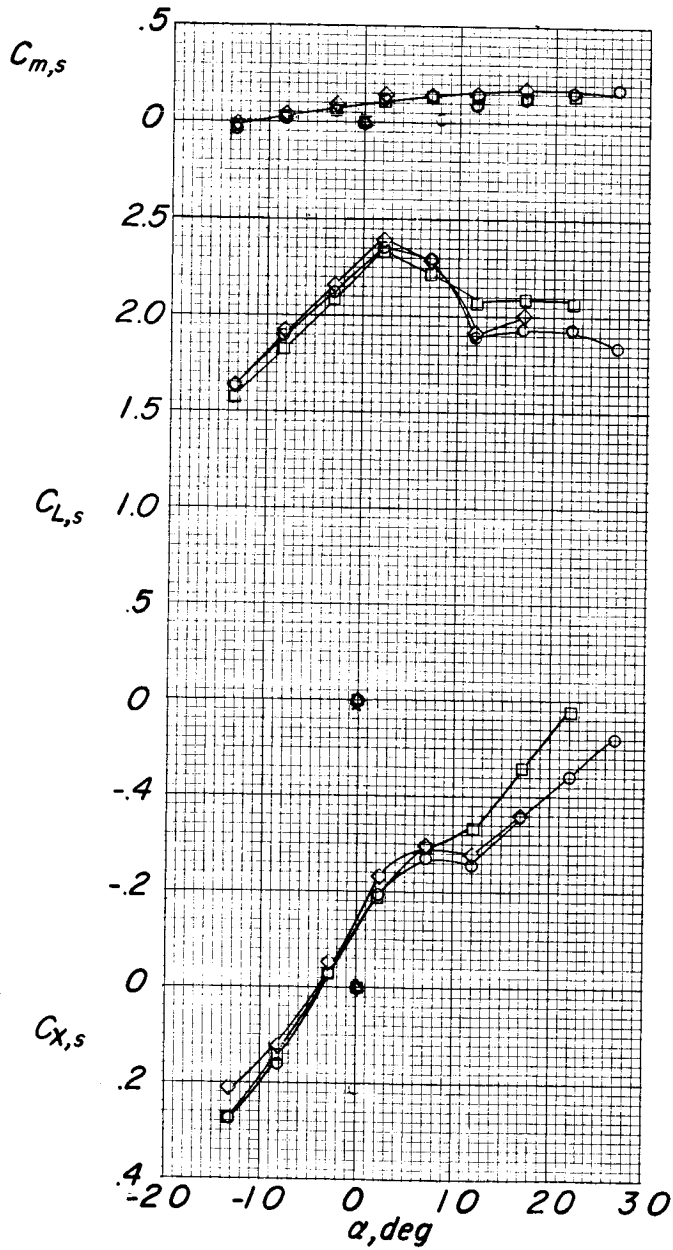
	$i_n,$ deg	Propeller rotation
○	5	Normal
□	5	Inboard reversed
◇	0	Normal



(a) Lift coefficient as function of longitudinal-force coefficient.

Figure 29.- Effect of propeller rotational direction and thrust-line incidence.  $C_{T,s} = 0.603$ ; tail off;  $\delta_{f,S}/\delta_{f,R} = 30/20.7$ .

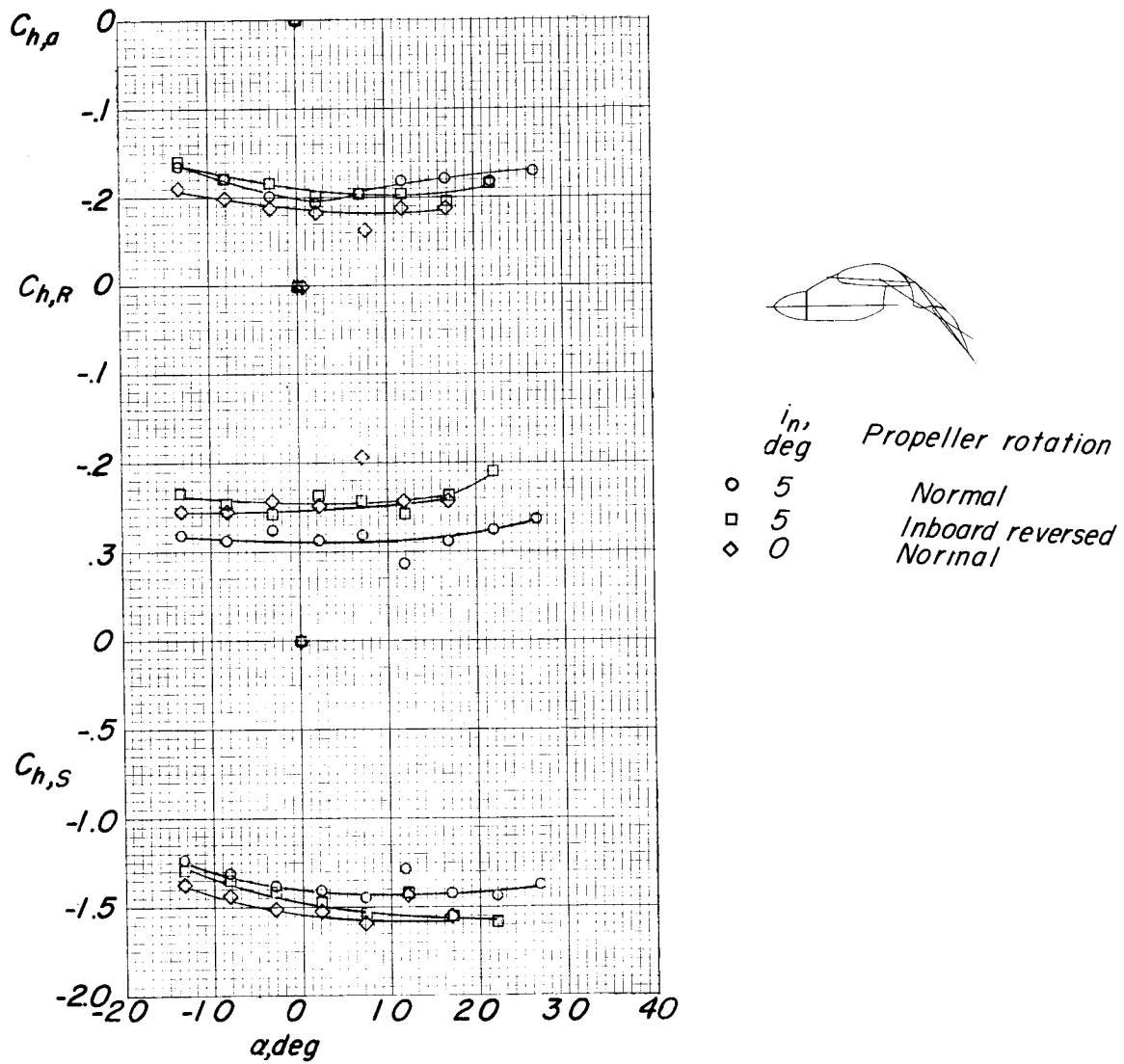
L-755



$i_n$ , deg	Propeller rotation
○ 5	Normal
□ 5	Inboard reversed
◇ 0	Normal

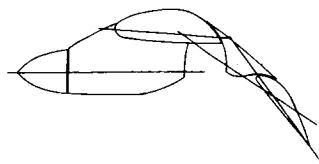
(b) Pitching-moment, lift, and longitudinal-force coefficients.

Figure 29.- Continued.

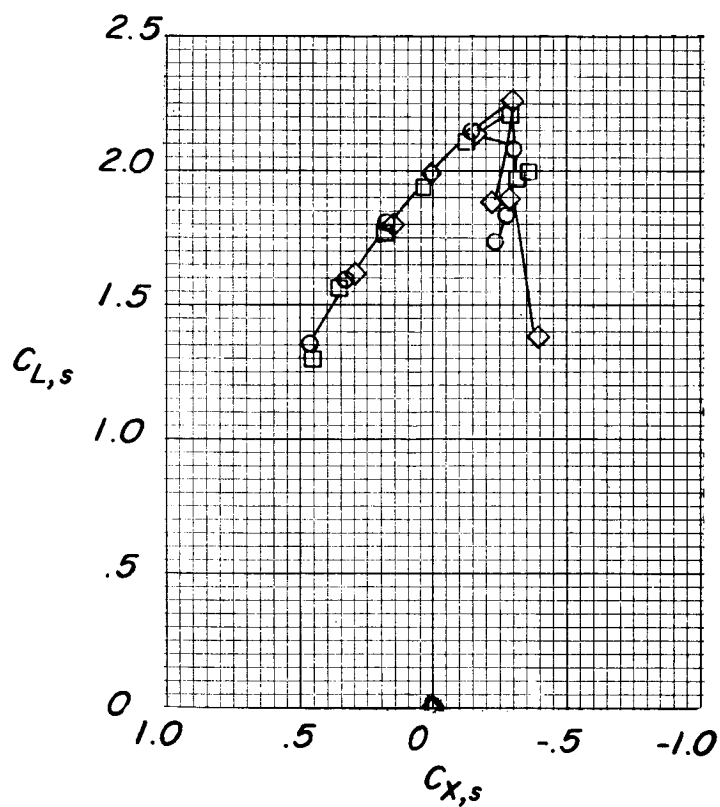


(c) Flap and aileron hinge-moment coefficients.

Figure 29.- Concluded.

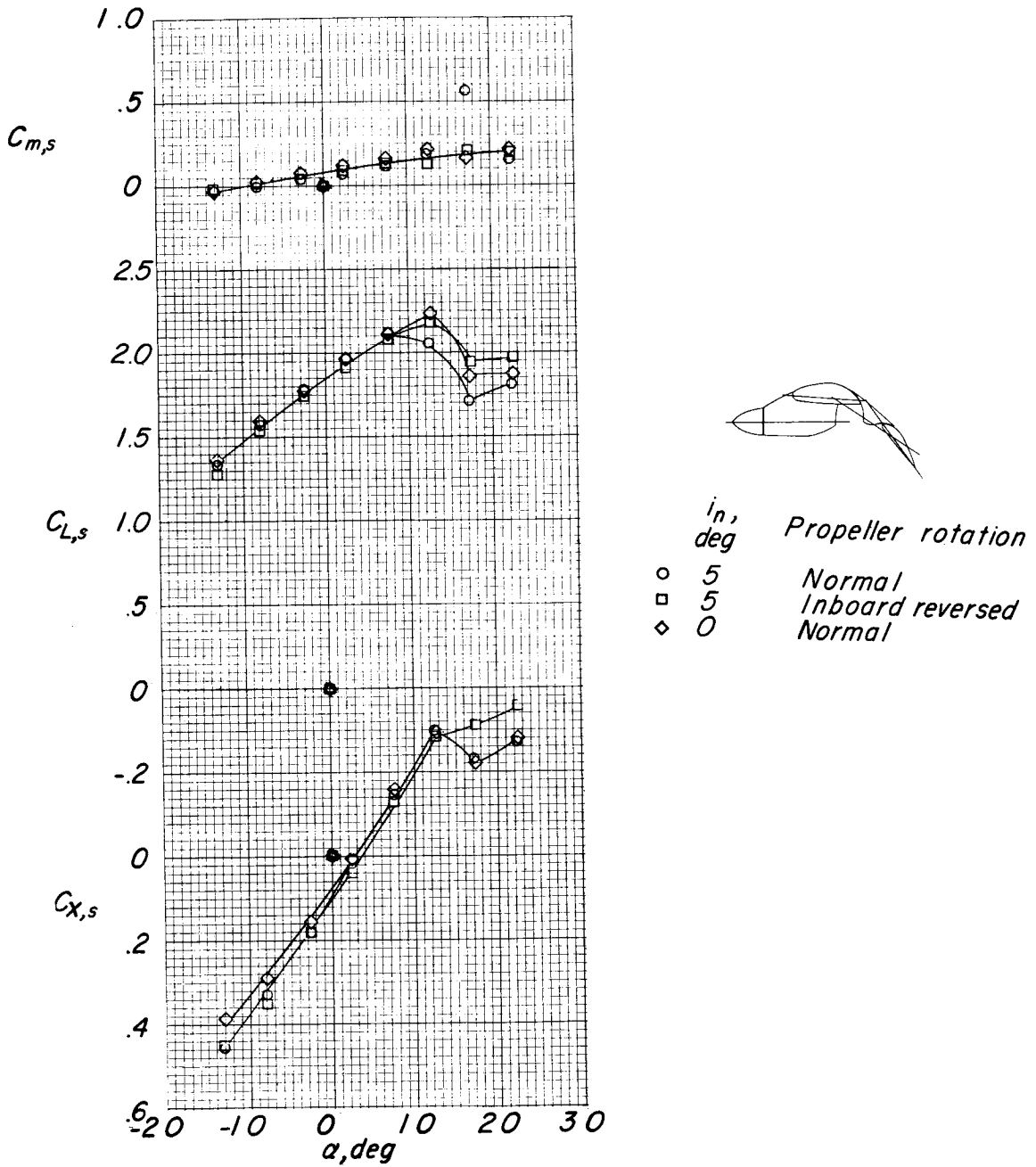


$i_n$ , deg	<i>Propeller rotation</i>
○ 5	<i>Normal</i>
□ 5	<i>Inboard reversed</i>
◇ 0	<i>Normal</i>



(a) Lift coefficient as function of longitudinal-force coefficient.

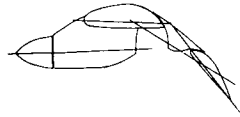
Figure 30.- Effect of propeller rotational direction and thrust-line incidence.  $C_{T,s} = 0.744$ ; tail off;  $\delta_{f,S}/\delta_{f,R} = 30/20.7$ .



(b) Pitching-moment, lift, and longitudinal-force coefficients.

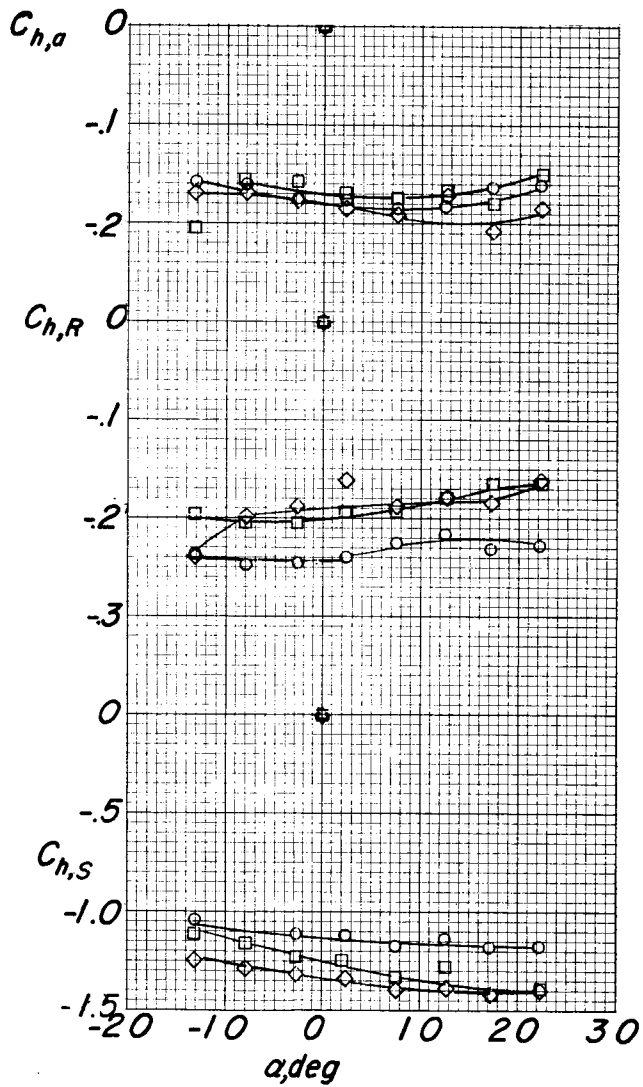
Figure 30.- Continued.

L-735



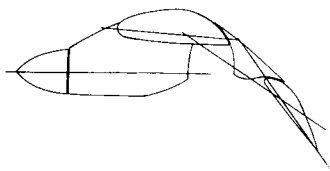
$i_n,$   
deg      Propeller rotation

- 5      Normal
- 5      Inboard reversed
- ◇ 0      Normal

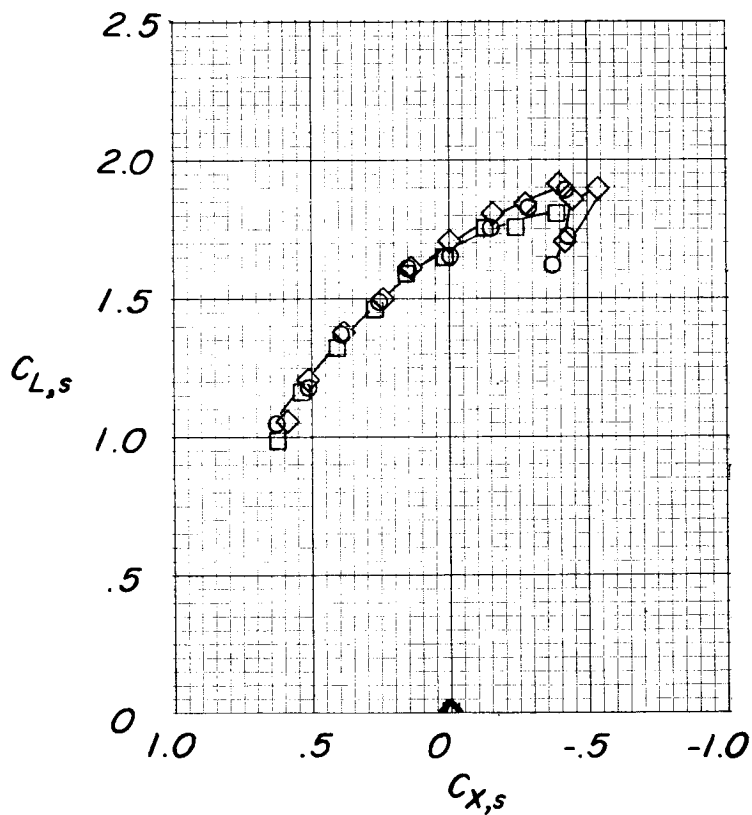


(c) Flap and aileron hinge-moment coefficients.

Figure 30.- Concluded.

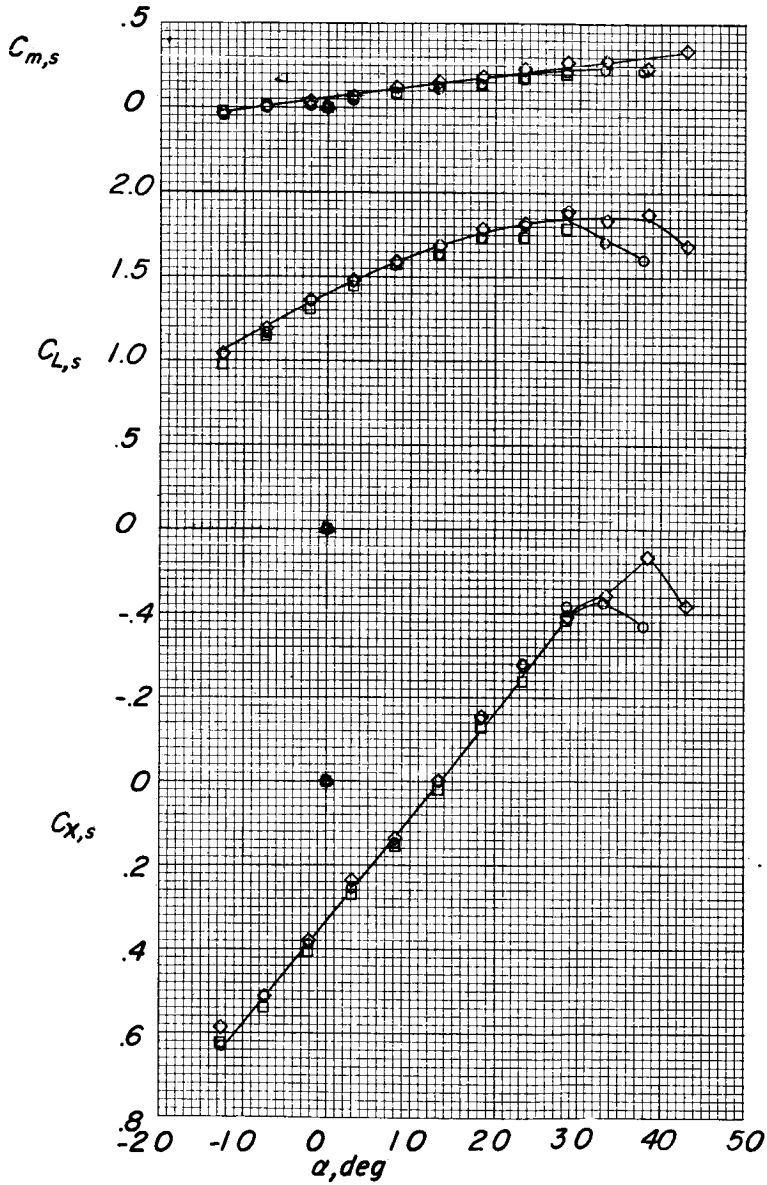


$i_n$ , deg	Propeller rotation
○	5 Normal
□	5 Inboard reversed
◇	0 Normal



(a) Lift coefficient as function of longitudinal-force coefficient.

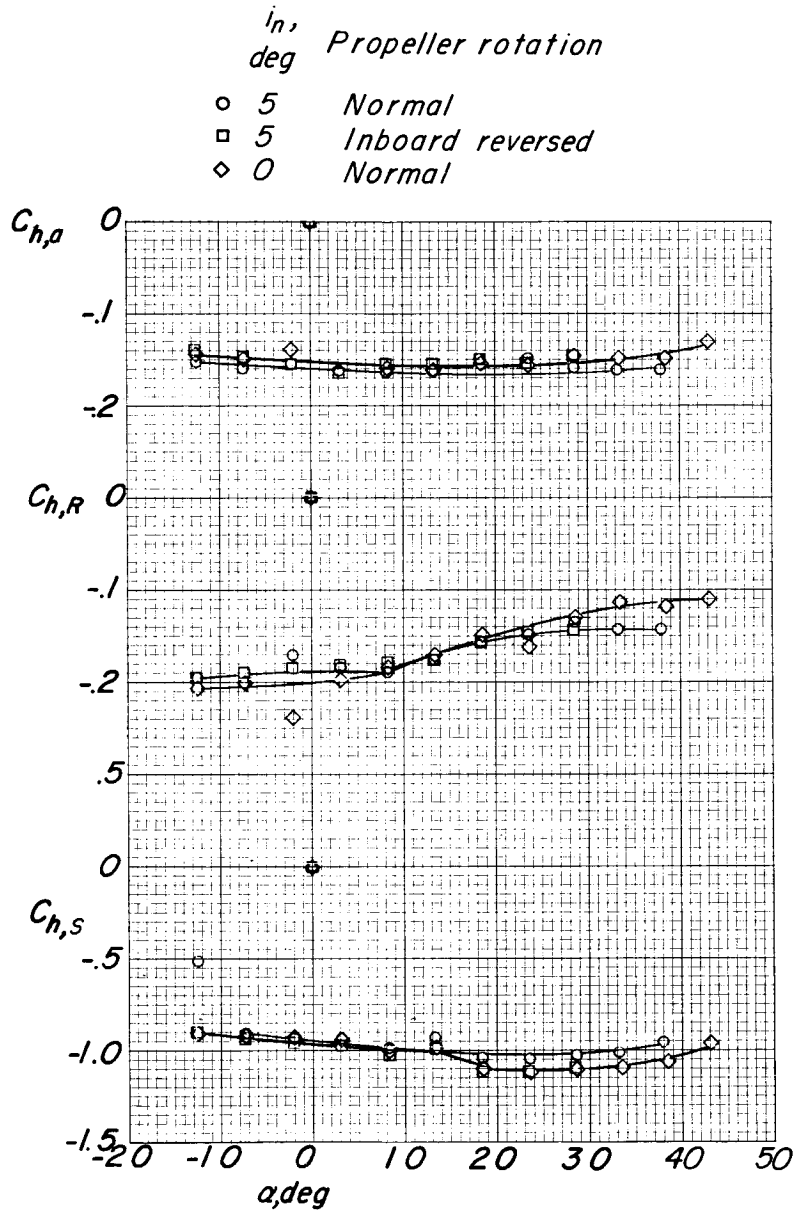
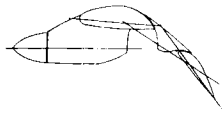
Figure 31.- Effect of propeller rotational direction and thrust-line incidence.  $C_{T,s} = 0.882$ ; tail off;  $\delta_{f,s}/\delta_{f,R} = 30/20.7$ .



(b) Pitching-moment, lift, and longitudinal-force coefficients.

Figure 31.- Continued.

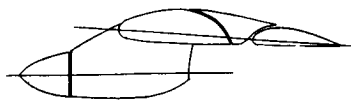
L-735



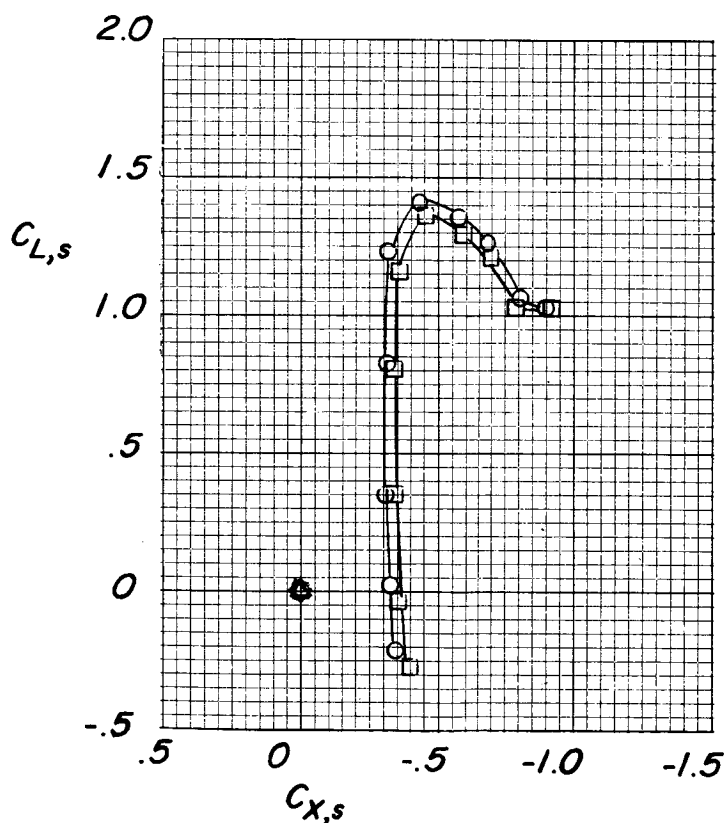
I-735

(c) Flap and aileron hinge-moment coefficients.

Figure 31.- Concluded.

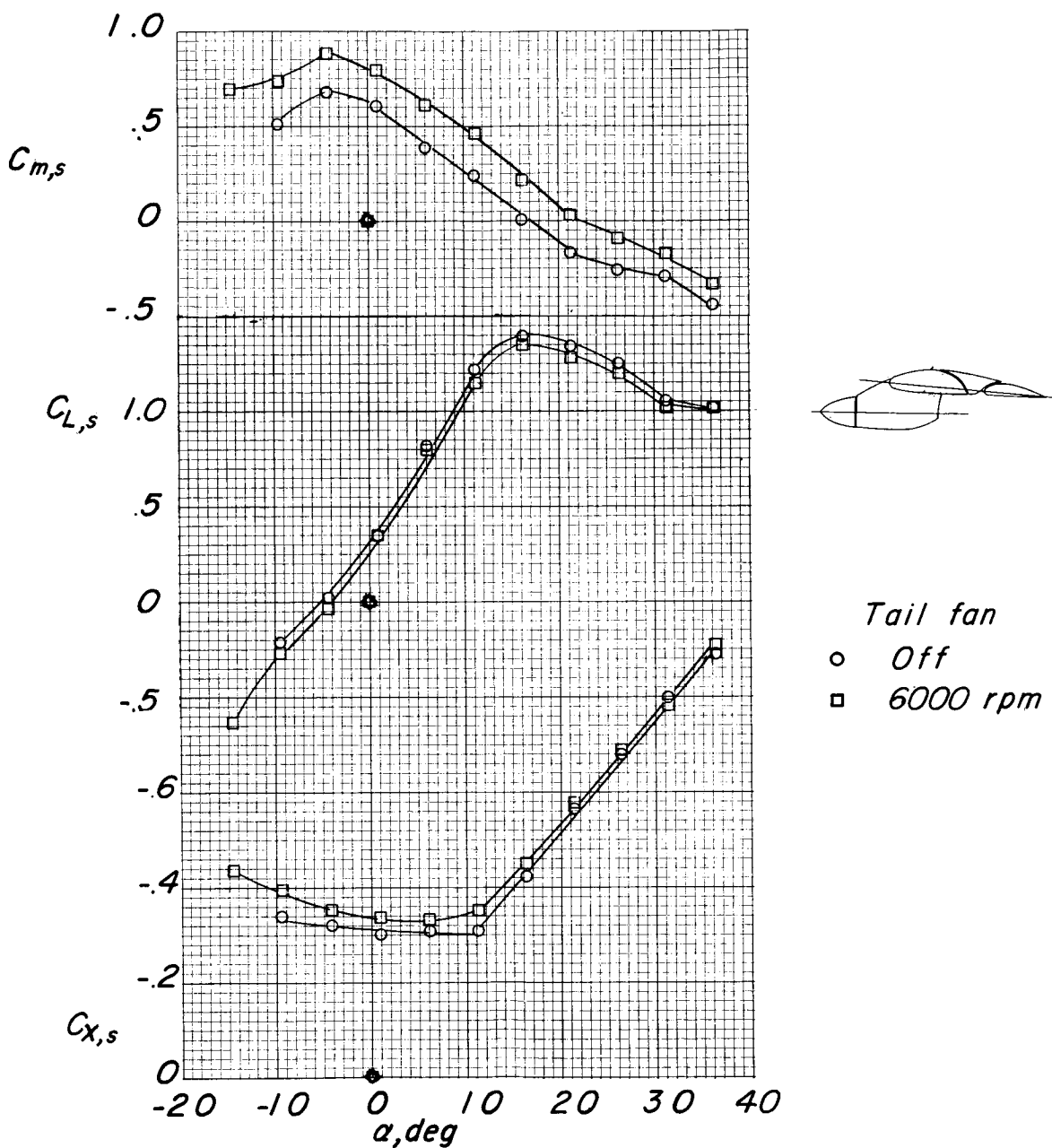


Tail fan  
 ○ Off  
 □ 6000 rpm



(a) Lift coefficient as function of longitudinal-force coefficient.

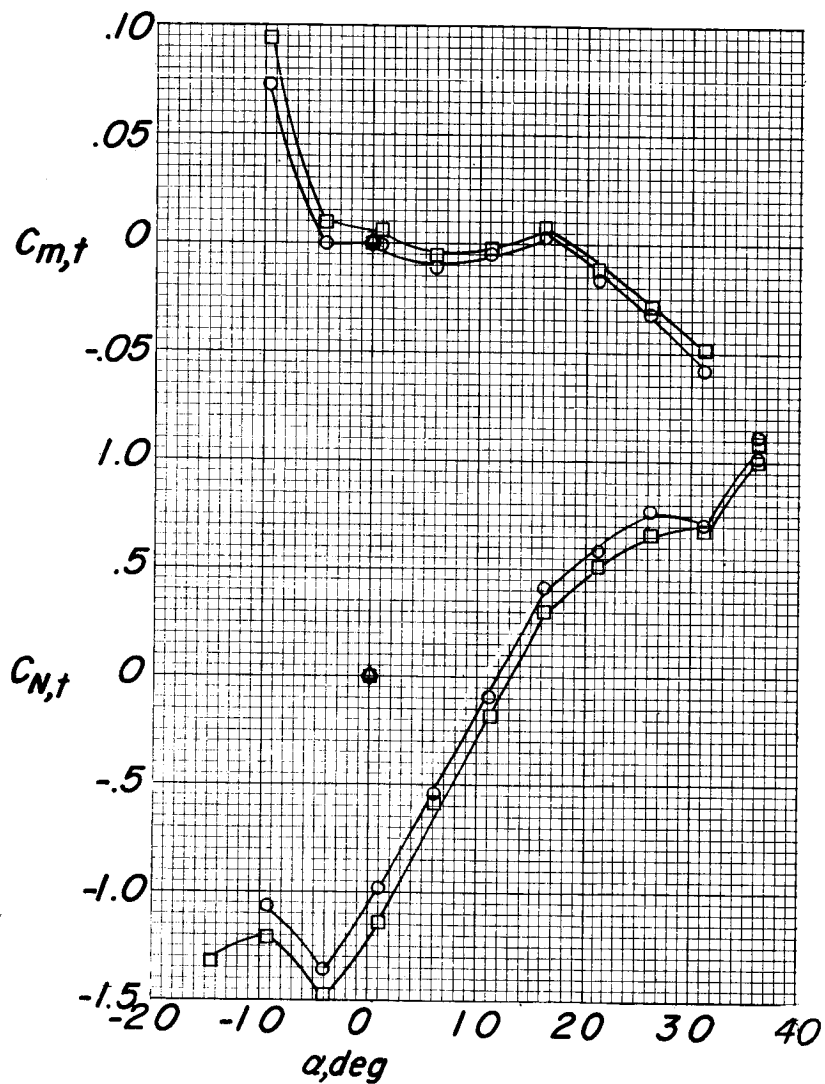
Figure 32.- Effect of tail fan. Propellers windmilling;  $i_t = -7.5^\circ$ ;  
 $\delta_{f,S}/\delta_{f,R} = 0/0$ .



(b) Pitching-moment, lift, and longitudinal-force coefficients.

Figure 32.- Continued.

L-735

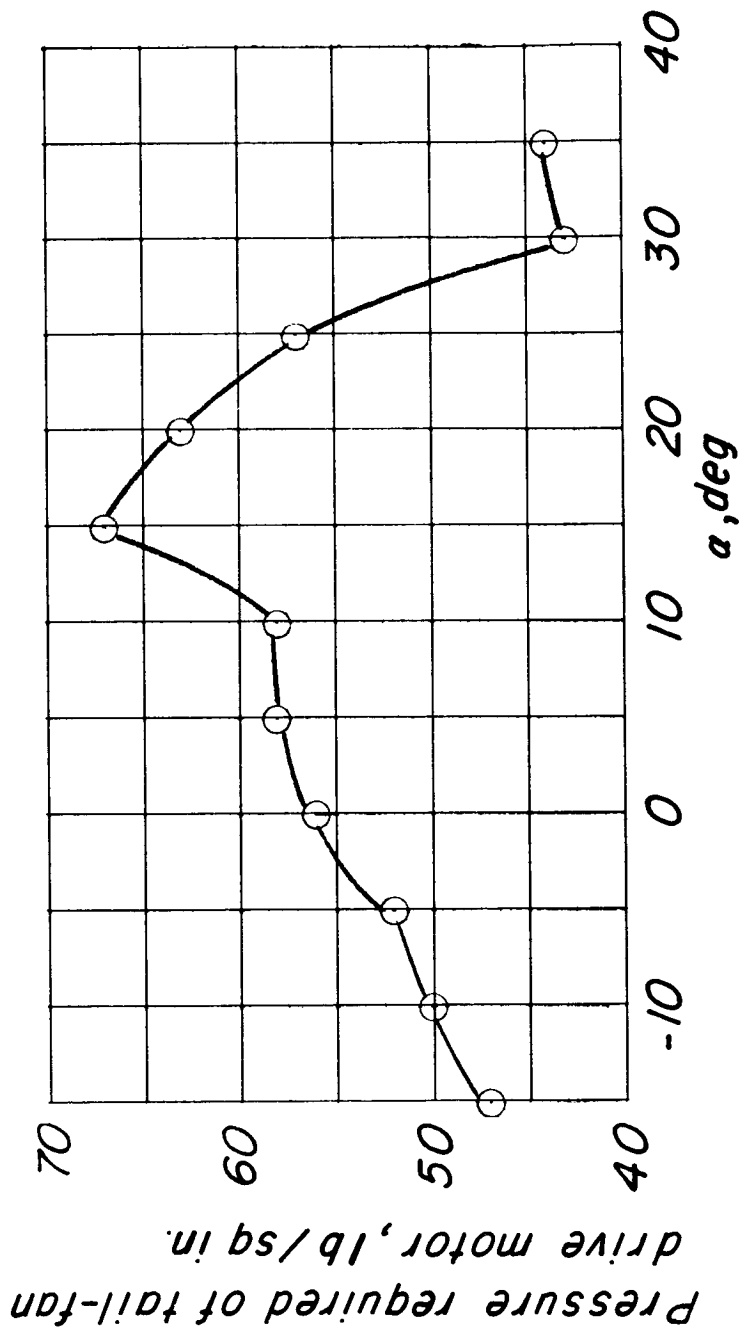


Tail fan

- Off
- 6000 rpm

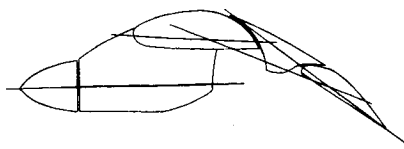
(c) Horizontal-tail pitching-moment and normal-force coefficients.

Figure 32.- Continued.



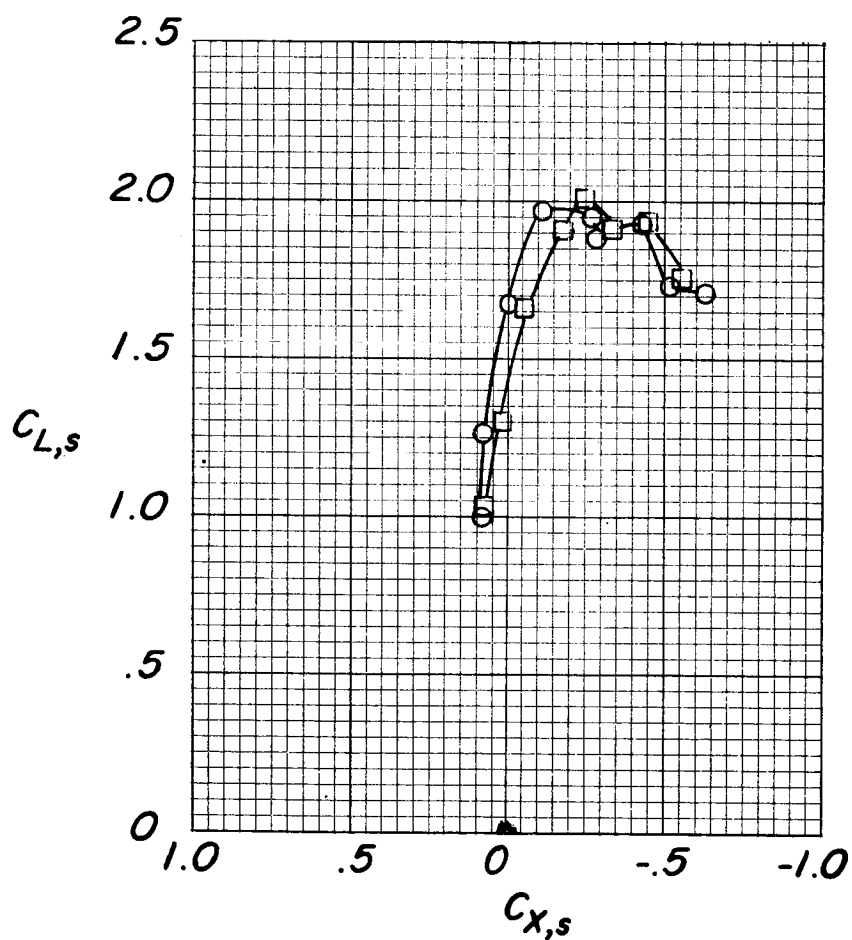
(d) Tail-fan pressure required for propeller rotational speed of 6,000 rpm.

Figure 32.- Concluded.



*Tail fan*

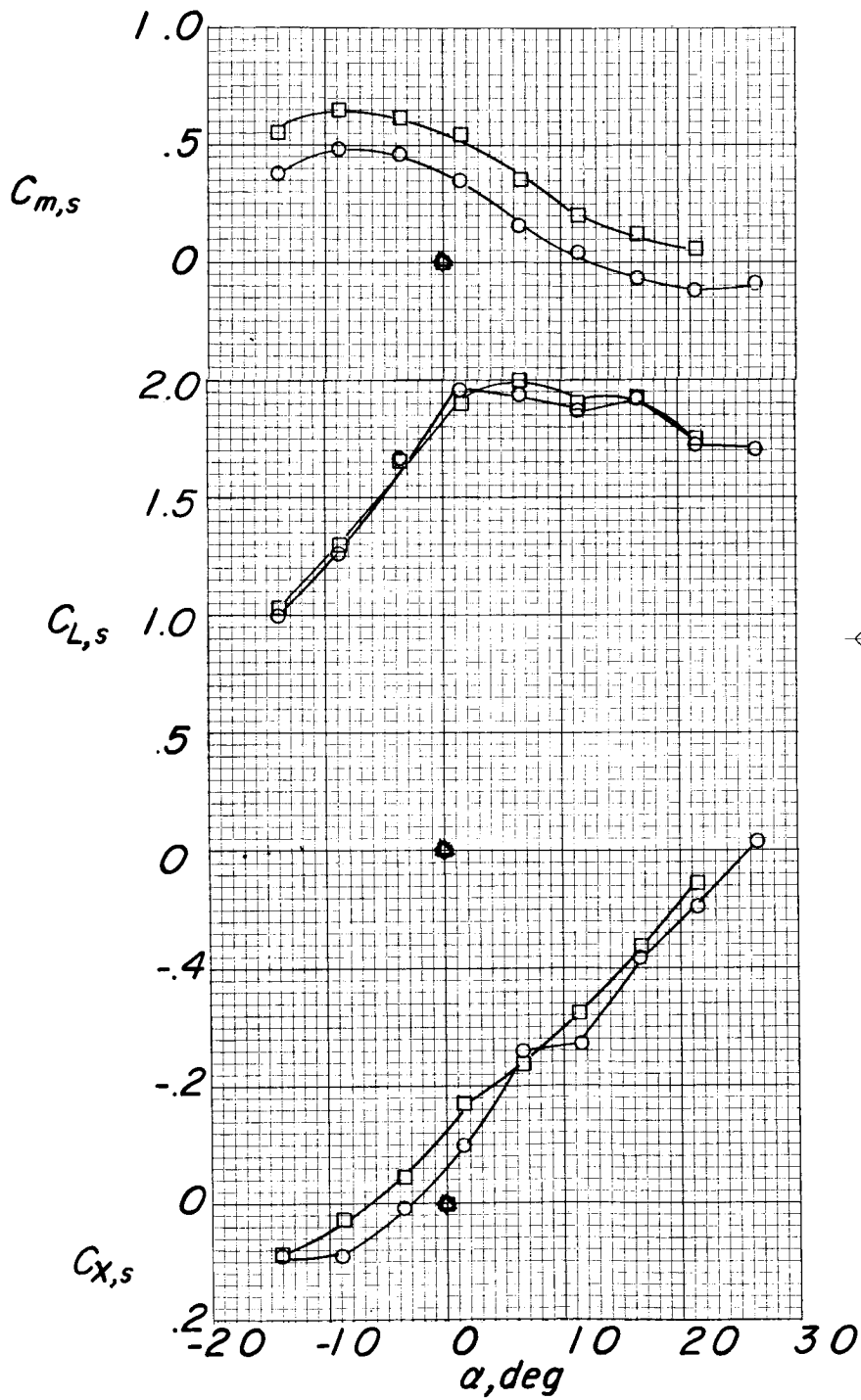
- *Off*
- *6000 rpm*



(a) Lift coefficient as function of longitudinal-force coefficient.

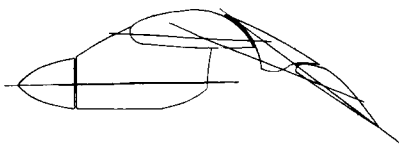
Figure 33.- Effect of tail fan.  $C_{T,S} = 0.366$ ;  $i_t = 0^\circ$ ;

$$\delta_{f,S}/\delta_{f,R} = 20/15.$$



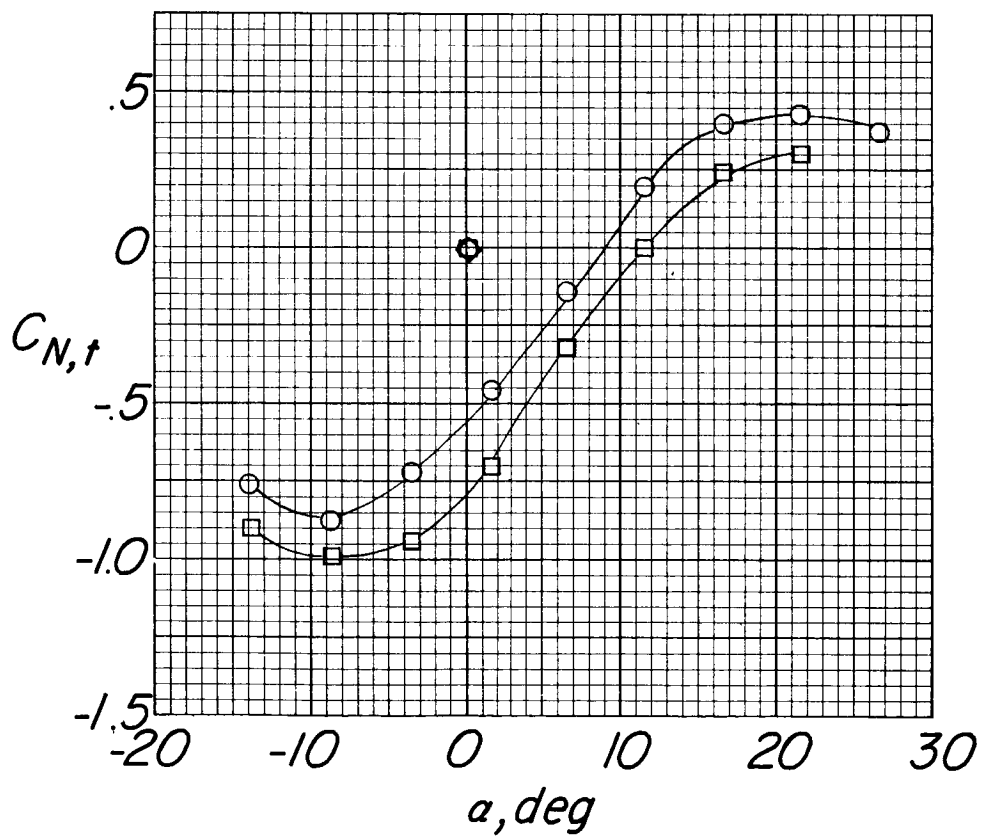
(b) Pitching-moment, lift, and longitudinal-force coefficients.

Figure 33.- Continued.



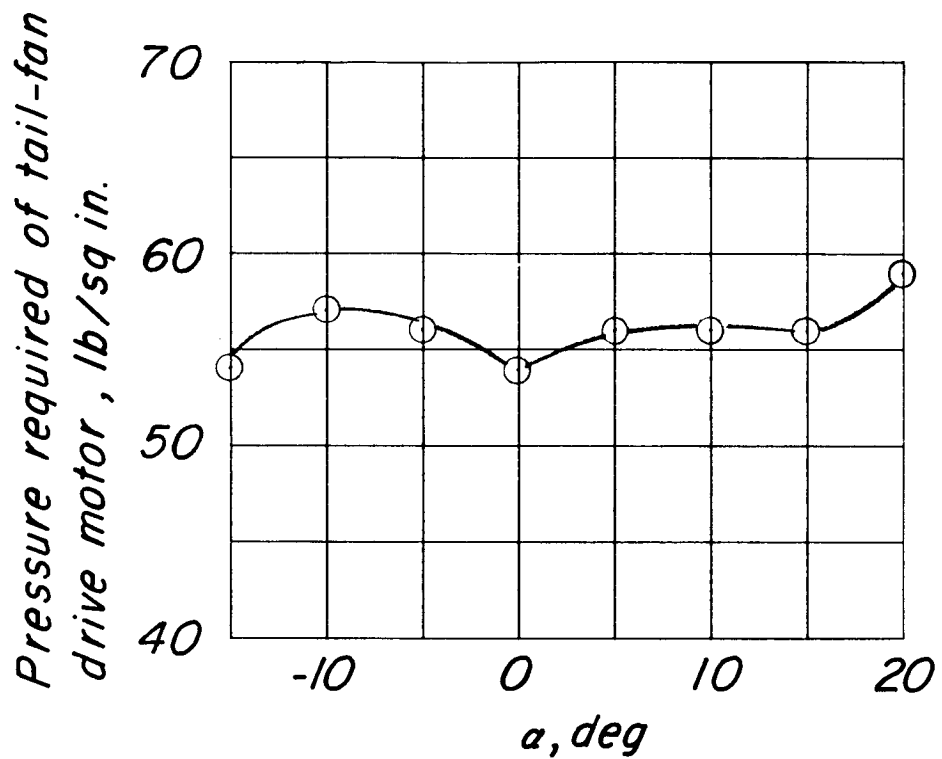
*Tail fan*

- *Off*
- *6000 rpm*



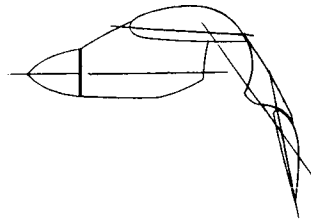
(c) Horizontal-tail normal-force coefficient.

Figure 33.- Continued.



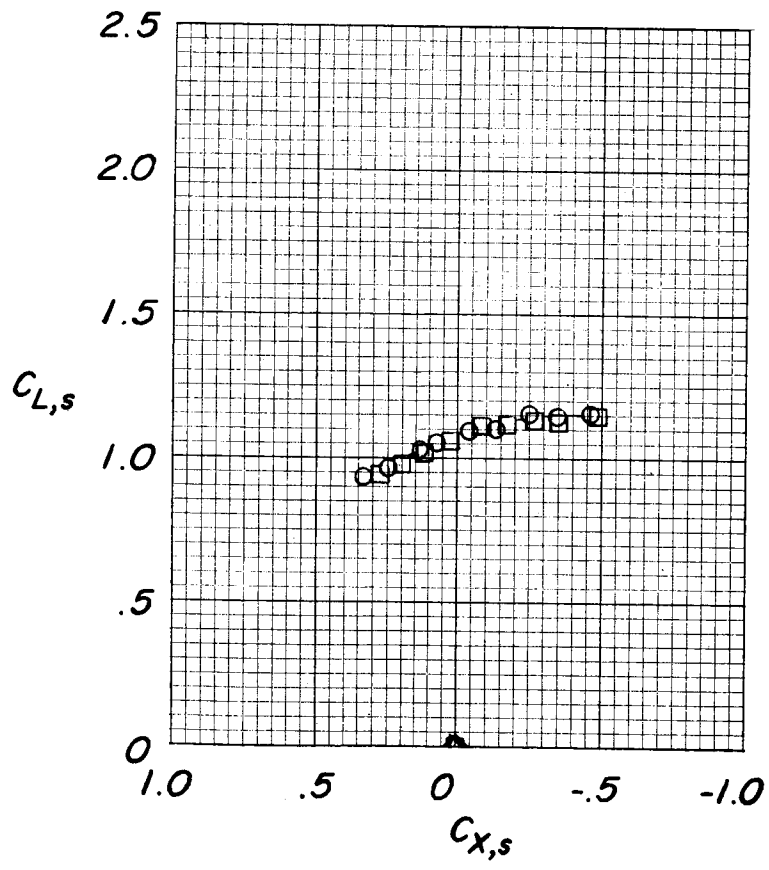
(d) Tail-fan pressure required for propeller rotational speed of 6,000 rpm.

Figure 33.- Concluded.



*Tail fan*

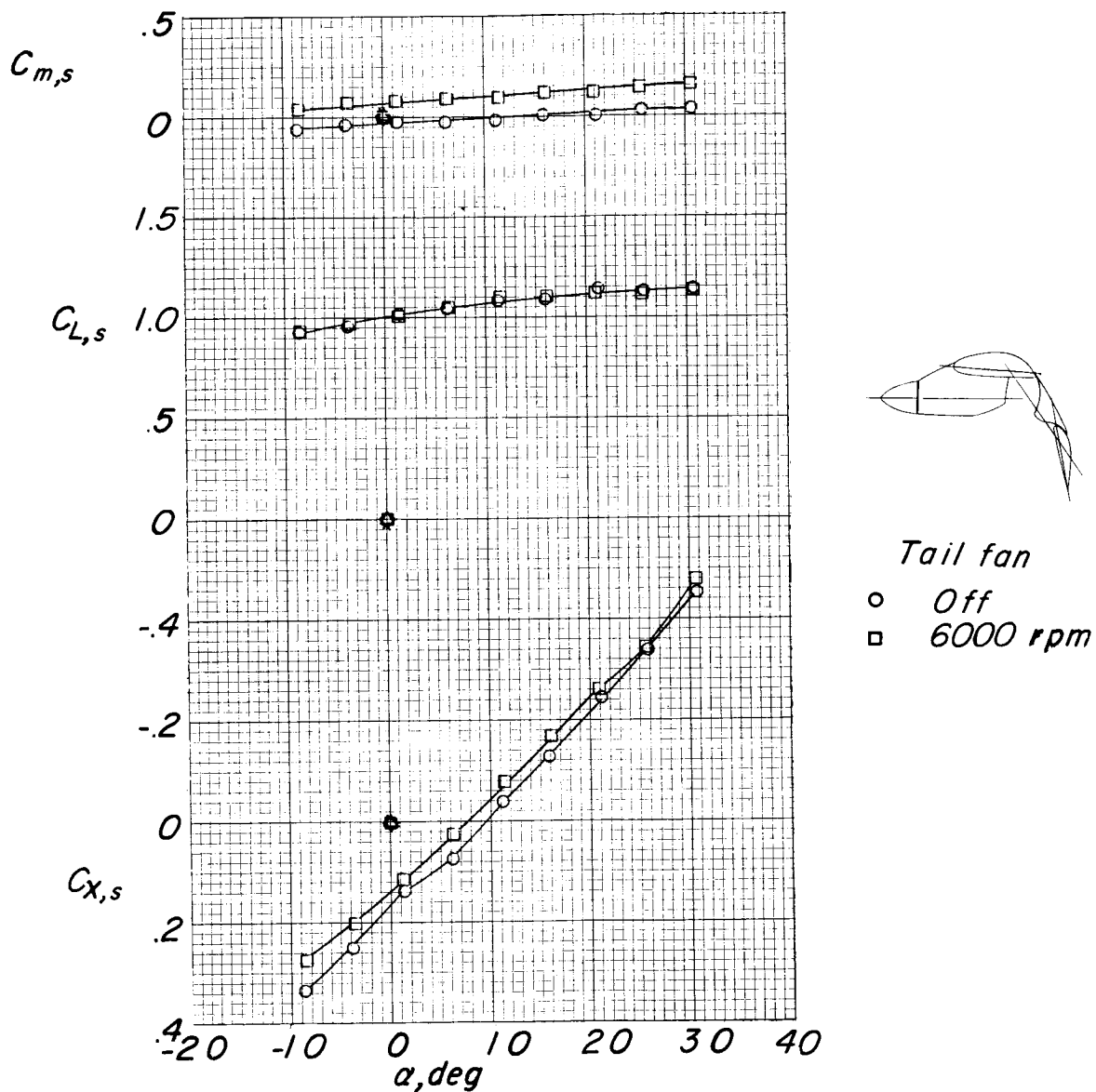
- *Off*
- *6000 rpm*



(a) Lift coefficient as function of longitudinal-force coefficient.

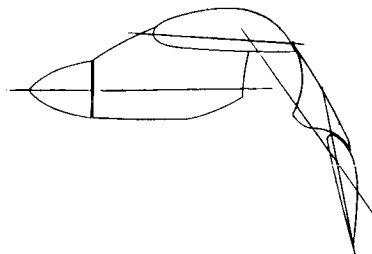
Figure 34.- Effect of tail fan.  $C_{T,s} = 0.978$ ;  $i_t = 0^\circ$ ;  
 $\delta_{f,S}/\delta_{f,R} = 50/25$ .

L-735



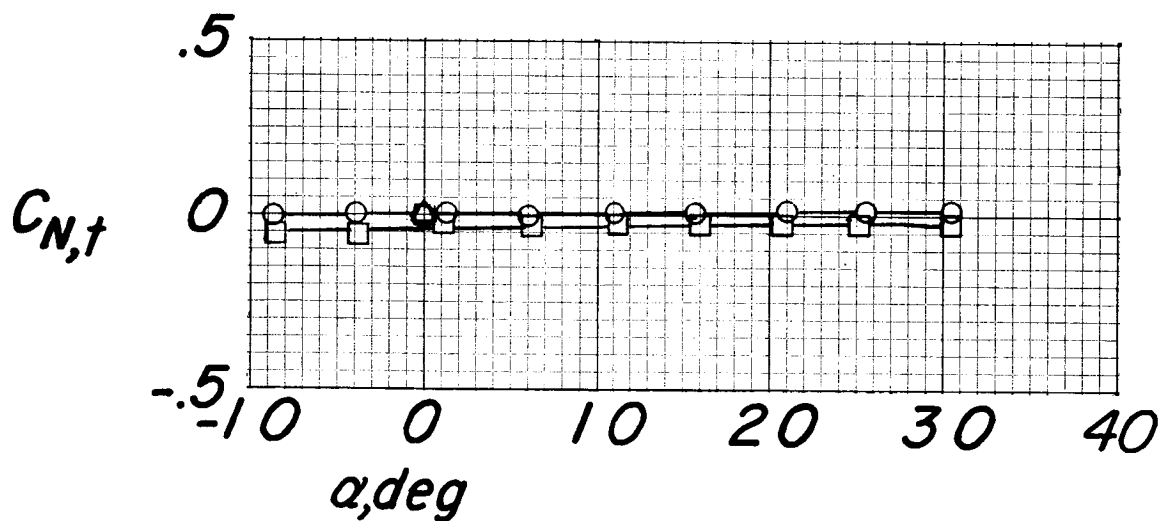
(b) Pitching-moment, lift, and longitudinal-force coefficients.

Figure 34.- Continued.



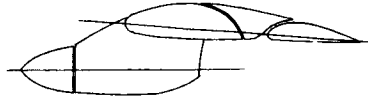
*Tail fan*

- *Off*
- *6000 rpm*



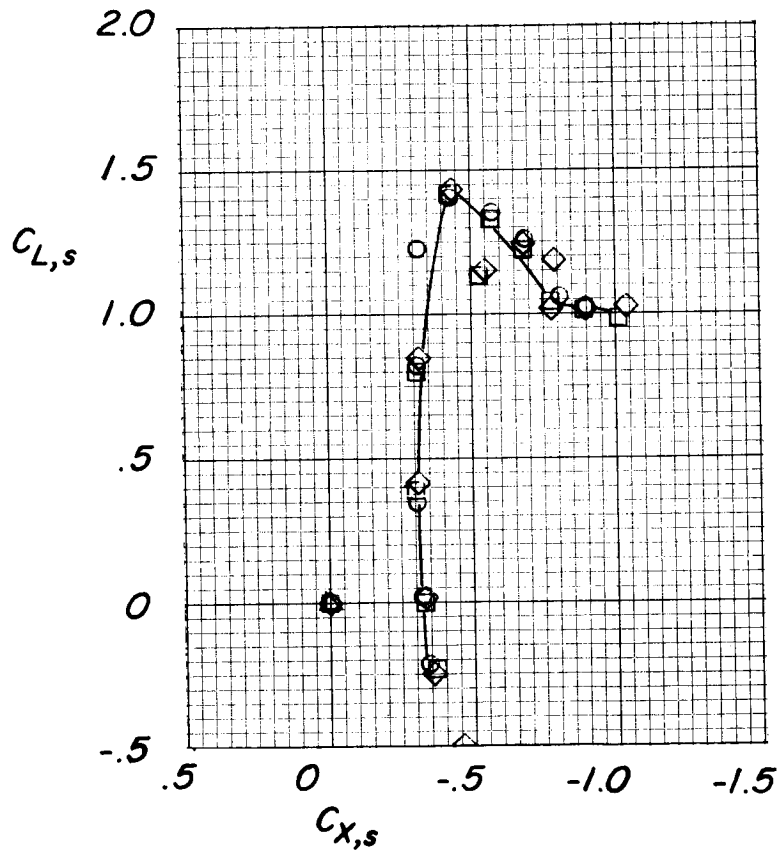
(c) Horizontal-tail normal-force coefficient.

Figure 34.- Concluded.



$\delta_{tab}$ ,  
deg

○ 0  
□ 5  
◇ 10

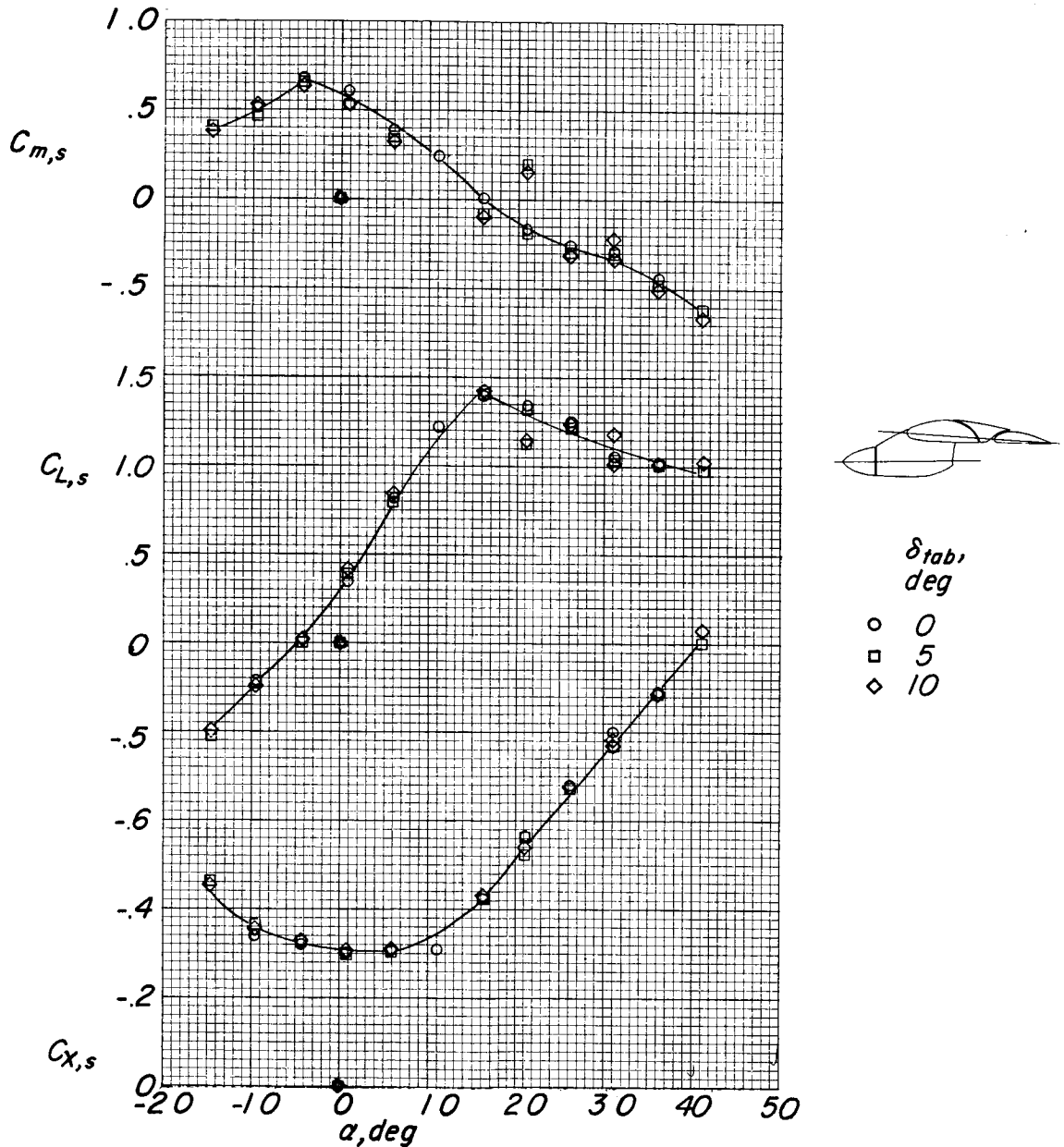


(a) Lift coefficient as function of longitudinal-force coefficient.

Figure 35.- Effect of tab setting. Propellers windmilling;  $i_t = -7.5^\circ$ ;

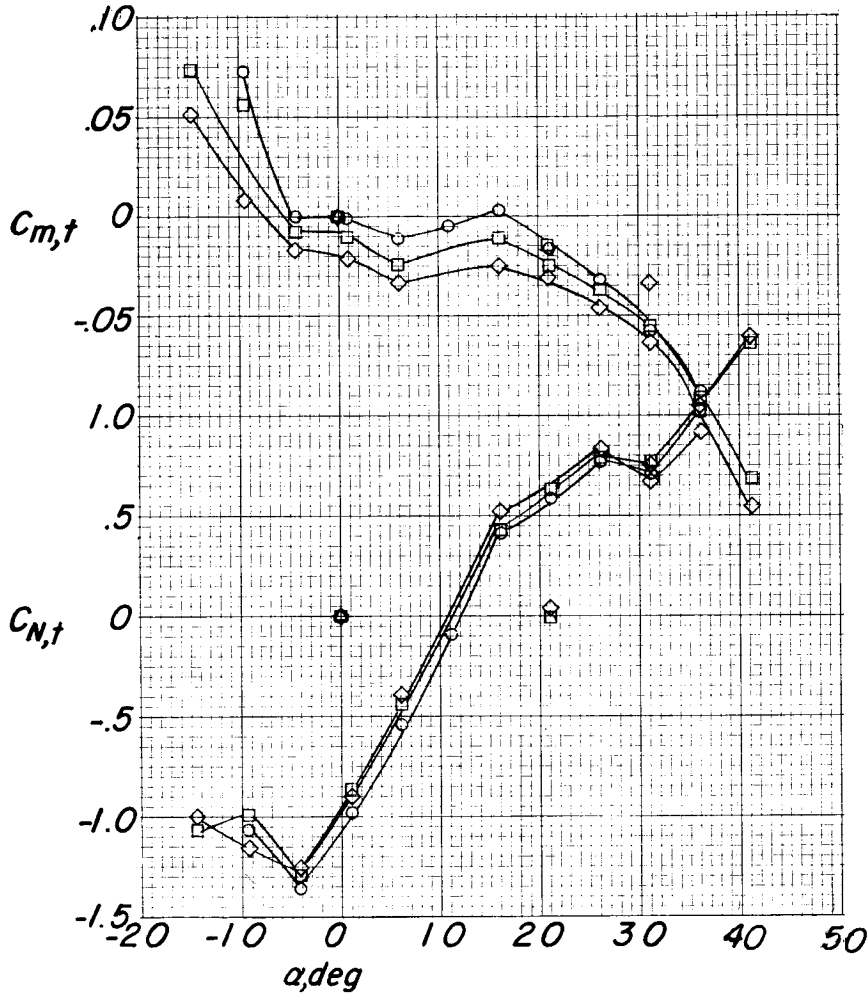
$$\delta_{f,S}/\delta_{f,R} = 0/0.$$

L-735



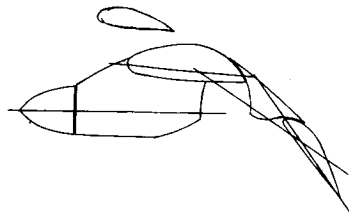
(b) Pitching-moment, lift, and longitudinal-force coefficients.

Figure 35.- Continued.



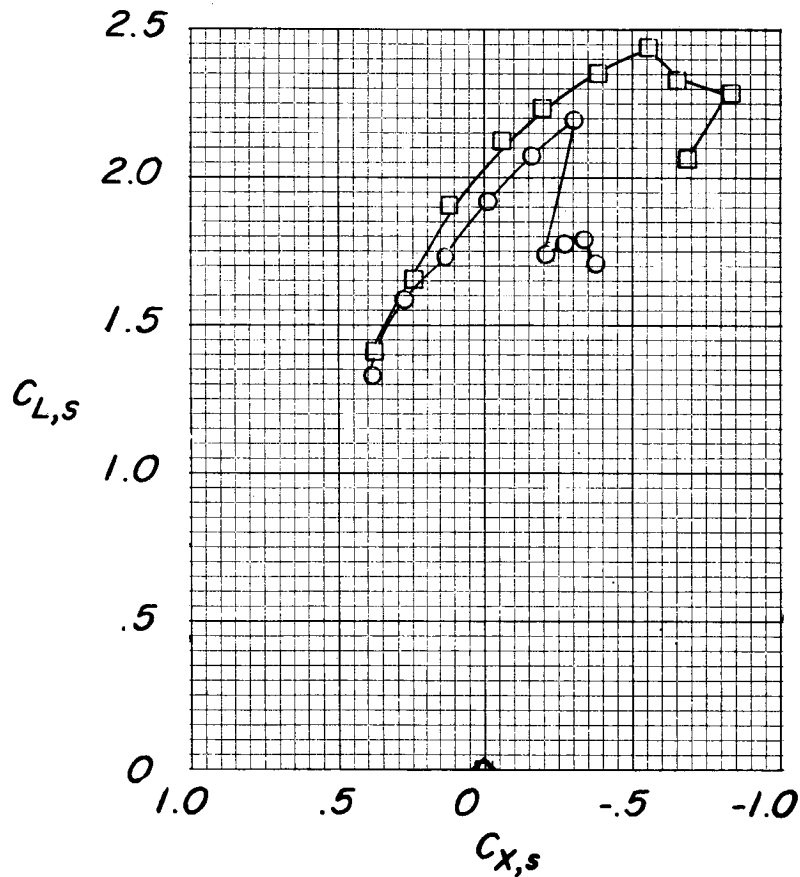
(c) Horizontal-tail pitching-moment and normal-force coefficients.

Figure 35.- Concluded.



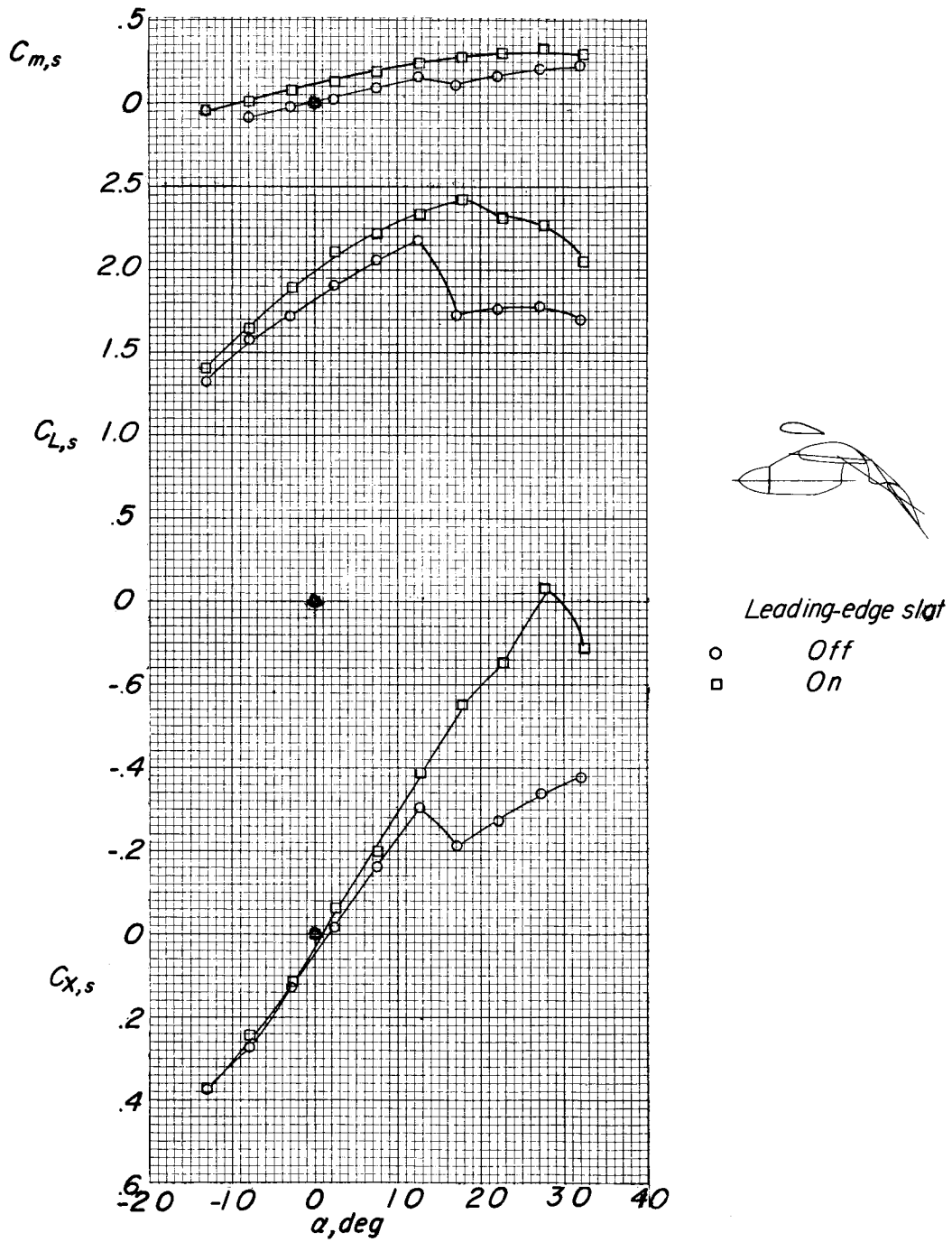
Leading-edge slat

○ Off  
 □ On



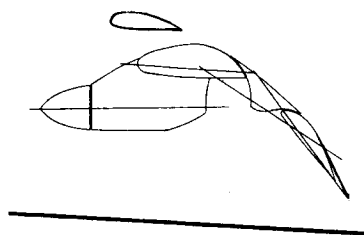
(a) Lift coefficient as function of longitudinal-force coefficient.

Figure 36.- Effect of leading-edge slat.  $C_{T,s} = 0.744$ ; tail off;  
 $\delta_{f,s}/\delta_{f,R} = 30/20.7$ .

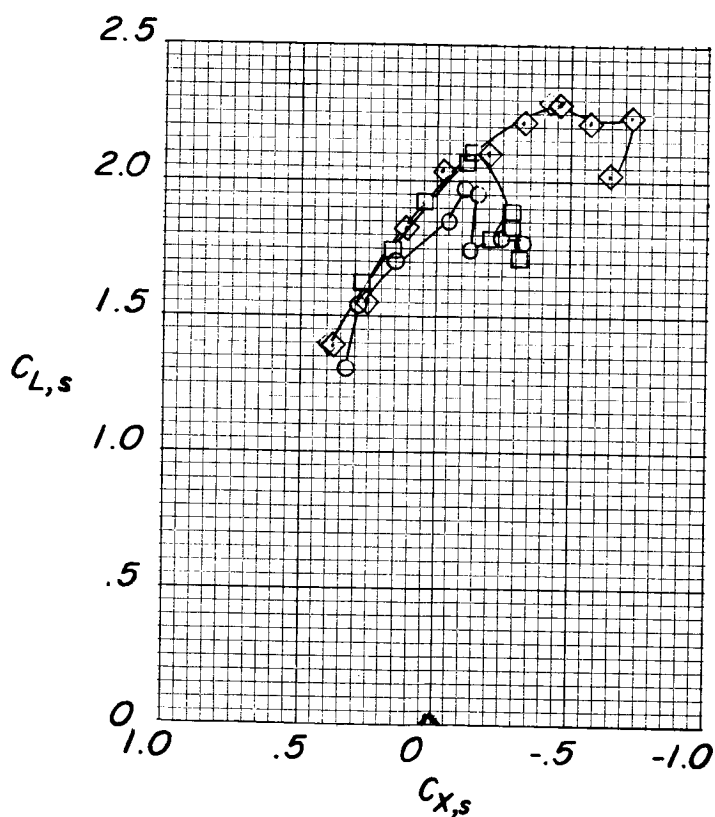


(b) Pitching-moment, lift, and longitudinal-force coefficients.

Figure 36.- Concluded.

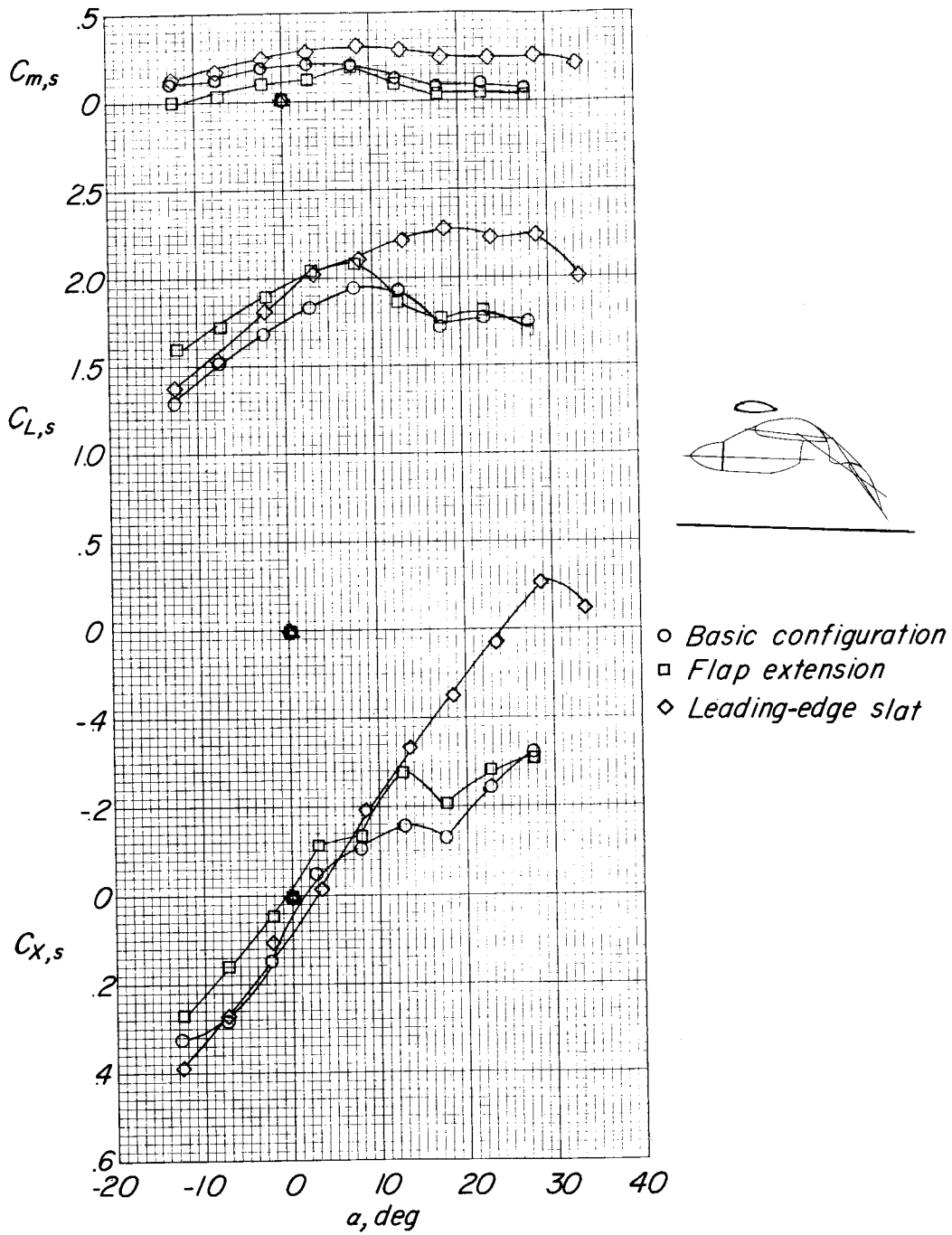


- *Basic configuration*
- *Flap extension*
- ◇ *Leading-edge slat*



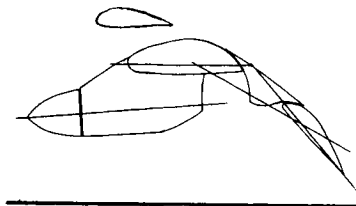
(a) Lift coefficient as function of longitudinal-force coefficient.

Figure 37.- Effect of flap extension or leading-edge slat in region of ground effect.  $C_{T,s} = 0.745$ ;  $i_t = 0^\circ$ ;  $\delta_{f,s}/\delta_{f,R} = 30/20.7$ ;  $h/D = 1.0$ .



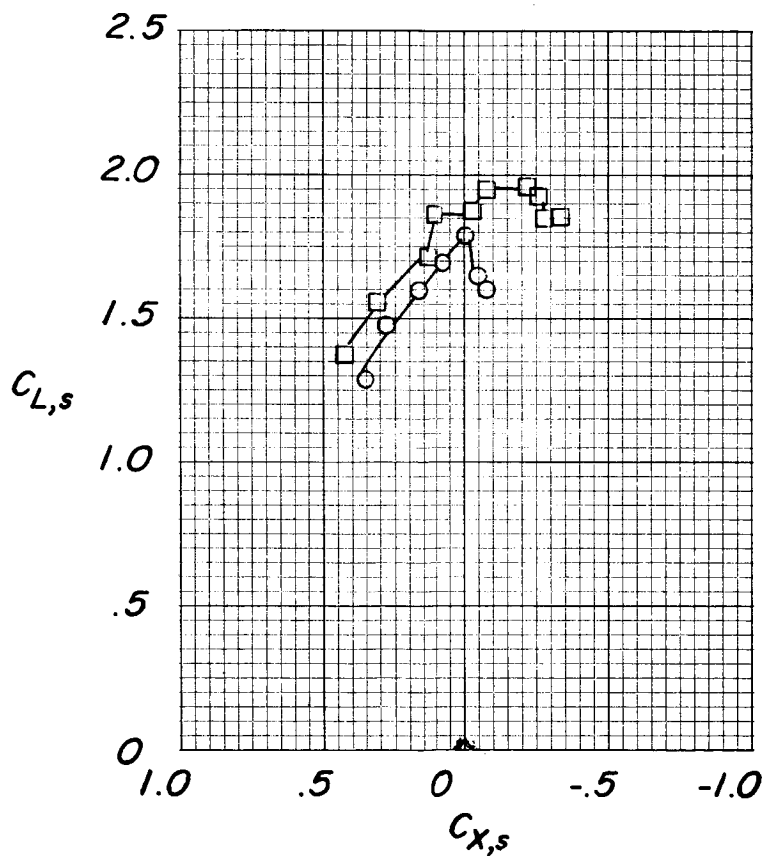
(b) Pitching-moment, lift, and longitudinal-force coefficients.

Figure 37.- Concluded.



*Leading-edge slat*

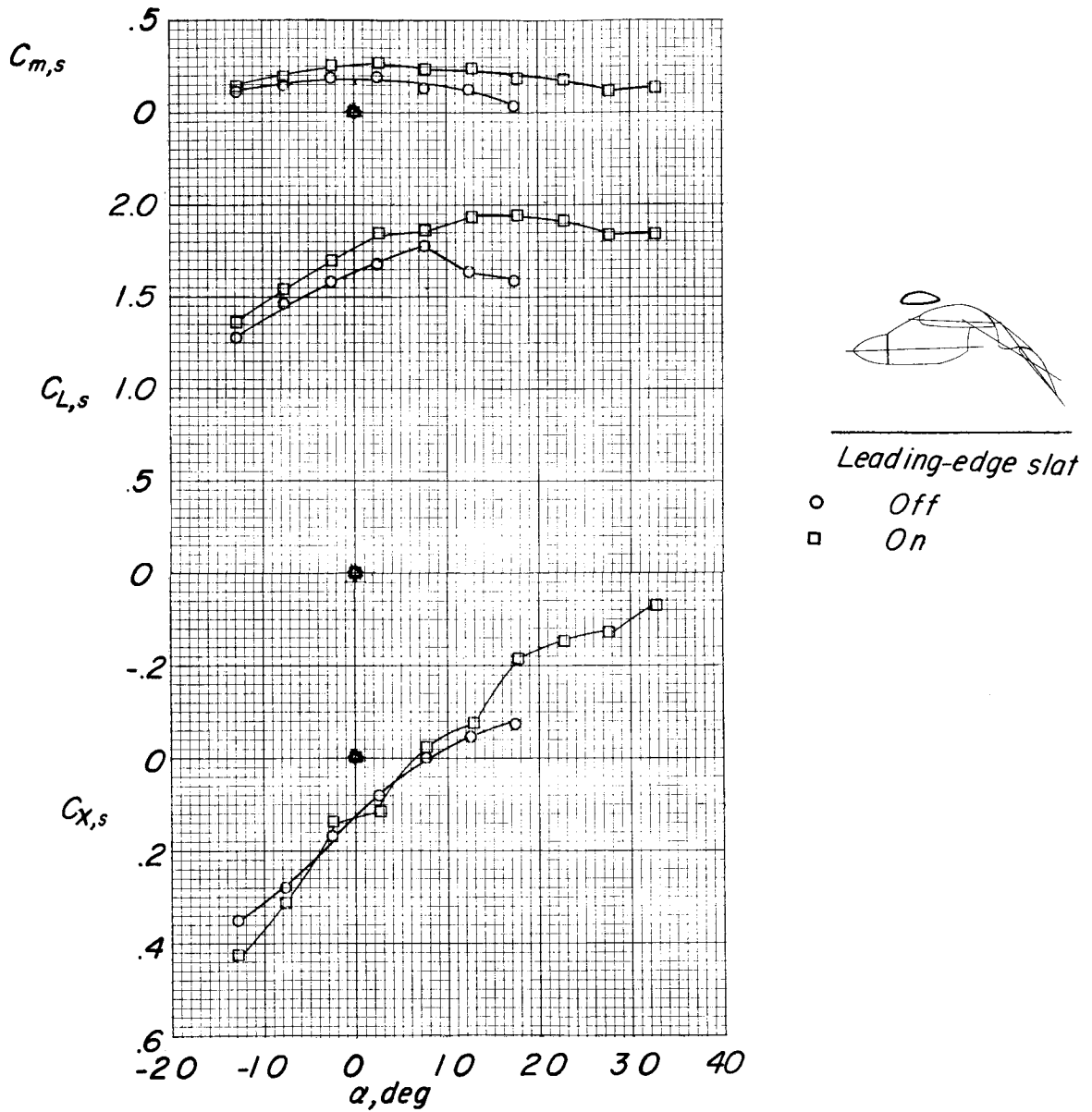
○ *Off*  
 □ *On*



(a) Lift coefficient as function of longitudinal-force coefficient.

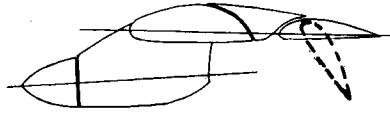
Figure 38.- Effect of leading-edge slat in region of ground effect.

$C_{T,s} = 0.745$ ;  $i_t = 0^\circ$ ;  $\delta_{f,S}/\delta_{f,R} = 30/20.7$ ;  $h/D = 0.33$ .

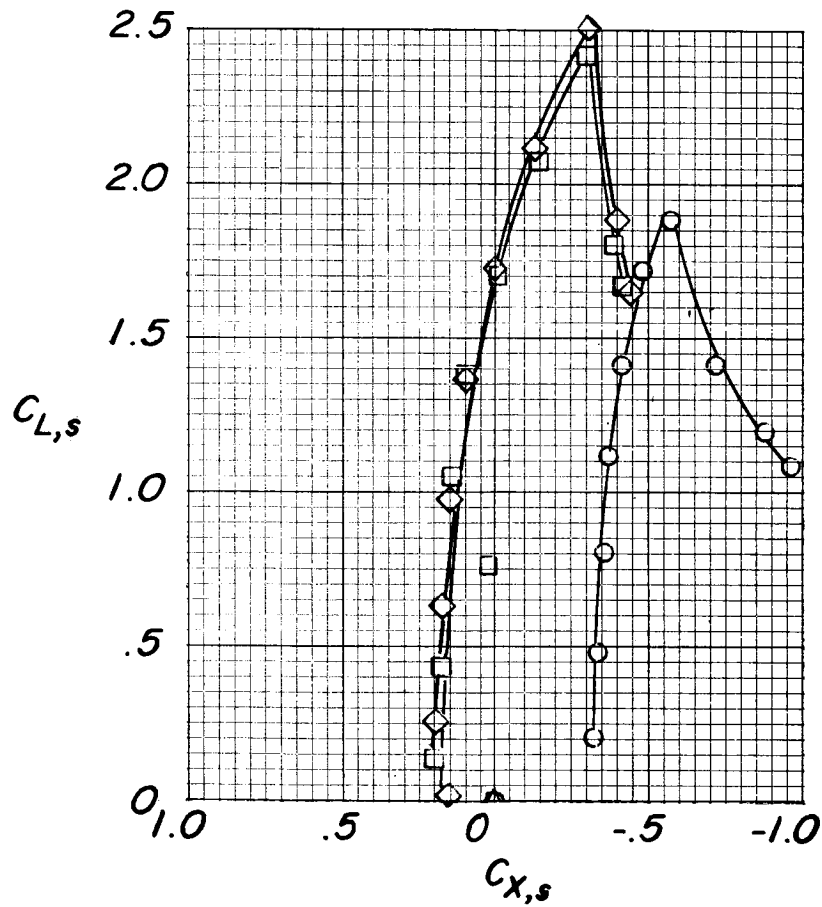


(b) Pitching-moment, lift, and longitudinal-force coefficients.

Figure 38.- Concluded.

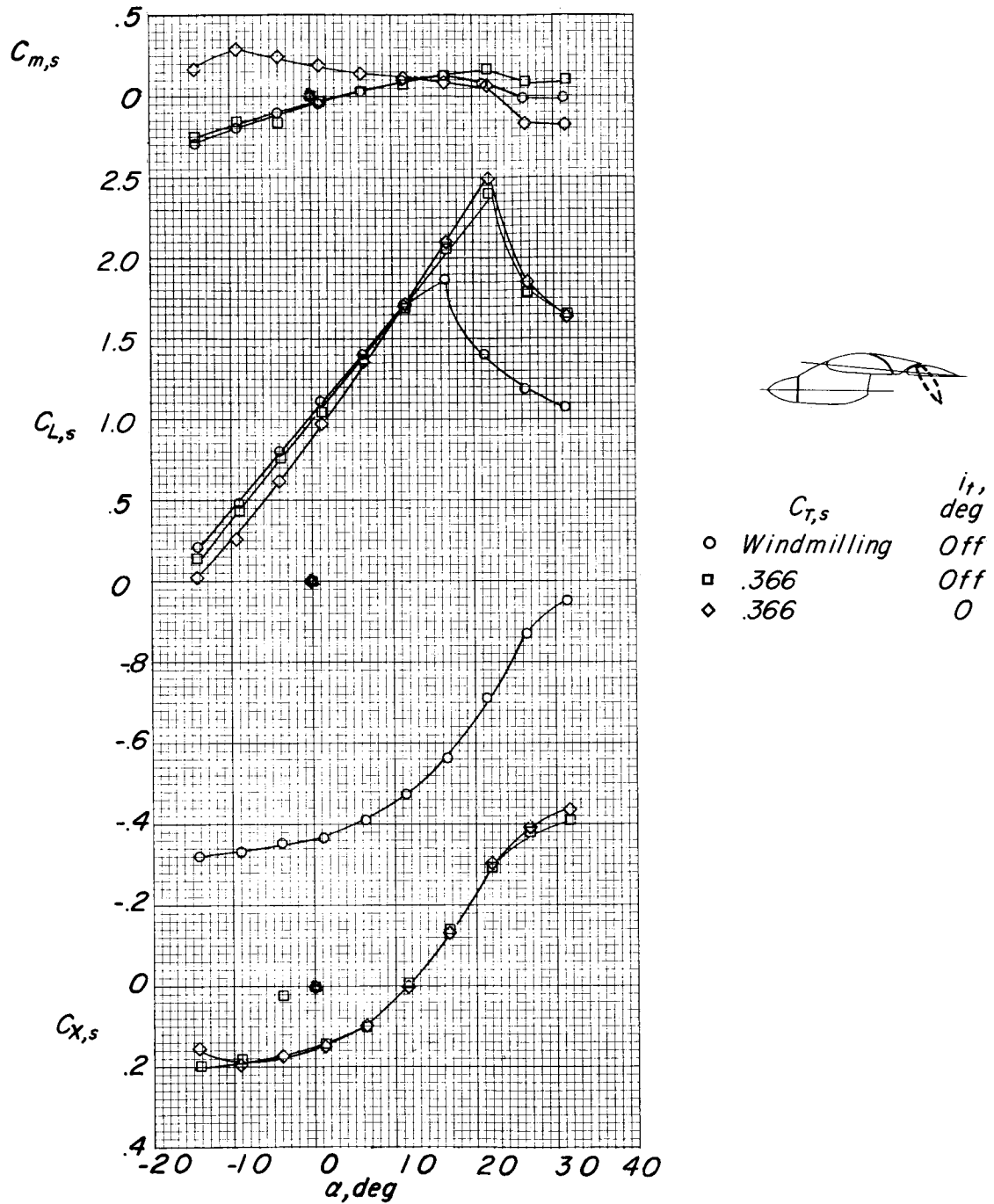


	$C_{T,s}$	$i_t$ , deg
○	Windmilling	Off
□	.366	Off
◇	.366	0



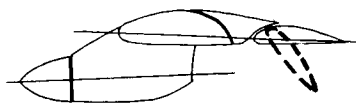
(a) Lift coefficient as function of longitudinal-force coefficient.

Figure 39.- Effect of thrust with inboard flap deflected  $40^\circ$ .

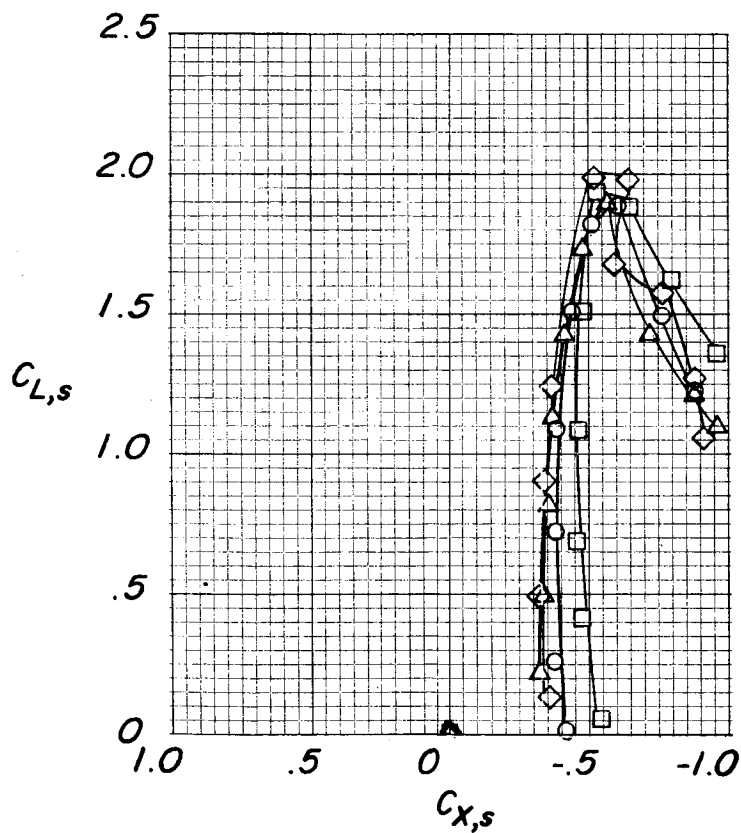


(b) Pitching-moment, lift, and longitudinal-force coefficients.

Figure 39.- Concluded.

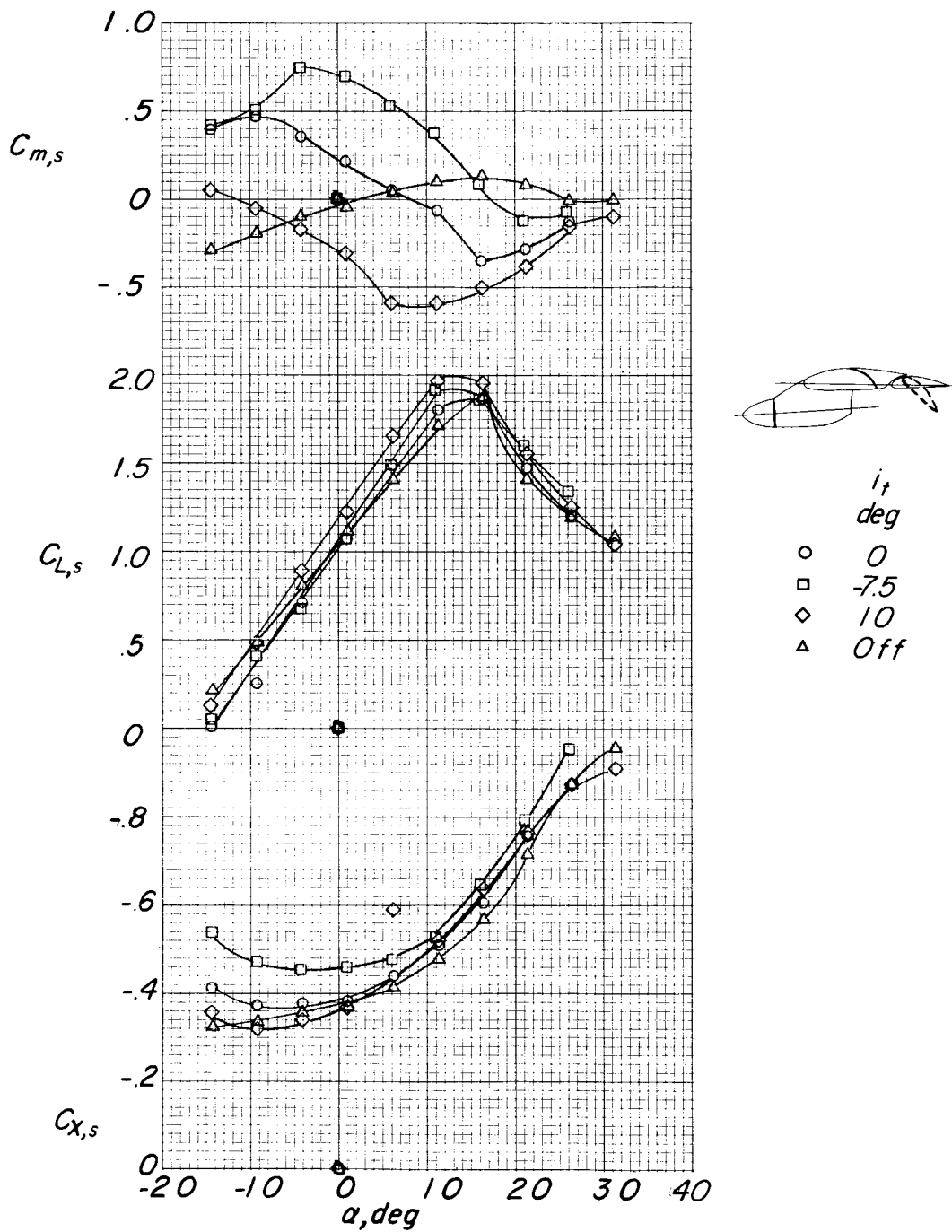


	$i_t$ , deg
○	0
□	-7.5
◇	10
△	Off



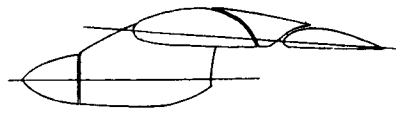
(a) Lift coefficient as function of longitudinal-force coefficient.

Figure 40.- Effect of tail incidence with inboard flap deflected  $40^\circ$ .  
Propellers windmilling.

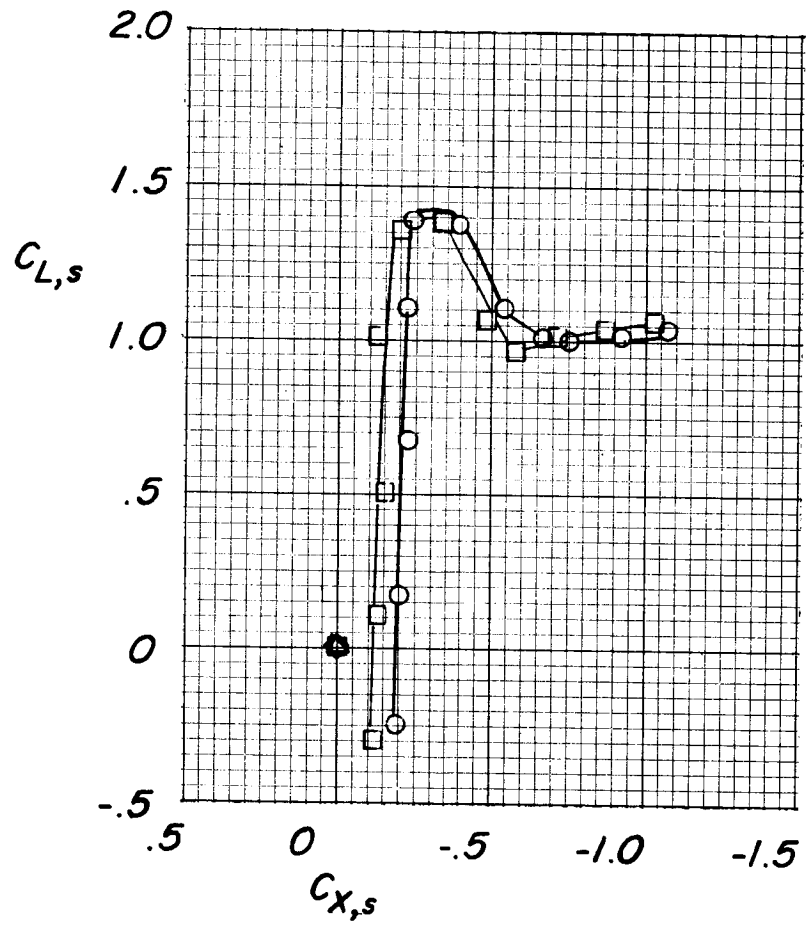


(b) Pitching-moment, lift, and longitudinal-force coefficients.

Figure 40.- Concluded.



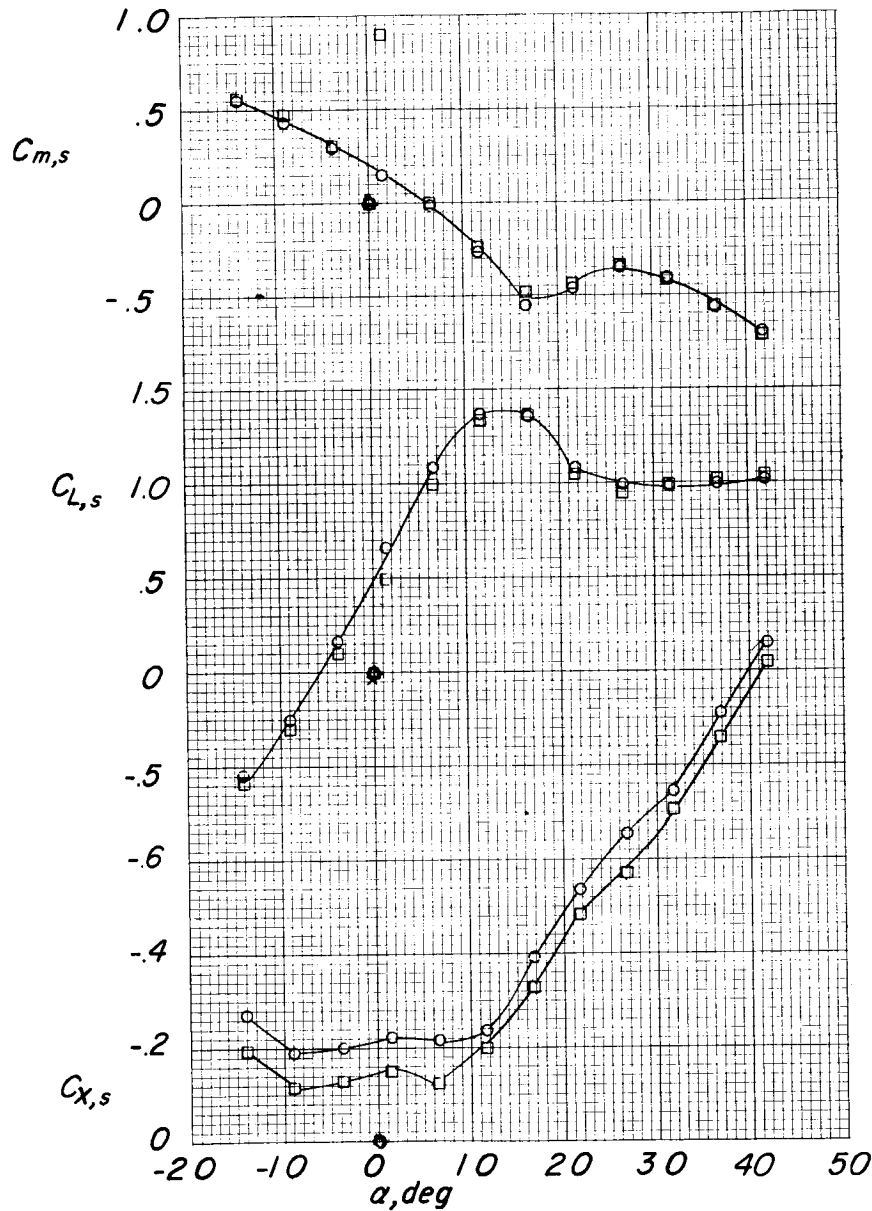
*Landing gear*  
 ○ *On*  
 □ *Off*



(a) Lift coefficient as function of longitudinal-force coefficient.

Figure 41.- Effect of landing gear. Propellers off;  $i_t = 0^\circ$ ;  
 $\delta_{f,S}/\delta_{f,R} = 0/0$ .

L-735



(b) Pitching-moment, lift, and longitudinal-force coefficients.

Figure 41.- Concluded.

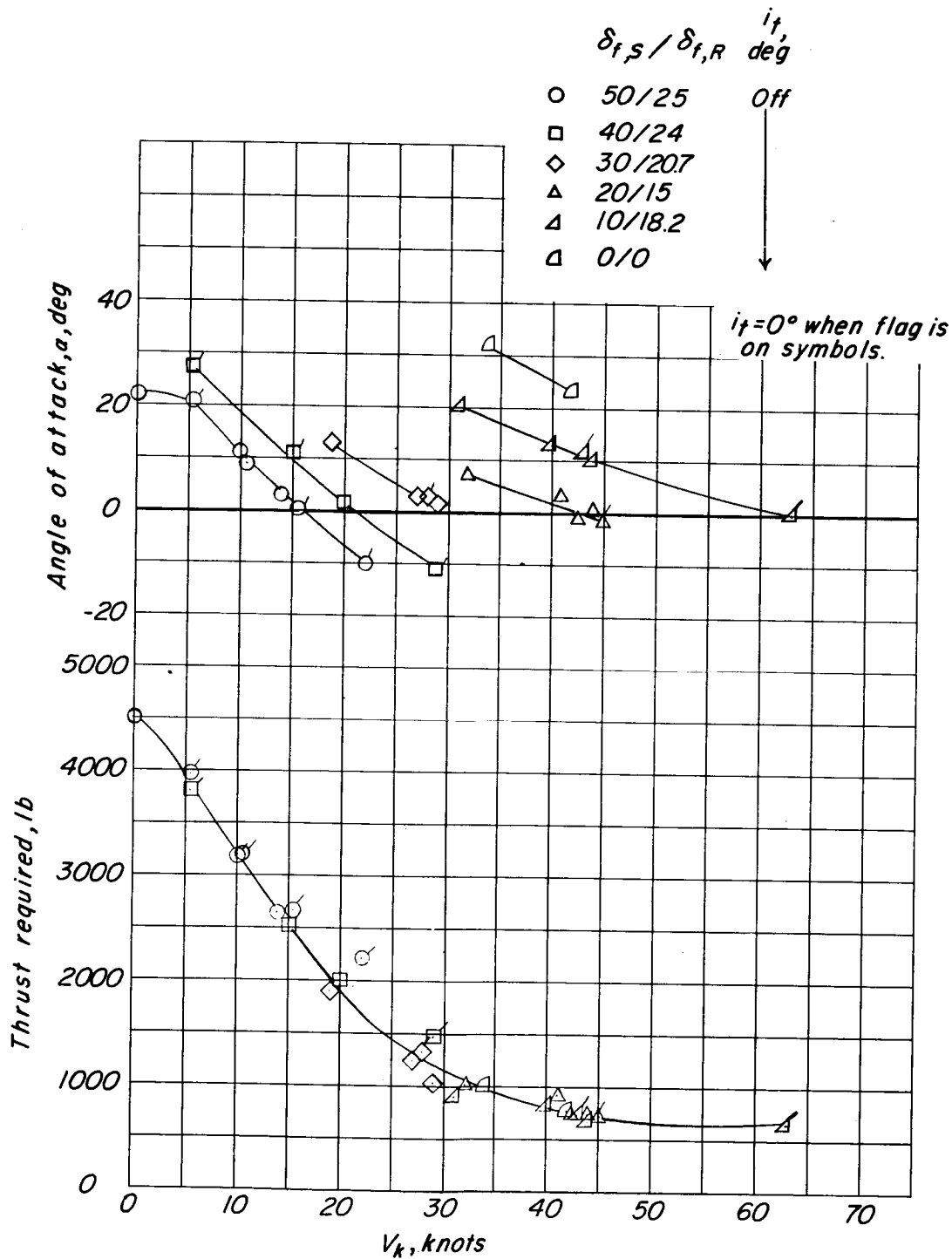
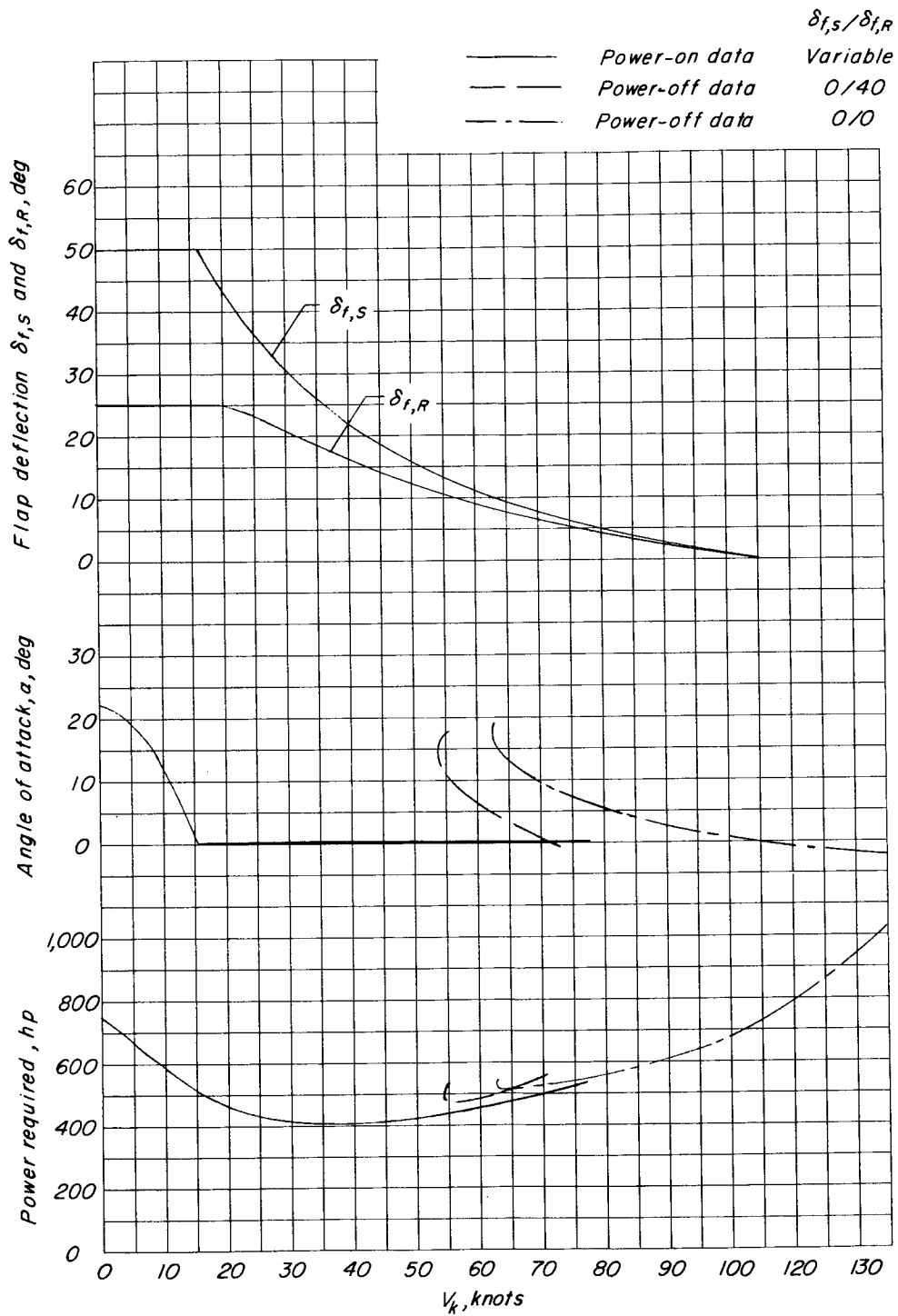


Figure 42.- Variation of angle of attack and thrust required for steady level flight for various flap deflections.

L-735



L-735

Figure 43.- Flap deflection, angle of attack, and power required in steady-level-flight transition.

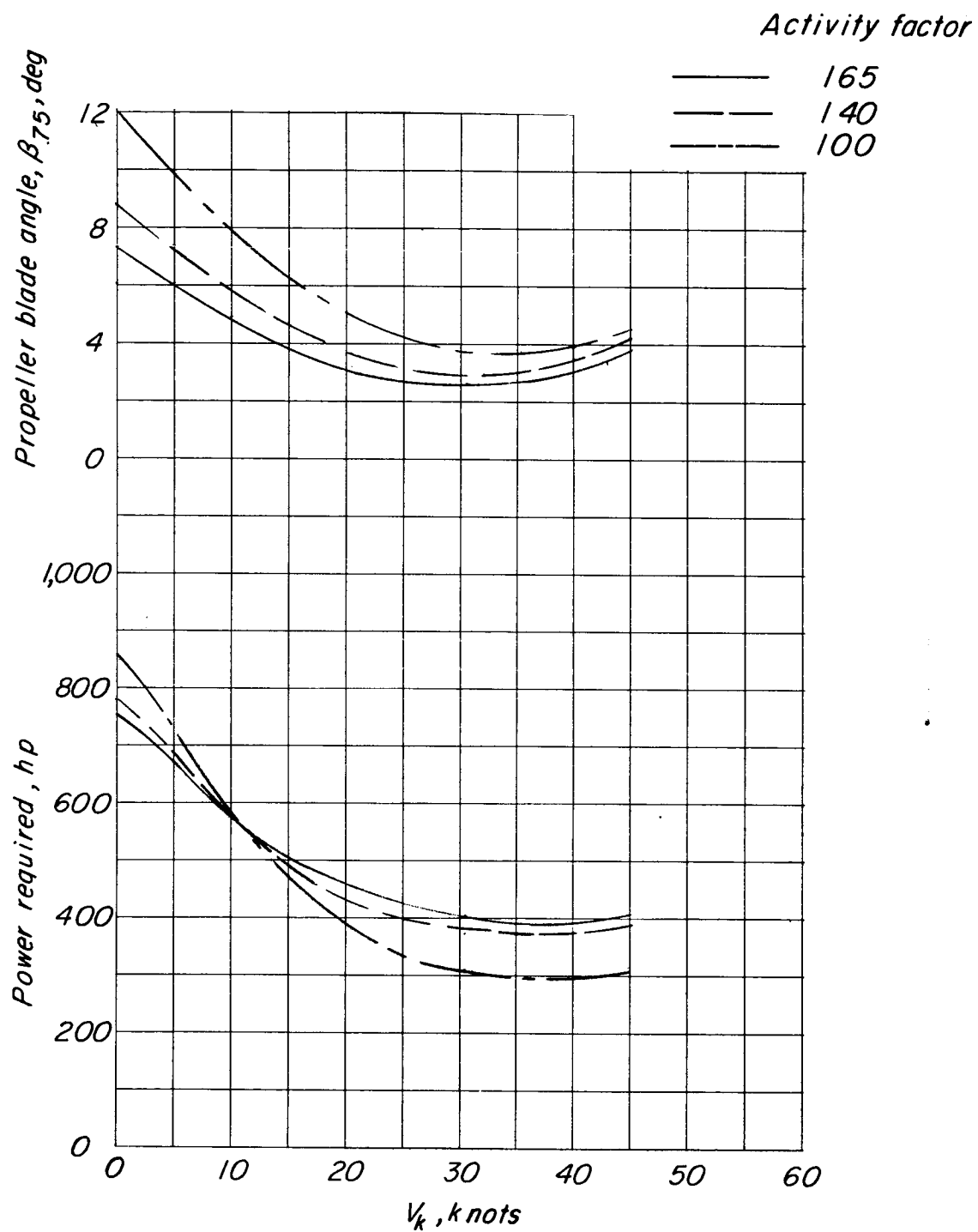


Figure 44.- Effect of propeller activity factor on blade angle and power required for steady-level-flight transition.

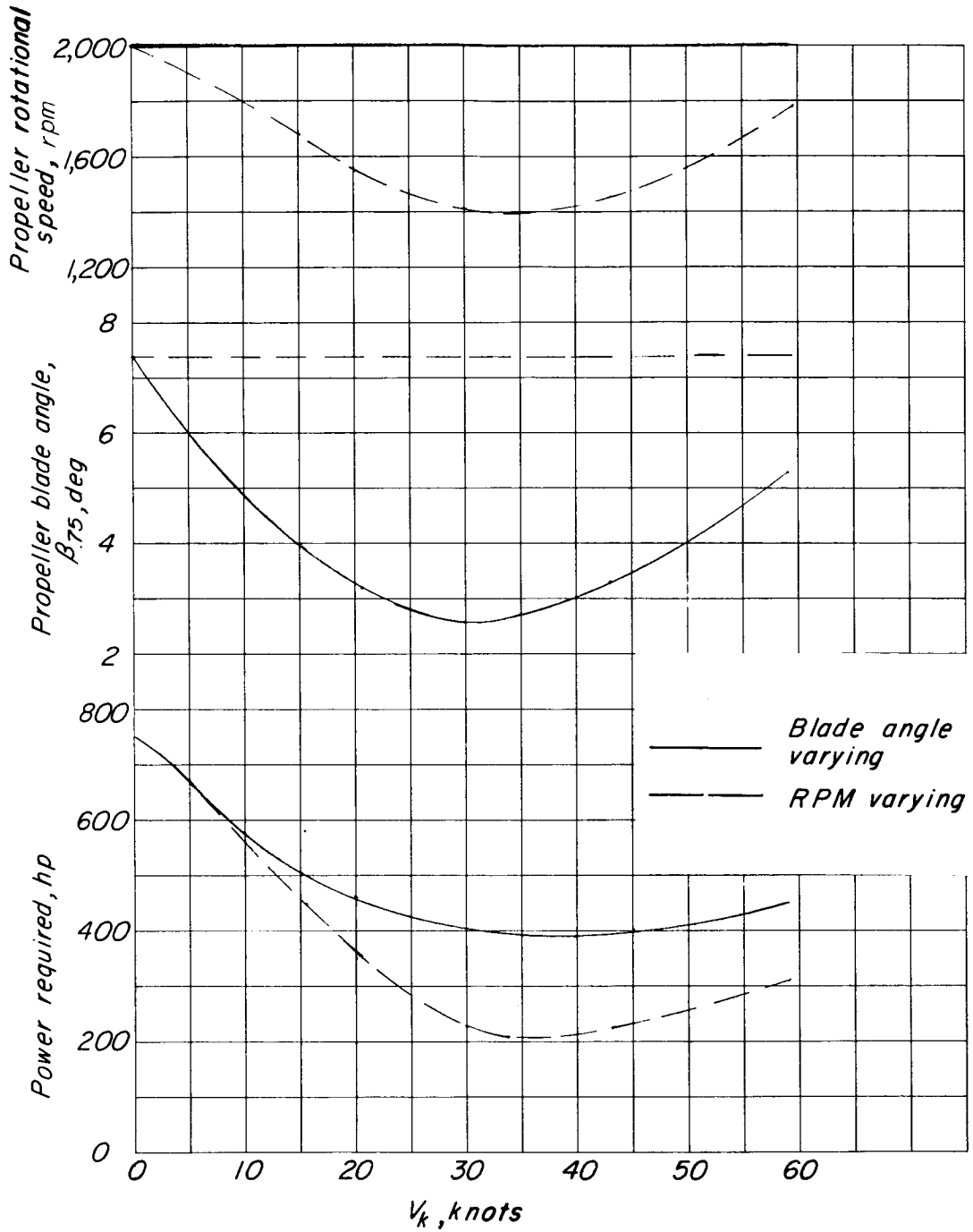


Figure 45.- Comparison of effect on power of varying propeller rotational speed or varying propeller blade angle to achieve steady-level-flight transition.

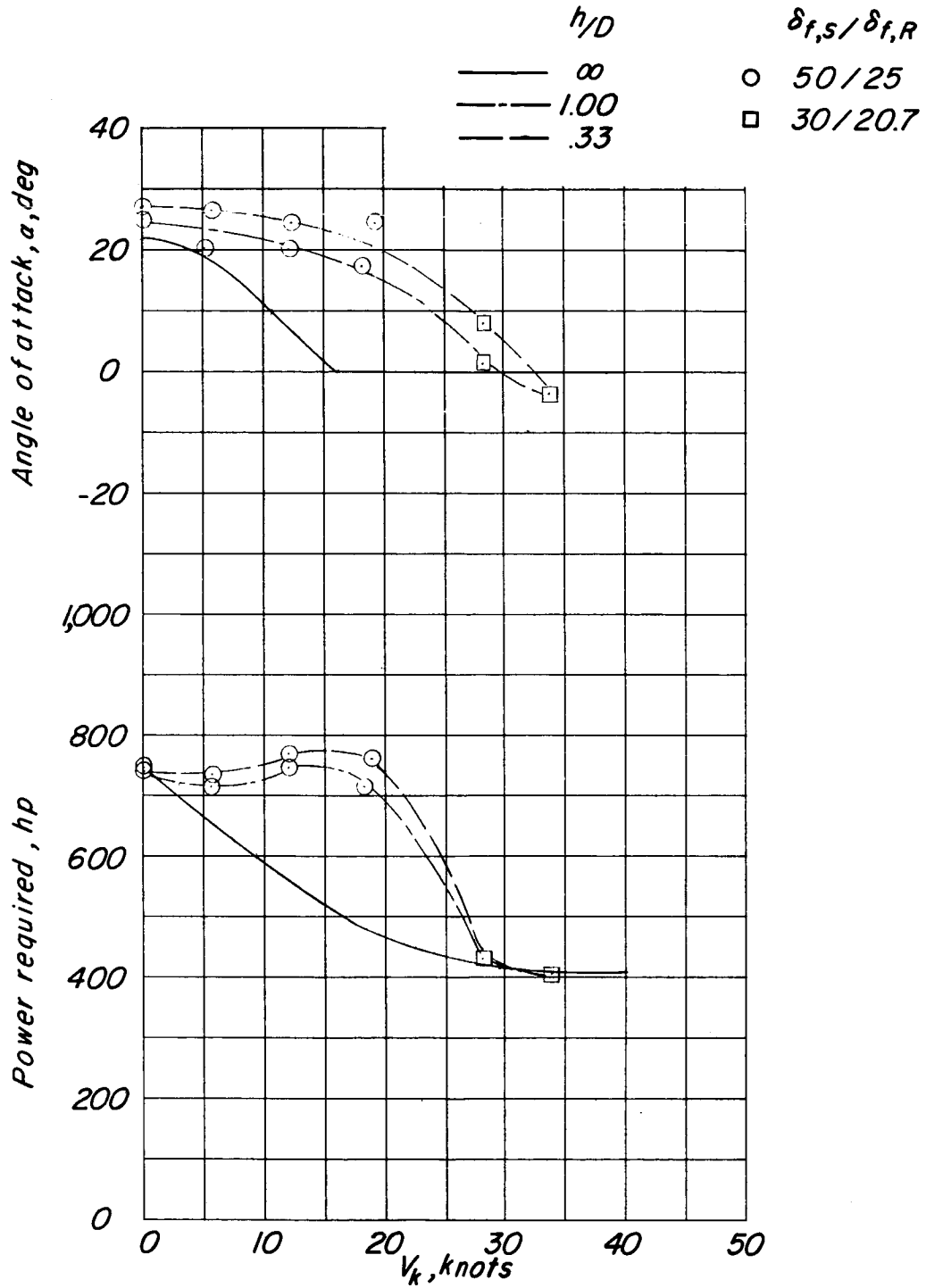


Figure 46.- Effect of ground proximity on angle of attack and power required for steady-level-flight transition.

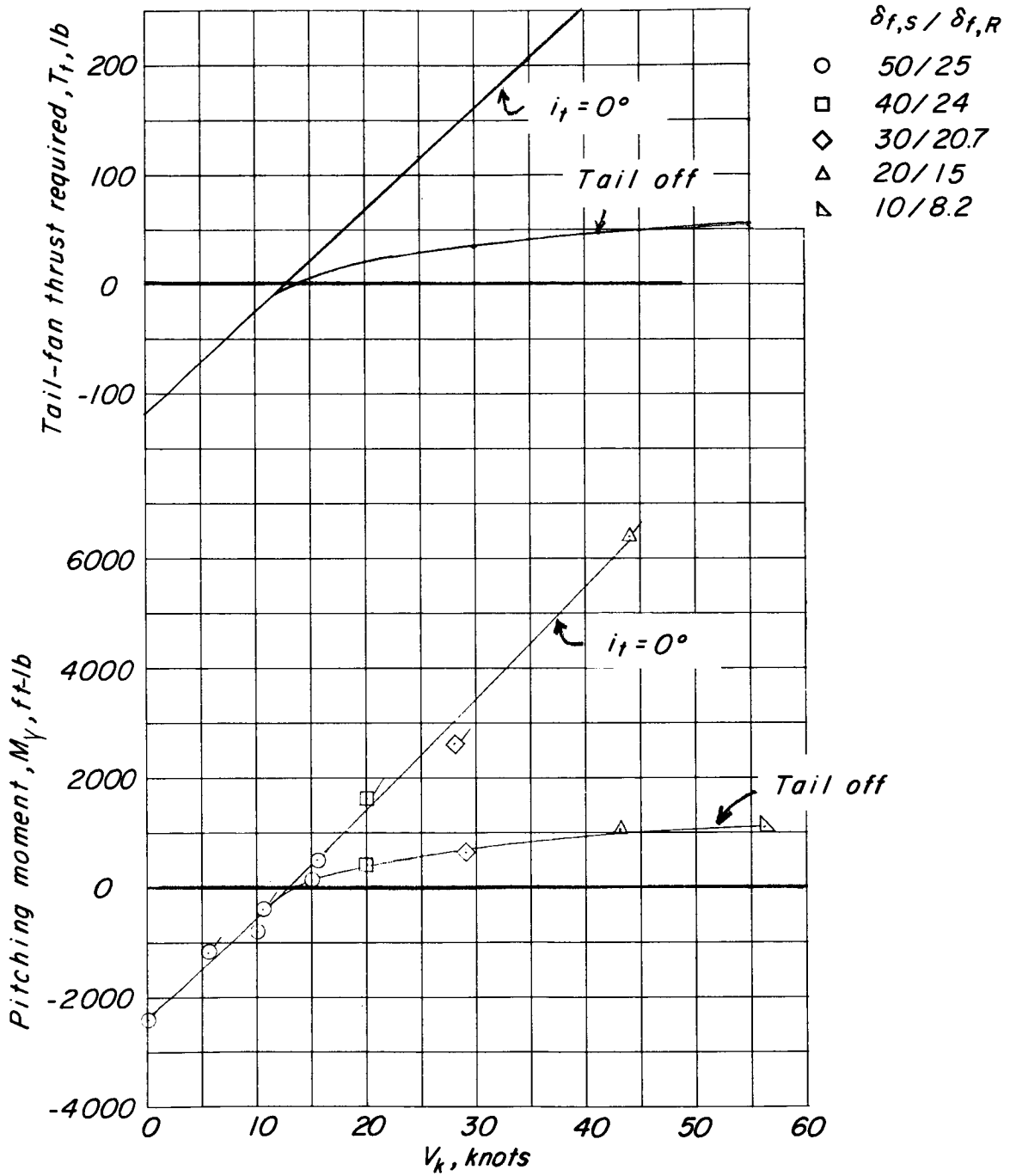


Figure 47.- Untrimmed pitching moment and tail-fan thrust required for trim in steady-level-flight transition.  $\alpha \approx 0^\circ$ .

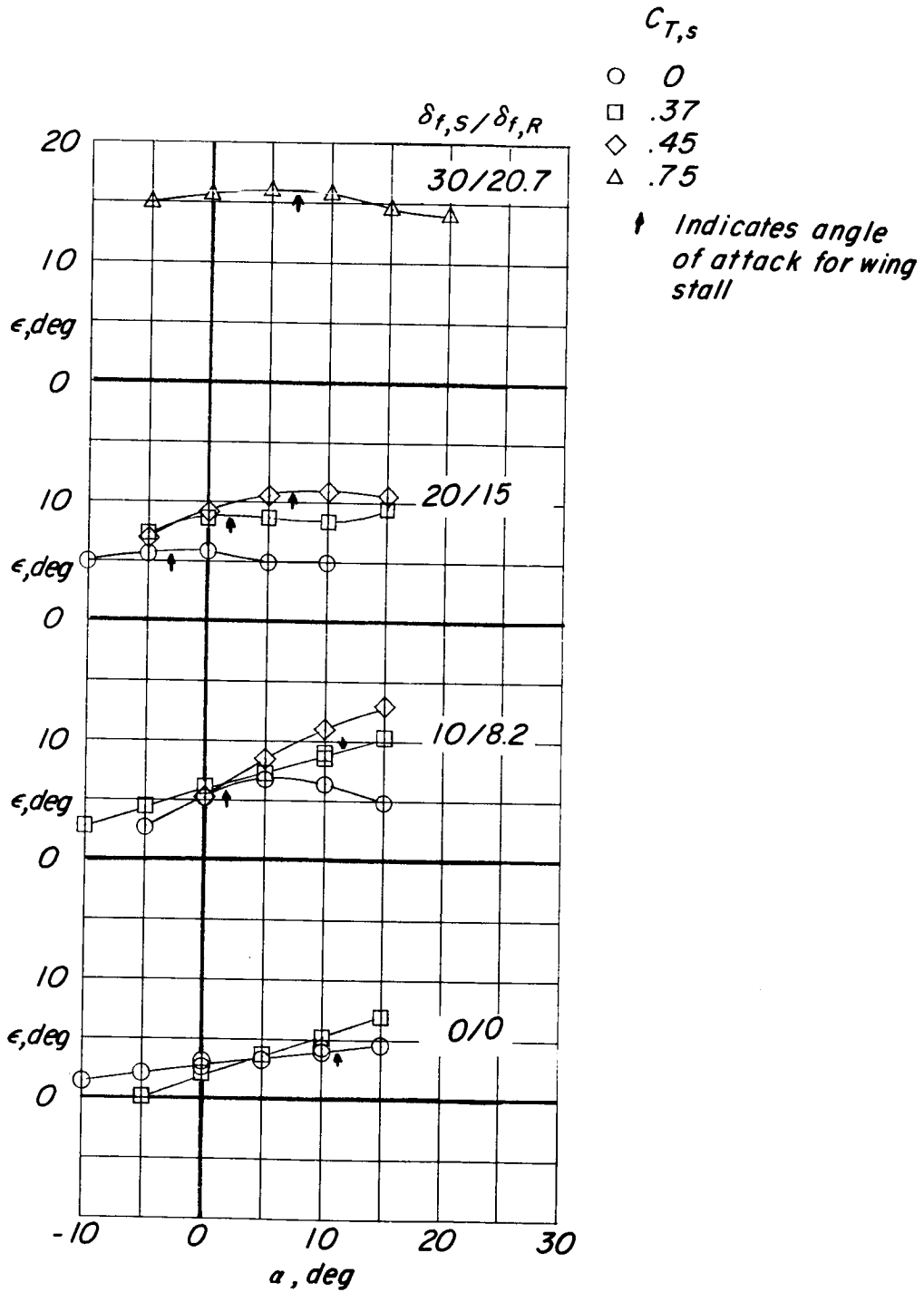
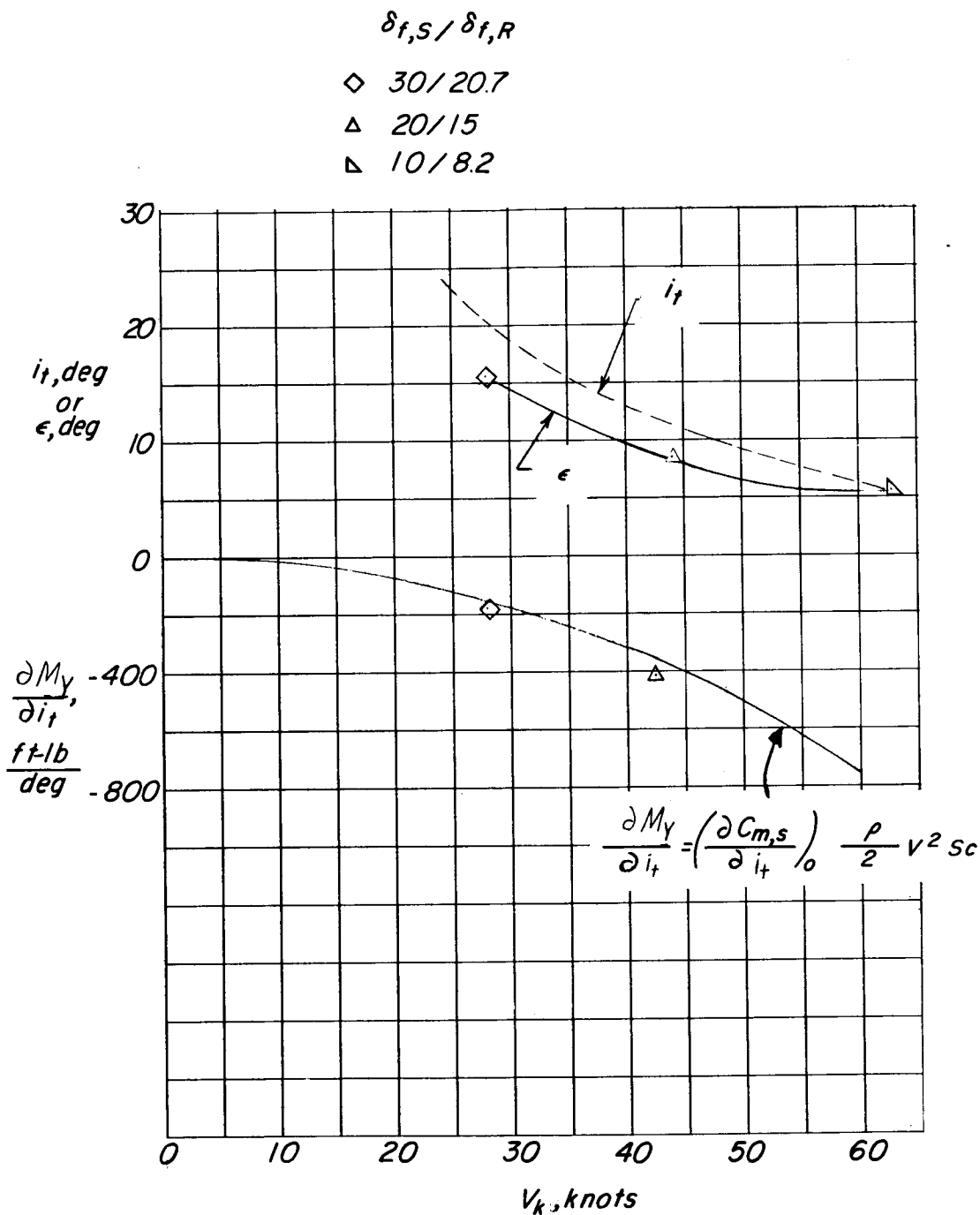


Figure 48.- Effect of flap deflection and thrust coefficient on downwash angle at horizontal tail.

L-735



L-735

Figure 49.- Horizontal-tail effectiveness, downwash angle, and stabilizer setting required for trim in steady-level-flight transition out of ground effect.  $\alpha = 0^\circ$ .

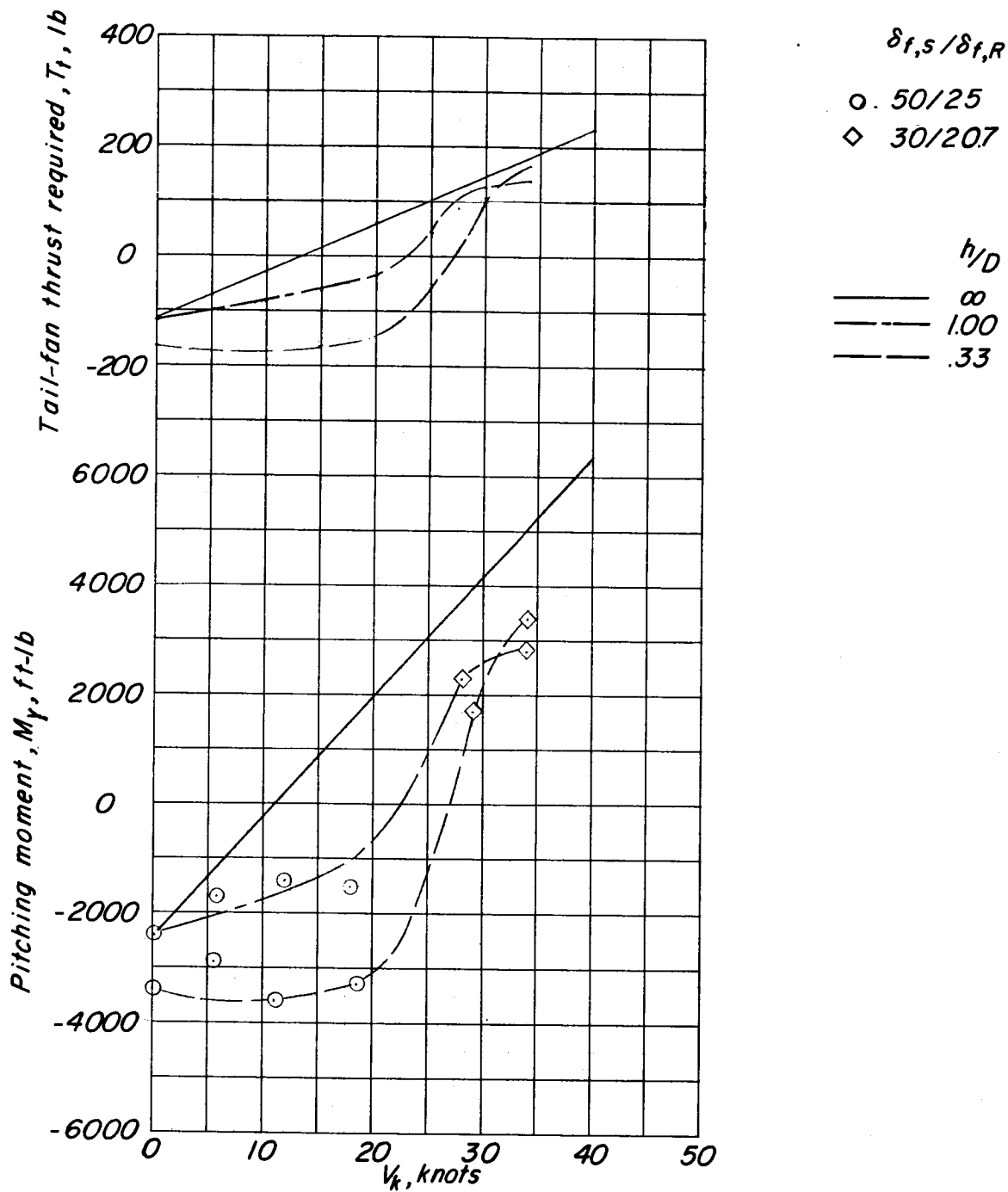


Figure 50.- Effect of ground proximity on untrimmed pitching moment and tail-fan thrust required for trim in steady-level-flight transition.  $\alpha = 0^\circ$ .

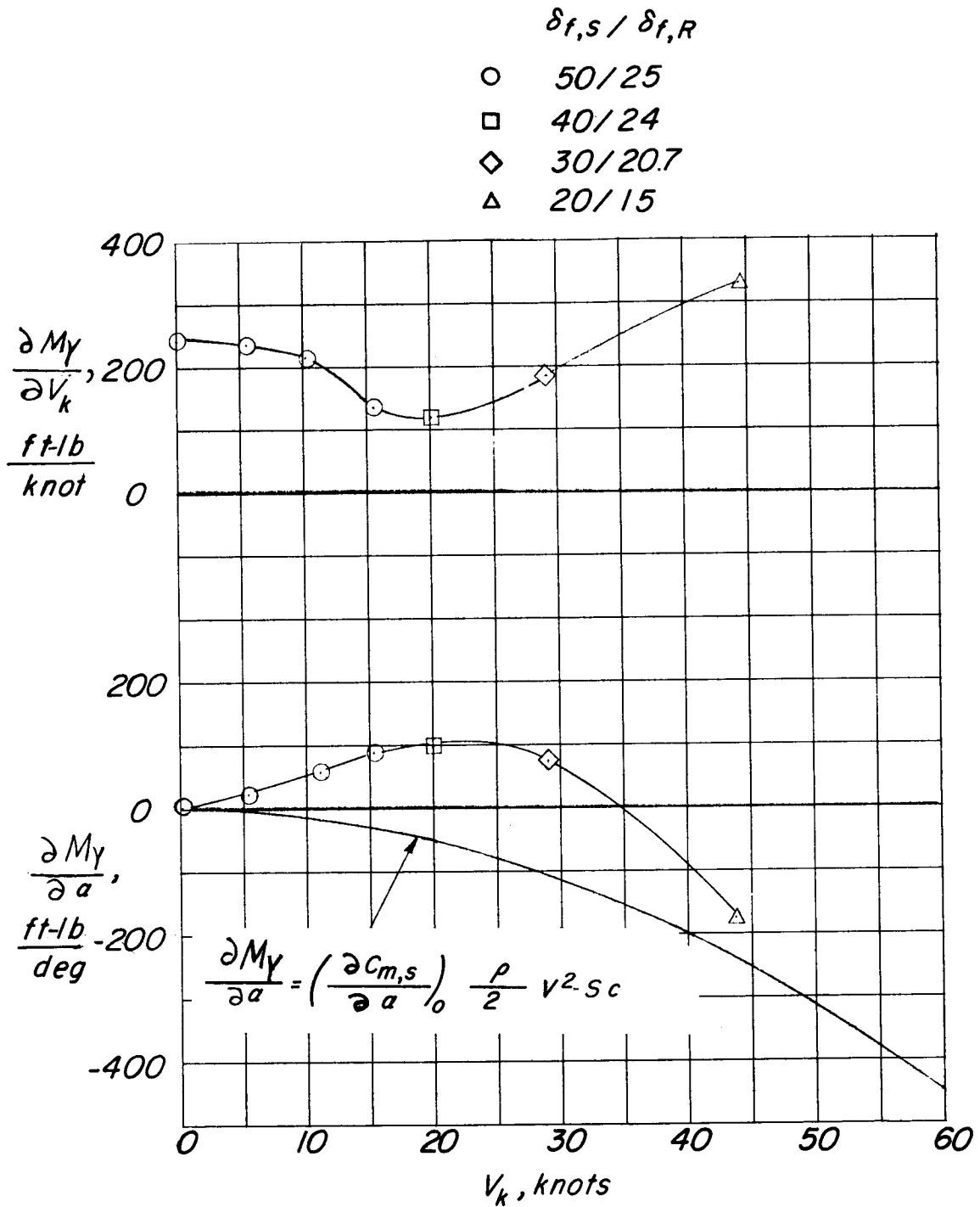


Figure 51.- Variation of speed-stability parameter  $\frac{\partial M_Y}{\partial V_k}$  and attitude-

stability parameter  $\frac{\partial M_Y}{\partial \alpha}$  in steady-level-flight transition.

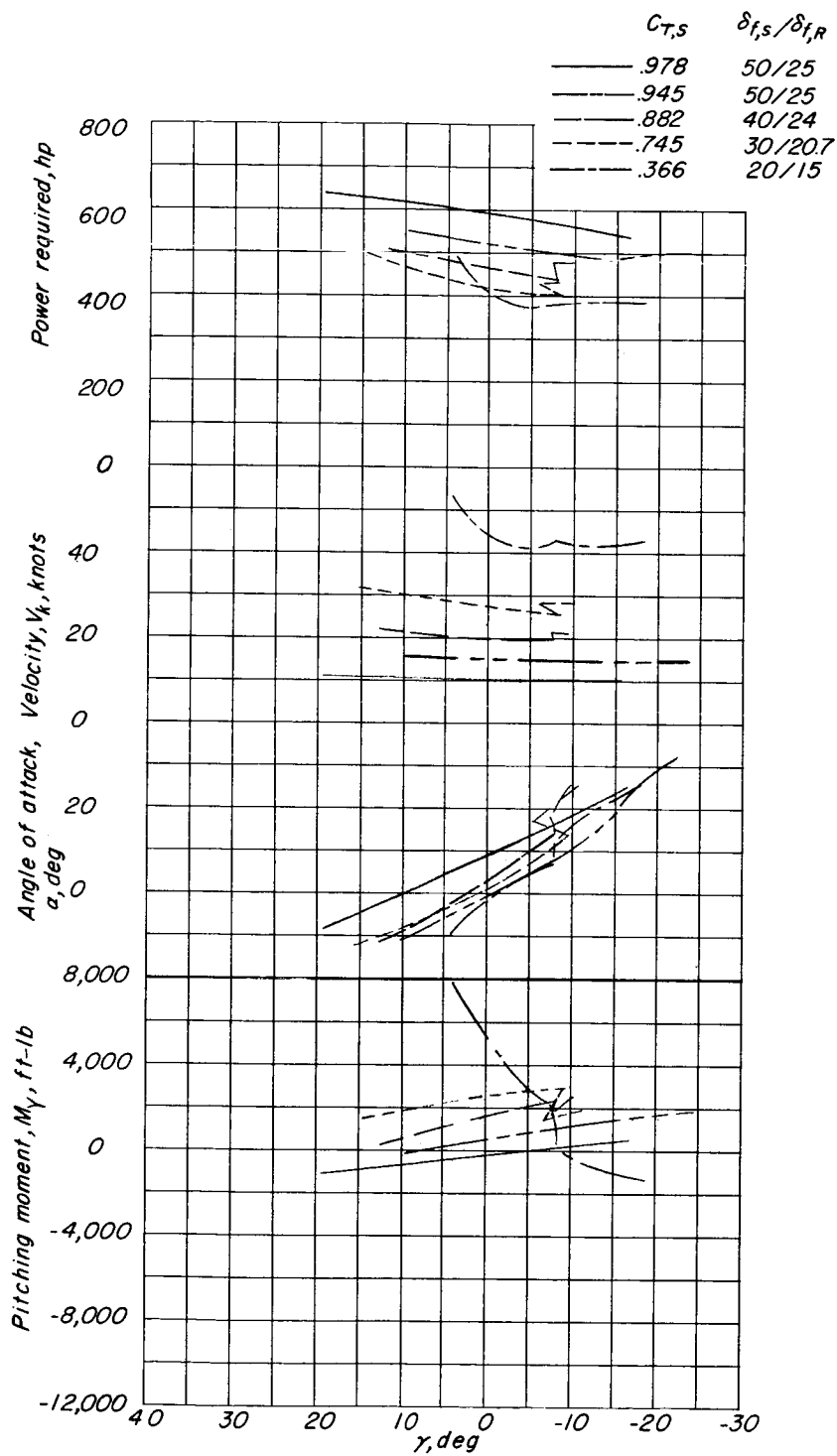
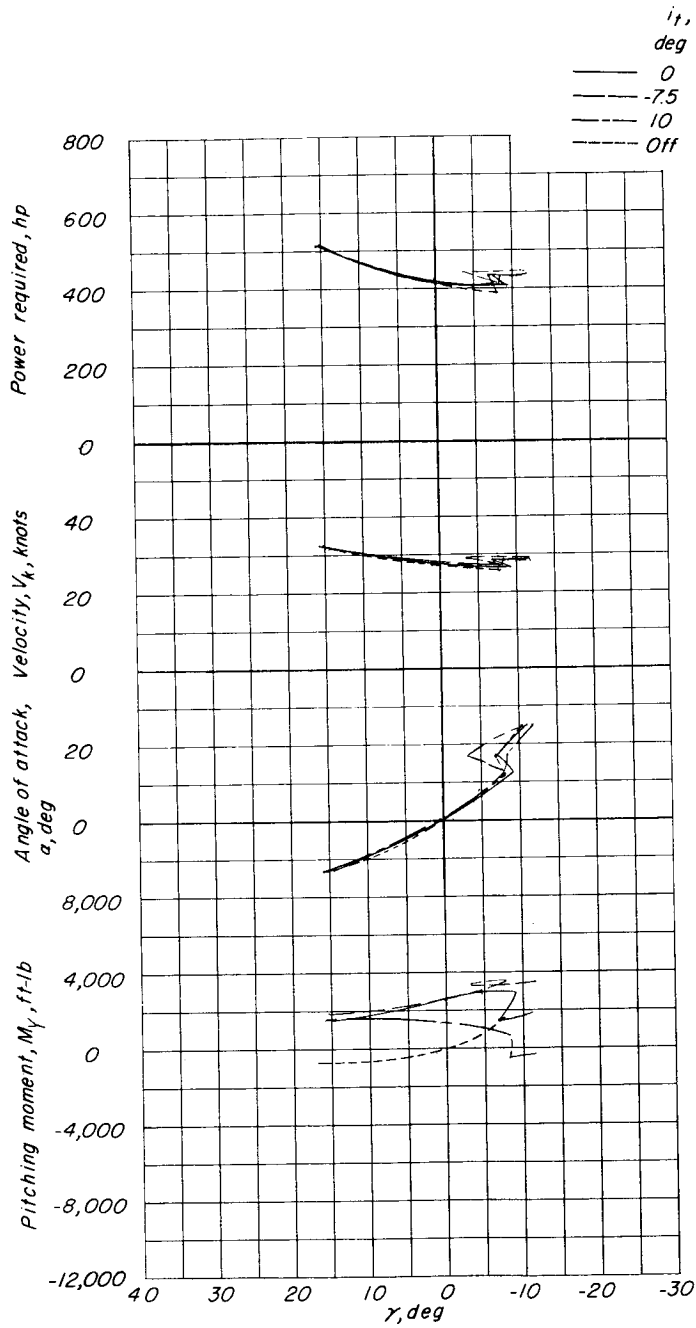


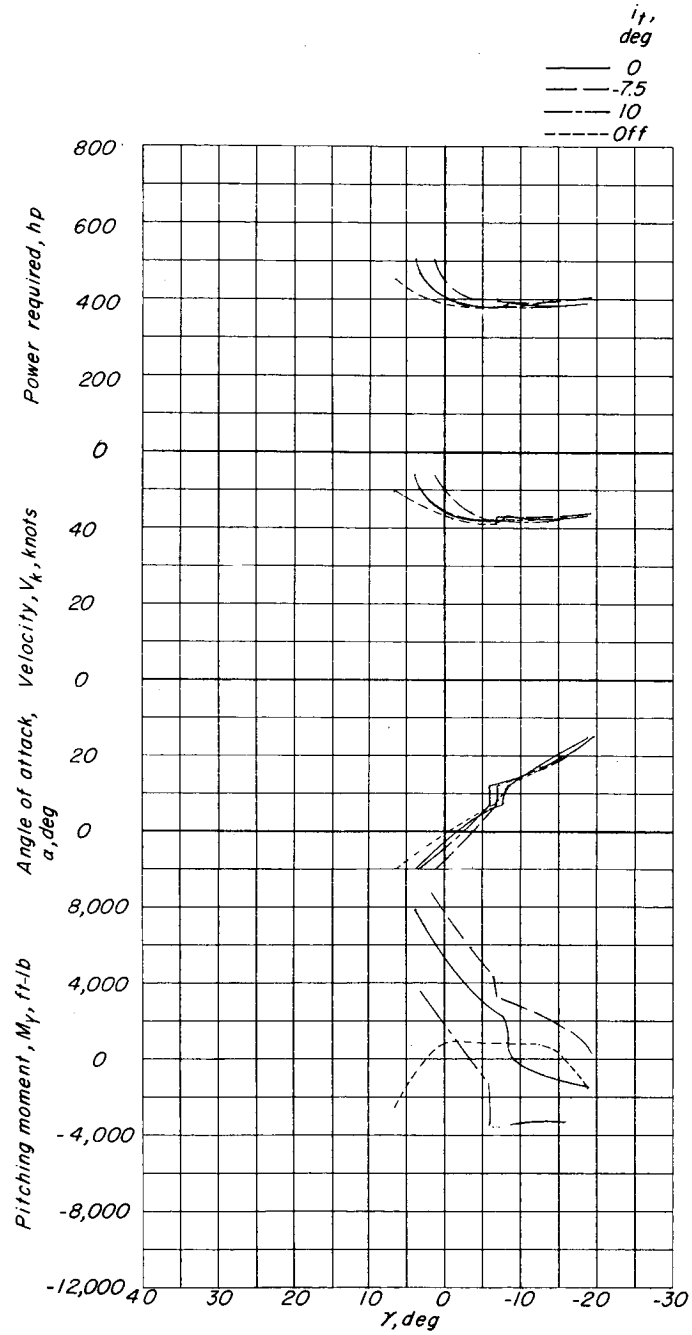
Figure 52.- Effect of flap deflection in climbing and descending flight.



(a)  $C_{T,S} = 0.745$ ;  $\delta_{f,S}/\delta_{f,R} = 30/20.7$ .

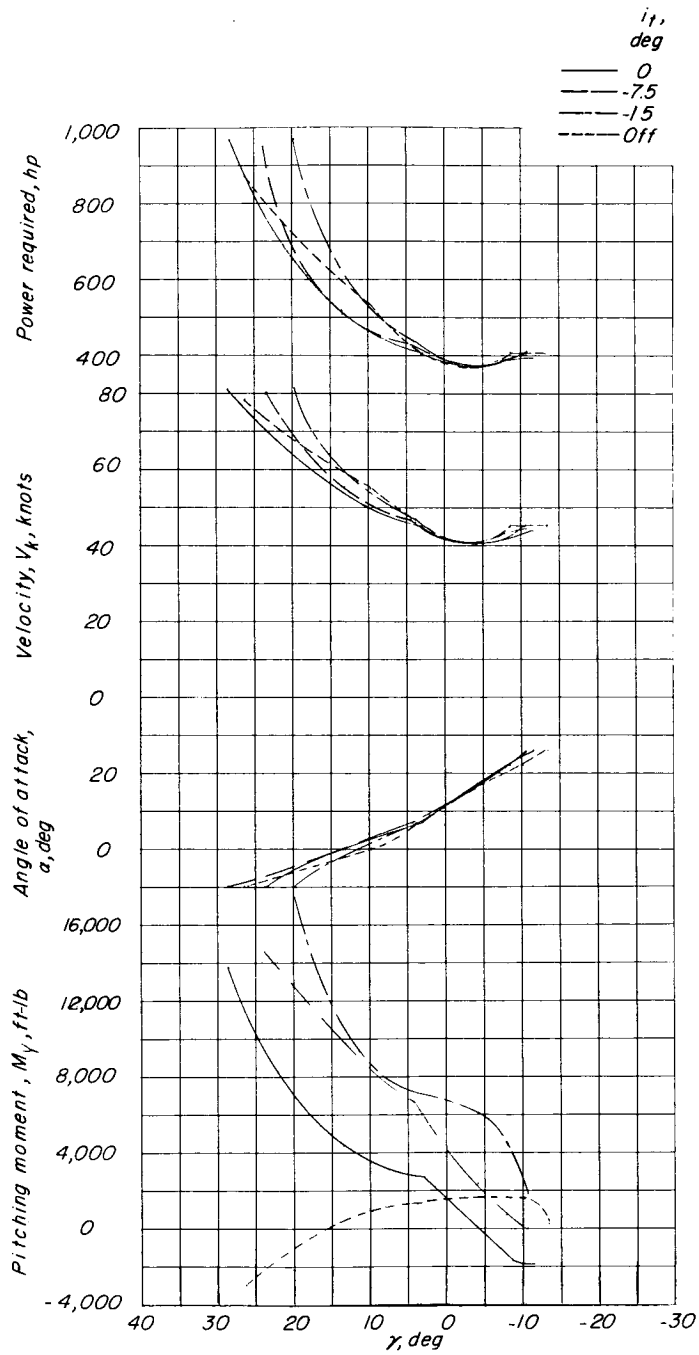
Figure 53.- Effect of horizontal tail in climbing and descending flight.

L-735



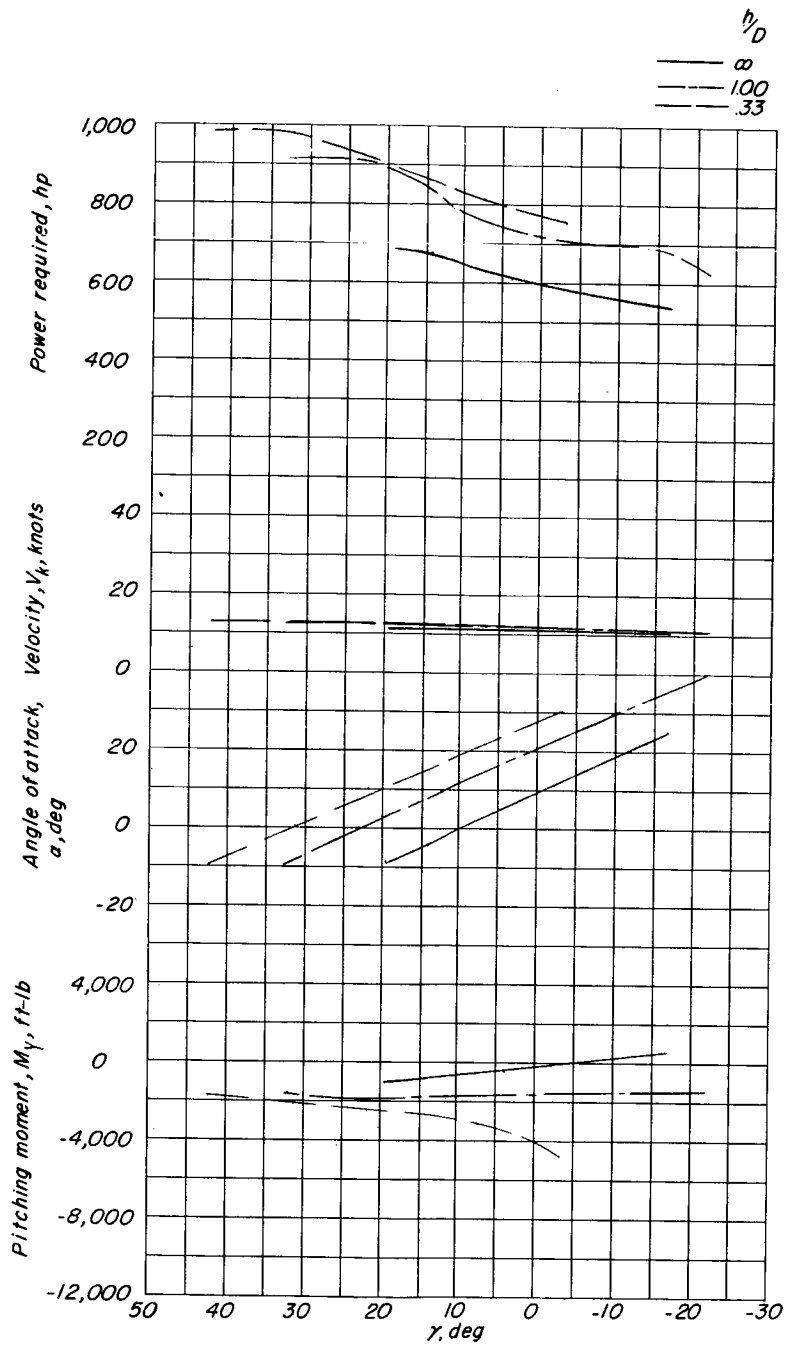
(b)  $C_{T,S} = 0.366$ ;  $\delta_{f,S}/\delta_{f,R} = 20/15$ .

Figure 53.- Continued.



(c)  $C_{T,s} = 0.366$ ;  $\delta_{f,S} / \delta_{f,R} = 10/8.2$ .

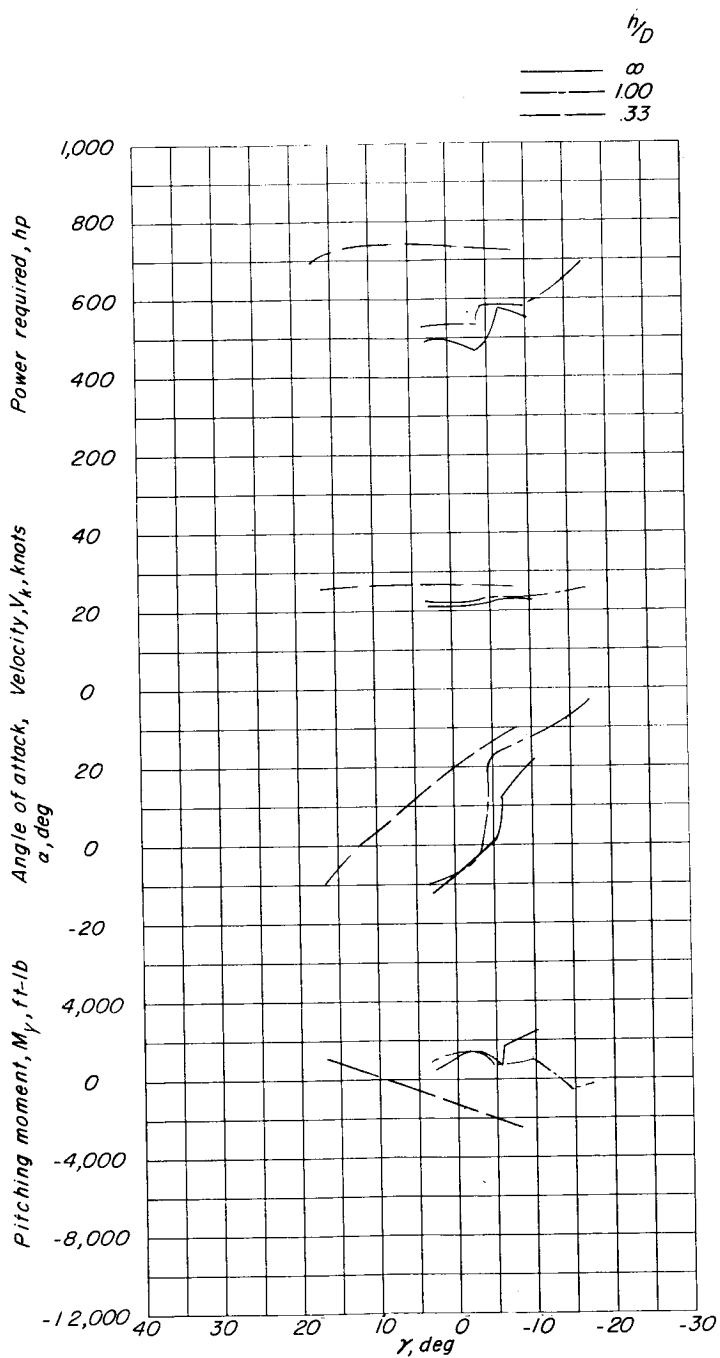
Figure 53.- Concluded.



(a)  $C_{T,S} = 0.978$ ;  $\delta_{f,S}/\delta_{f,R} = 50/25$ .

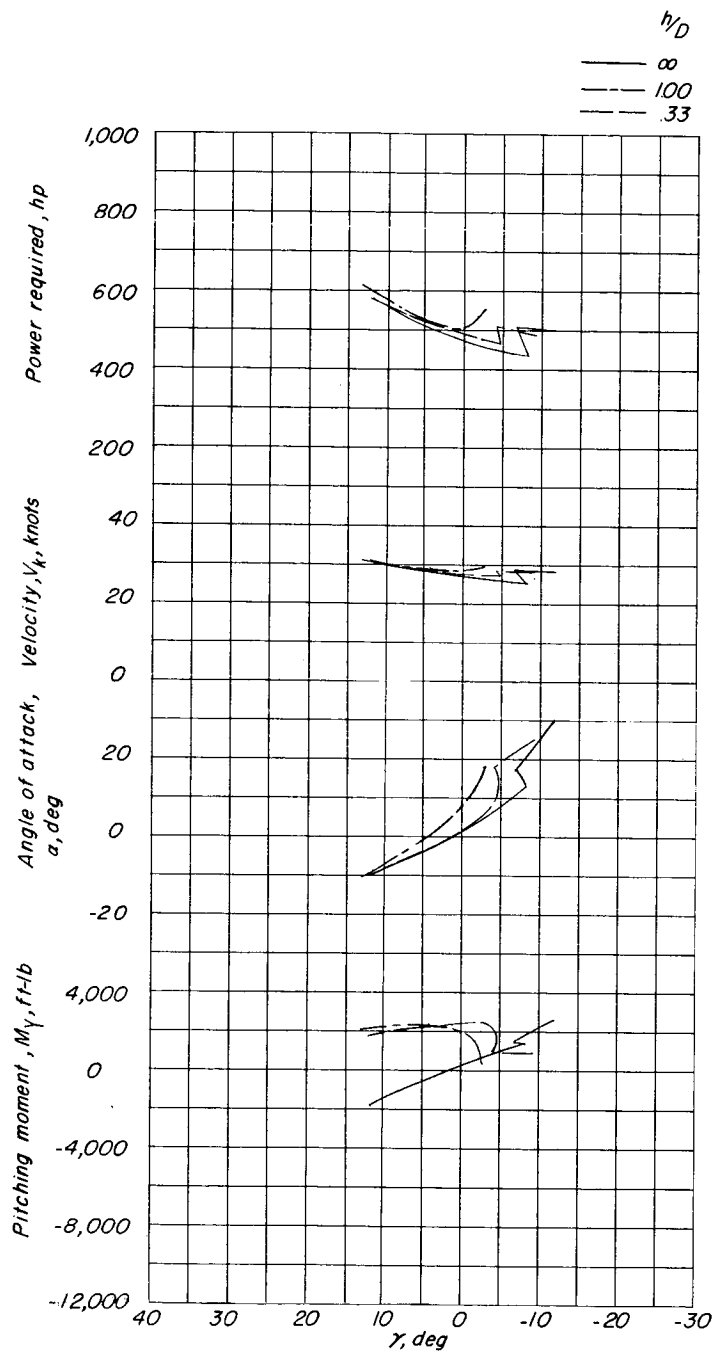
Figure 54.- Effect of ground proximity on climbing and descending flight.

L-735



(b)  $C_{T,s} = 0.882$ ;  $\delta_{f,S}/\delta_{f,R} = 50/25$ .

Figure 54.- Continued.



(c)  $C_{T,s} = 0.745$ ;  $\delta_{f,S}/\delta_{f,R} = 30/20.7$ .

Figure 54.- Concluded.

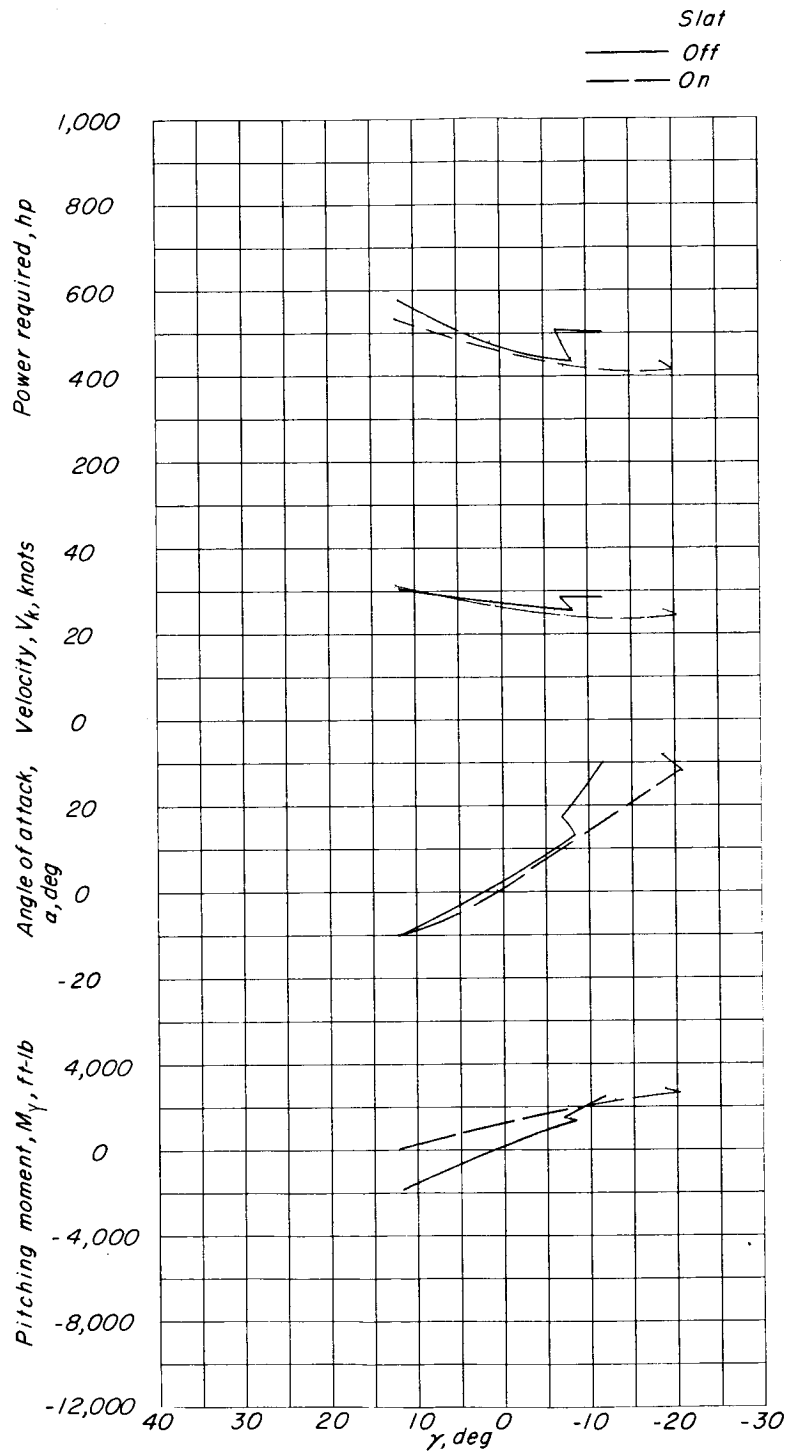


Figure 55.- Effect of slat in climbing and descending flight.  
 $\delta_{f,S}/\delta_{f,R} = 30/20.7$ .